Power Electronics Intensive Energy Management Solutions for Hybrid Electric Vehicle Energy Storage Systems

Zahra Amjadi

A Thesis

in

The Department

of

Electrical and Computer Engineering

Presented in Partial Fulfillment of the Requirements for the Degree of

Doctor of Philosophy

Concordia University

Montréal, Québec, Canada

February 2011

CONCORDIA UNIVERSITY
SCHOOL OF GRADUATE STUDIES

This is to certify that the thesis prepared
By: Zahra Amjadi

Entitled: "Power Electronics Intensive Energy Management Solutions for Hybrid Electric Vehicle Energy Storage Systems"

And submitted in partial fulfillment of the requirements for the degree of

DOCTOR OF PHILOSOPHY (Electrical & Computer Engineering)

Complies with the regulations of the University and meets the accepted standards with respect to originality and quality.

Signed by the final examining committee:

_____ Chair

Dr. S. Rakheja

_____ External Examiner

Dr. N. Kar

_____ External to Program

Dr. A. Bagchi

_____ Examiner

Dr. S. Hashtrudi Zad

_____ Examiner

Dr. P. Pillay

_____ Thesis Supervisor

Dr. S. Williamson

Approved by _____

Dr. M. Kahrizi, Graduate Program Director

February 8, 2011 _____

Dr. Robin A.L. Drew, Dean

Faculty of Engineering & Computer Science

ABSTRACT

Power Electronics Intensive Energy Management Solutions for Hybrid Electric and Plug-in Hybrid Electric Vehicle Energy Storage Systems

Zahra Amjadi, Ph.D

Concordia University, 2011

Batteries, ultra capacitors (UCs), and fuel cells (FCs) are widely being proposed for electric and plug-in hybrid electric vehicles (EVs/PHEVs) as energy sources. The increasing popularity of EVs and PHEVs can be attributed to the savings in fuel costs, compared to conventional internal combustion engine (ICE) vehicles. EVs and PHEVs save energy due to the employment of reverse regenerating braking, during the deceleration cycle. This recuperated energy can be proficiently stored in batteries and/or ultra-capacitors. In general, the design of an intelligent control strategy for coordinated power distribution is a critical issue for ultra-capacitor supported PHEV energy storage systems. Implementation of several control methods have been presented in related literature, with the goal of improving battery life and overall vehicle efficiency. The control objectives vary with respect to vehicle velocity, power demand, and state-of-charge of both the batteries and ultra-capacitors. Hence, an optimal control strategy design is a critical aspect of an all-electric/plug-in hybrid electric vehicle operational characteristic.

This thesis deals with the detailed analysis and novel hybrid controller design for bidirectional energy management solutions, using smart power electronic DC/DC converter solutions. More specifically, an intelligently designed novel digital control technique is presented for a 4-quadrant switched-capacitor *Luo* (4Q SC *Luo*) DC/DC converter. Features of voltage step-down, step-up, and bi-directional power flow are integrated into a single circuit. The novel control strategy enables simpler dynamics, compared to a standard buck converter with input filter, superior regulation capability, lower source current ripple, ease of control, and continuous input current waveform in buck and boost modes of operation. Furthermore, the proposed novel control strategy depicts high converter power density, high efficiency, and simple structure.

ACKNOWLEDGEMENTS

The author would like to express her sincere gratitude to her research supervisor, Prof. Sheldon Williamson for his extremely useful guidance, advice, friendship, willingness to teach, and financial support throughout this study period.

The author would like to thank her colleagues in the Power Electronics and Energy Research Group, at the P. D. Ziogas Power Electronics Laboratory, for their helpful discussions and suggestions. In particular, the author would like to express her sincere gratitude towards Prof. Pragasen Pillay, Prof. Shahin Hashtrudi Zad, and Prof. Ashutosh Bagchi for their valuable suggestions and comments.

Last, but not least, the author is very grateful towards her husband and parents, for their encouragement and support, which made it possible to complete this study.

To my husband and my parents

TABLE OF CONTENTS

LIST OF FIGURES

LIST OF TABLES

LIST OF ABBREVIATIONS

UC	Ultra-Capacitor
EV	Electric Vehicle
HEV	Hybrid Electric Vehicle
PHEV	Plug-In Hybrid Electric Vehicle
HESS	Hybrid Energy Storage System
ADVISOR	Advanced Vehicle Simulator
SUV	Sport Utility Vehicle
ICE	Internal Combustion Engine
SCC	Switched Capacitor Converter
SC *Luo*	Switched Capacitor *Luo*
4- Q	4- Quadrant
RFC	Regenerative Fuel Cell
FCV	Fuel Cell Vehicle
HV	High Voltage
LV	Low Voltage
SOC	State of Charge
IC	Integrated Circuit
DSP	Digital Signal Processor
Ah	Ampere Hour
HP	Hours Power
PMDC	Permanent Magnet DC Machine

PCB	Printed Circuit Board
ADC	Analog to Digital Converter
DAC	Digital to Analog Converter
I.B	Interface Board
Li-ion poly	Lithium-Ion Polymer
Op-Amp	Operational Amplifier

LIST OF SYMBOLS

I_a	Armature Current
I_F	Field Current
Te	Electrical Torque
ω_m	Speed of DC Machine
T	Switching Period
$\bar{I}$	Average Current
S	Switch
D	Diode
C	Capacitor
V_C	Capacitor Voltage
I_C	Capacitor Current
V_{UC}	Ultra-Capacitor Voltage
$V_{battery}$	Battery Voltage
V_m	Motor Voltage
r_S	Parasitic Resistance of Switch
r_C	Capacitor Equivalent Resistance
V_D	Voltage Drop of Diode
KT	State-On Period
(1- K)T	State-Off Period
P_I	Input Power
P_O	Output Power

I_I	Input Current
I_O	Output Current
η	Transfer Efficiency
f	Frequency
ΔV_C	Variation of Capacitor Voltage
K	Conduction Duty (Duty Cycle)
V_{GS}	Gate- to- Source Voltage
kW/kg	kilowatt per Kilogram
Wh/Kg	Watt Hours per Kilogram
T_L	Load Torque
P_L	Load Power
V_a	Armature Voltage

PUBLICATIONS

ACCEPTED JOURNAL PAPERS

[1] **Z. Amjadi** and S. S. Williamson, "Modeling, simulation, and control of an advanced *Luo* converter for plug-in hybrid electric vehicle energy storage system," *IEEE Transactions on Vehicular Technology*, vol. 60, no. 1, pp. 64-75, Oct. 2010.

[2] **Z. Amjadi** and S. S. Williamson, "Design and control of a *Luo* converter for variably loaded hybrid electric vehicle energy storage system," (accepted, under press) *International Journal of Power Electronics*, March 2010.

[3] **Z. Amjadi** and S. S. Williamson, "A novel control technique for a switched capacitor converter based hybrid electric vehicle energy storage system," *IEEE Transactions on Industrial Electronics*, vol. 57, no. 3, pp. 926-934, Feb. 2010.

[4] **Z. Amjadi** and S. S. Williamson, "Power-electronics-based solutions for plug-in hybrid electric vehicle energy storage and management systems," *IEEE Transactions on Industrial Electronics*, vol. 57, no. 2, pp. 608-616, Feb. 2010.

[5] **Z. Amjadi** and S. S. Williamson, "Advanced digital control for a switched capacitor and interleaved switched capacitor hybrid electric vehicle energy management system," (accepted, under press) *Journal of Electrical Engineering and Technology*, Feb. 2010.

SUBMITTED JOURNAL PAPERS

[1] **Z. Amjadi** and S. S. Williamson, "Novel Digital Control of a Bidirectional DC/DC Switched Capacitor Converter for Hybrid Electric Vehicle Energy Storage System Applications," (submitted, under review) *IEEE Transactions on Power Electronics,* Jan. 2011.

[2] **Z. Amjadi** and S. S. Williamson, "Prototype Design and Controller Implementation for a Battery-Ultracapacitor Hybrid Electric Vehicle Energy Storage System," (submitted, under review) *IEEE Transactions on Smart Grid*, Jan. 2011.

[3] **Z. Amjadi** and S. S. Williamson, "Design and Verification of a Novel Hybrid Electric Vehicle Battery-Ultracapacitor Power Electronic Energy Management System," (submitted, under review) *IEEE Transactions on Industrial Electronics,* Nov. 2010.

[4] **(Invited) Z. Amjadi** and S. S. Williamson, "Suitability of switched capacitor converters for hybrid electric vehicle energy management systems," (submitted, under review) *IEEE Power Electronics Society Magazine,* Oct. 2010.

ACCEPTED CONFERENCE PAPERS

[1] **Z. Amjadi** and S. S. Williamson, "Efficiency Modeling and Comparison of Switched Capacitor, *Luo*, and Interleaved Switched Capacitor Converters for Electric Vehicle Energy Storage Systems," in Proc. *Annual Conf. of the IEEE Industrial Electronics Society*, Phoenix, AZ, Nov. 2010, pp. 1811-1817.

[2] **Z. Amjadi** and S. S. Williamson, "On the suitability of interleaved switched capacitor converter as an interface for electric vehicle dual energy storage system," in Proc. *World Energy Congress*, Montreal, Canada, Sept. 2010.

[3] **Z. Amjadi** and S. S. Williamson, "Performance comparison and efficiency modeling of a *Luo* converter and 2-quadrant switched capacitor converter for HEV energy management," in Proc. *IEEE Vehicle Power and Propulsion Conf.*, Lille, France, Sept. 2010.

[4] **(Invited) Z. Amjadi** and S. S. Williamson, "Comparative analysis between a 2-quadrant DC/DC converter and a *Luo* converter for a battery/ultracapacitor HEV energy storage system," in Proc. *IEEE Vehicle Power and Propulsion Conf.*, Lille, France, Sept. 2010.

[5] **Z. Amjadi** and S. S. Williamson, "Novel controller design for a *luo* converter electric vehicle energy management system," in Proc. *IEEE Canada Electrical Power and Energy Conf.*, Halifax, Nova Scotia, Aug. 2010, pp. 1-6.

[6] **Z. Amjadi** and S. S. Williamson, "Design and implementation of a bidirectional HEV energy management strategy using a switched capacitor *Luo* converter," in Proc. *IEEE Canadian Conf. on Electrical and Computer Engineering*, Calgary, Alberta, May 2010, pp. 1-5.

[7] **Z. Amjadi** and S. S. Williamson, "Efficiency modeling and analysis of a switched capacitor converter for a plug-in hybrid electric vehicle energy storage system," in Proc. *35th Annual Conf. of the IEEE Industrial Electronics Society*, Porto, Portugal, Nov. 2009, pp. 3723-3728.

[8] **Z. Amjadi** and S. S. Williamson, "Review of alternate energy storage systems for hybrid electric vehicles," in *Proc. IEEE Canada Electrical Power and Energy Conf.*, Montreal, QC, Oct. 2009, pp. 1 – 7.

[9] **(Invited) Z. Amjadi** and S. S. Williamson, "Dynamic analysis of a bi-directional switched capacitor DC/DC converter for fuel cell vehicle energy storage," in *Proc. IEEE Vehicle Power and Propulsion Conf.*, Dearborn, MI, Sept. 2009, pp. 1 – 7.

[10] **Z. Amjadi** and S. S. Williamson, "Novel control strategy design for multiple hybrid electric vehicle energy storage systems," in *Proc. IEEE Applied Power Electronics Conf. and Expo.*, Washington, DC, Feb. 2009, pp. 597 – 602.

CHAPTER 1

INTRODUCTION

With the reduction of fossil fuel and increasing fuel costs, the introduction of new transportation technologies has attracted much attention. These technologies consist of electric vehicles (EV), hybrid electric vehicles (HEV), plug-in hybrid electric vehicles (PHEV), and fuel cell vehicles (FCV). A hybrid electric vehicle (HEV) is one which combines a conventional internal combustion engine (ICE) system with an electric propulsion system. A PHEV is similar to an HEV from the drivetrain point of view, except that it has a larger on-board battery pack, which can be charged from an external electricity source. The electric traction motor either assists the ICE (in parallel HEVs) or is the only mechanical link to the wheels (in series HEVs). The feature of external battery charging poses the advantage of allowing the vehicle to run for some distance without use of the ICE, thus reducing the use of fuel. EVs and PHEVs save energy due to the employment of regenerative braking during the deceleration cycle. This recuperated energy can be proficiently stored in batteries and/or ultra-capacitors [1], [2].

1.1. BATTERY AND ULTRA-CAPACITOR CHARACTERISTICS

An electric vehicle (EV) battery is able to store large amounts of energy (in the order of 1kW/kg; 100Wh/kg). However, it is not suitable for supplying a large amount of power in a very short time, due to low power output density. An increase in efficiency of energy source can be achieved by using a smaller battery, with a lower peak output power. The lead acid, alkaline, and lithium-ion batteries are generally used for portable

utilities and industry applications. As for the lithium-ion battery, it has the advantage of high working cell voltage, low environmental population, low self-discharge rate, and high power density in volume as well as high specific energy and energy density. Therefore that voltage in a single battery cell is inherently low. Series-connected lithium-ion battery packs are usually employed for EVs, hybrid electric vehicles (HEVs), and plug-in hybrid electric vehicles (PHEVs). [3]-[7].

A UC has low storage capacity, but possesses the ability to supply a large burst of power (in the order of 10kW/kg; 1Wh/kg) and short charge/discharge time. Due to the low voltage of a single UC cell, which is typically 2.5-3.0 V in a fully charged state; series connected UC strings with the bus voltage in the range of 300V-400V is necessary for high voltage applications such as EV, HEV and PHEV [8], [9].

The battery is used to supply a large amount of power at light loads, thereby increasing the total efficiency, whereas the UC bank is used for satisfying EV/HEV acceleration and regenerative braking requirements. Such a scenario also helps improve the on-board battery life time. The combination of battery and UC results in reduced size and weight of the overall energy storage system. Together, an UC and battery can combine to meet the storage and peak current characteristics. This is achieved by connecting 2 energy sources in a parallel configuration [3]-[5].

1.2. HYBRID ELECTRIC DRIVETRAIN ARCHITECTURES

Primarily, three HEV drive train configurations exist, namely; series, parallel, and series-parallel configurations. Due to the varying sizes of the drive trains and the availability of space on the vehicle; parallel and series-parallel hybrid drive trains are used in smaller passenger vehicles, while the series configuration is deemed suitable for

larger vehicles [10]-[22]. Each configuration will be discussed in detail in the following sections.

1.2.1. SERIES HYBRID ELECTRIC DRIVETRAINS

A series hybrid electric drive train is consisted of 2 power sources feed a single electric motor. The unidirectional energy source is a fuel tank and unidirectional energy converter is an ICE coupled to a generator. Also, output of generator is connected to a DC/DC bidirectional converter.

The bidirectional energy source is an electrochemical battery bank, connected to DC/DC converter. Therefore, drive train needs to battery charger to charge of battery cells. The DC/DC bidirectional converter is connected to controller of electric motor and electric traction motor can be controlled as a motor or generator in a forward or reverse mode.

Main advantage of series configuration is that ICE output power is buffered by the battery bank, which allow ICE operate at steady state in its most efficient mode to provide minimum fuel consumption and low emissions. An example of series HEV is *Chevrolet Volt* with plug-in option. Fig. 1-1 is depicted a series hybrid electric drive train.

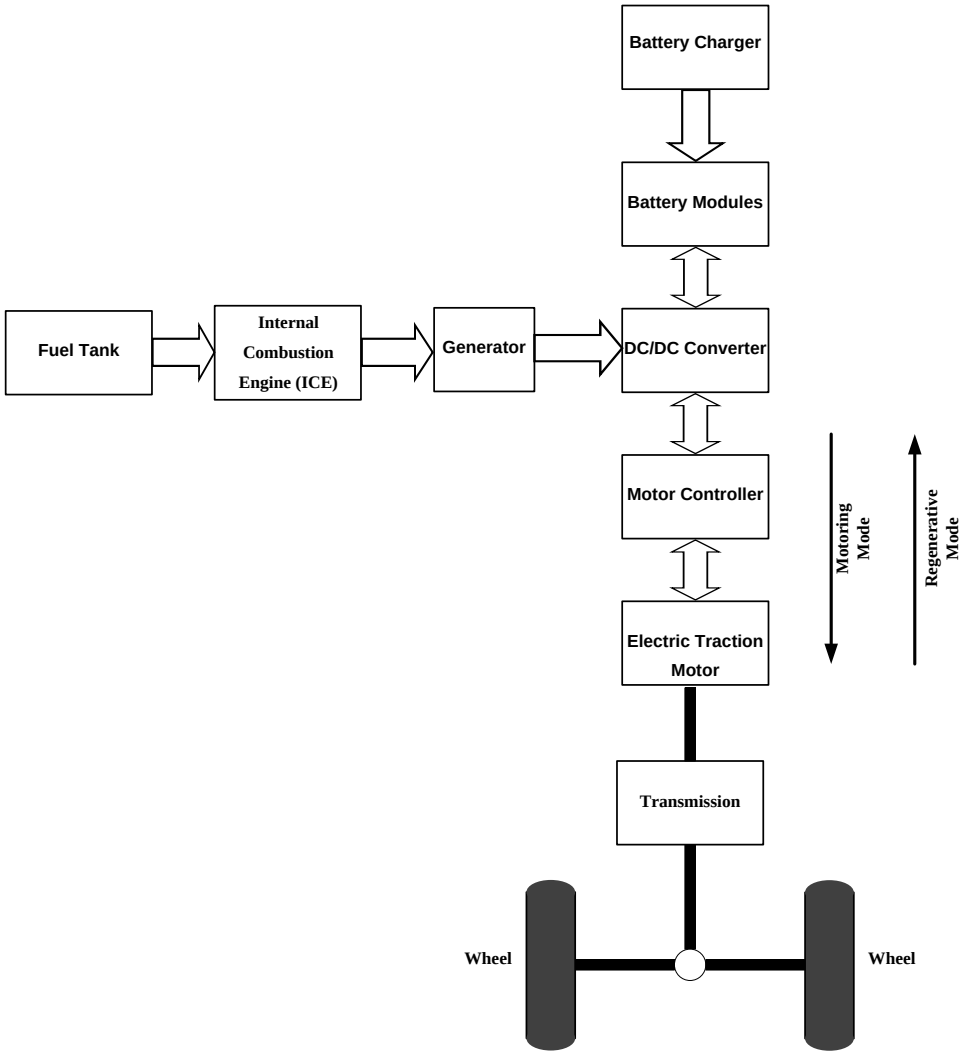

Fig. 1-1. Series hybrid electric drive train.

The battery cells can be replaced by other hybrid energy sources such as UC's or flywheels [23].

1.2.2. PARALLEL HYBRID ELECTRIC DRIVETRAINS

A parallel hybrid electric drive train is configuration with 2 power paths; also that ICE or electric population system or both can be used to produce the power to turn the wheels. The engine is used for high way driving and electric traction motor provides added power during hill climbs, acceleration and other periods of high demand.

Main advantage of parallel configuration is in term of transfer efficiency in compared to series hybrid electric drive trains, because ICE power need not convert to electrical energy before being delivered to the wheels. In this technique, electric traction motor can be used as a generator for charge of the battery cells during regenerative brake or absorb power from engine when its output power is greater than that required to drive the wheels [23]. Examples of Parallel HEVs include the *Honda Insight*, *Honda Civic*, and *Honda Accord*. Fig. 1-2 is shown a parallel hybrid electric drive train.

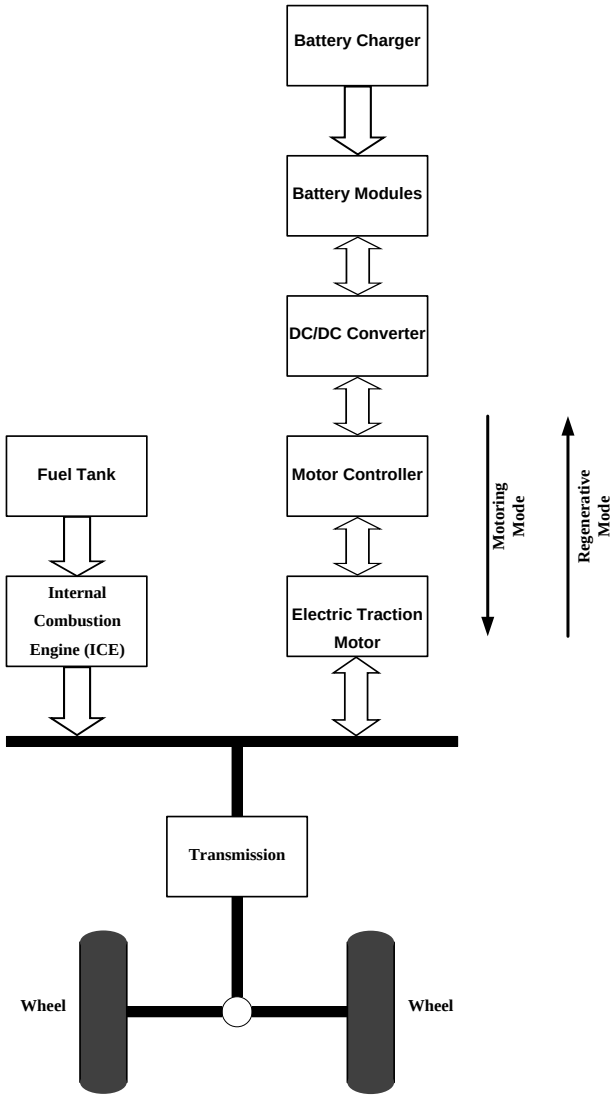

Fig. 1-2. Parallel hybrid electric drive train.

1.2.3. SERIES-PARALLEL HYBRID ELECTRIC DRIVETRAINS

The series-parallel hybrid electric drive train is combined series and parallel configurations. But this technique involves an additional mechanical link as compared with series hybrid vehicle and also, an additional generator as compared with parallel hybrid vehicle [23]. An example of a series-parallel HEV is the popular *Toyota Prius*. Fig. 1-3 is shown a series- parallel hybrid electric drive train.

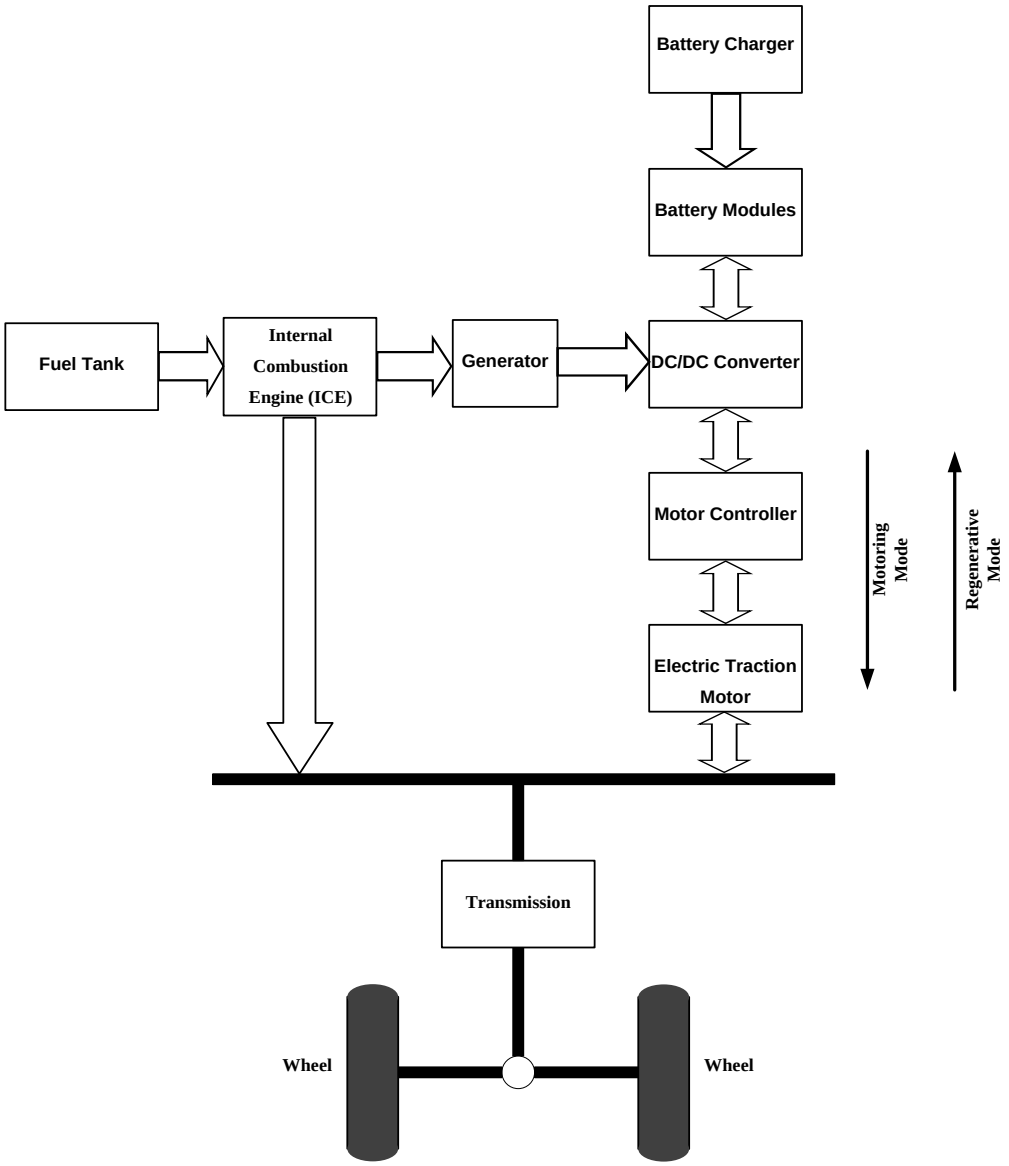

Fig. 1-3. Series- parallel hybrid electric drive train.

A combination of UC and battery results in a hybrid energy storage system (HESS). This configuration can be either passively or actively connected. An actively connected configuration requires power electronic components, which drive their costs upwards. The actively connected HESS regulates transfer of energy to and from each component as well as the system, through a controllable power electronics buffer, between the battery cells and the UC bank. The advantage of a HESS is that the overall mass of the system can be potentially smaller than that of a passive configuration for the same load [10]-[22]. A parallel connection of battery and UC for an all-electric vehicle results in a simple configuration, as shown in Fig. 1-4.

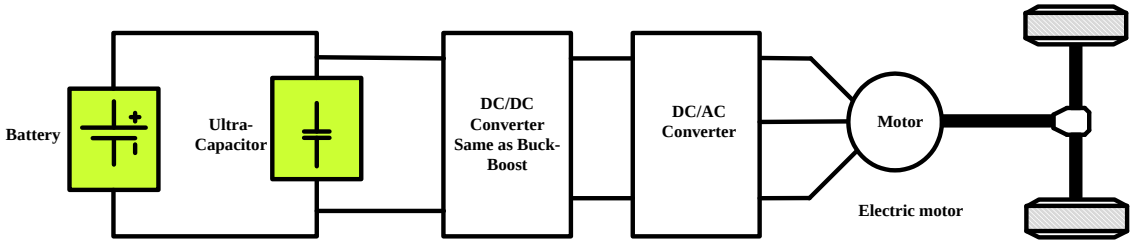

Fig. 1-4. Parallel connection of battery and UC for an all-electric vehicle.

The arrangement for a typical 3-way PHEV ESS consists of a regenerative fuel cell (RFC), a UC bank, and a battery unit system. The RFC generator acts as the main energy source. However, it has a poor efficiency at light loads, thus relying on the battery pack, for light-load energy requirements. A bi-directional step-up/step-down DC/DC converter, as shown in Fig. 1-5, connects each power source to the DC link.

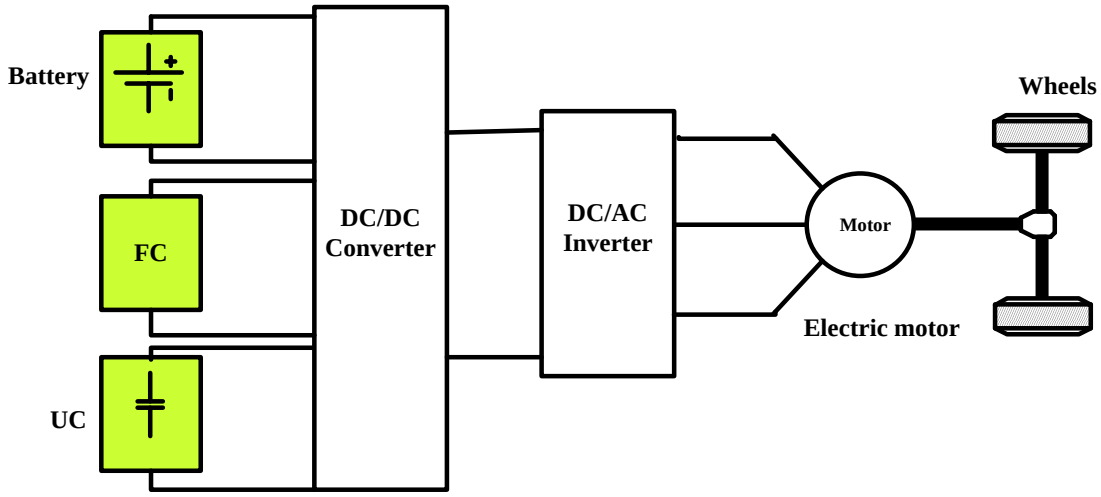

Fig. 1-5. Typical 3-way hybrid energy storage system.

As aforementioned, for transferring energy from each source to the DC link, a step-up mode of operation is used, while for charging both the UC bank and the battery storage system, as well as recovering braking energy, the step-down operation is used [11]-[13]. In this research study, Li-ion battery cells are used, the model of which includes a voltage source and an internal resistance (R_{bat}), which characterizes the system accurately. Also, UC is modeled by an internal resistance (R_{eq}) and an equivalent capacitance (C_{eq}) [24]. The UC and battery models used are shown in Fig. 1-6.

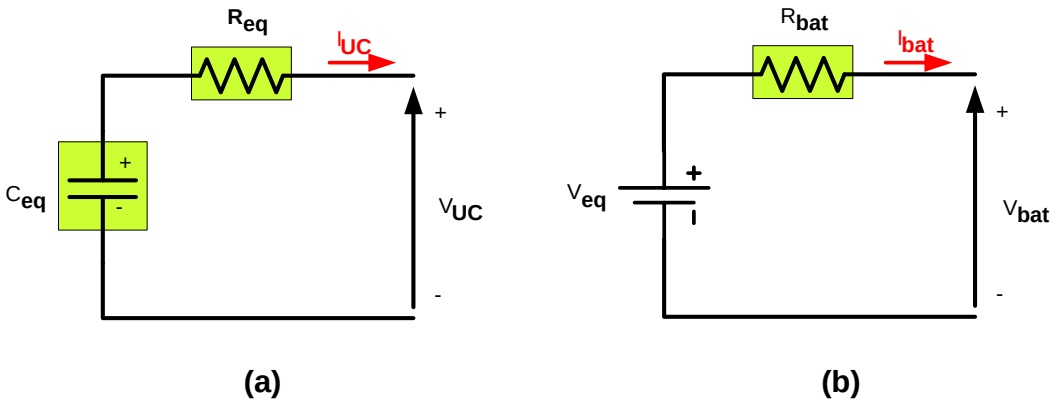

Fig. 1-6. (a) Ultra-capacitor model, (b) Battery model.

1.3. GOALS AND OBJECTIVES OF THE DISSERTATION

This dissertation deals with the design of a smart novel control technique for bidirectional power electronic energy management systems for EV/PHEV energy storage systems. More specifically, the digital control technique is proposed for the popular 4Q switched-capacitor (SC) DC/DC converter as well as the *Luo* DC/DC converter. The main advantage of using SCCs for EV/PHEV energy management is the absence of transformers and inductors, which makes the complete integration of switching converters possible. In addition, switches are controlled by capacitors, which are charged and discharged through different paths, and transfer their stored energy to either the high voltage (HV) battery side, or the low voltage (LV) ultra-capacitor side. Furthermore, an SCC enables good regulation capability, low electromagnetic interference (EMI), lower source current ripple, ease of control, and continuous input current waveform, in both buck and boost modes of operation, which are critical aspects when dealing with sensitive current applications, such as an EV battery or UC system. For the boost mode, the voltage lift technique presents an excellent method to practically implement the proposed control strategy. Hence, by using a suitable combination of the SCC and voltage lift technique, a new converter with high voltage gain, high power density, high efficiency, low EMI, ease of control, and small size can be easily constructed.

1.4. SUMMARY

This chapter provided an introduction to the concept of multiple-input DC/DC power converters, devoted to combine power flows of multiple energy sources of on-board EV/PHEV energy storage systems. A hybrid arrangement, with a parallel combination of batteries and UCs, can significantly reduce the volume and weight of the overall EV

energy storage system. Furthermore, overall battery life can be significantly improved, due to the decrease in the output current. An electric vehicle (EV) battery is able to store large amounts of energy. However, it is not suitable for supplying a large amount of power in a very short time, due to low power output density. A UC has low storage capacity, but possesses the ability to supply a large burst of power and short charge/discharge time.

CHAPTER 2

THEORETICAL BACKGROUND

2.1. 2-Q ENERGY SHARING CONVERTER ALGORITHM

A two-quadrant (2-Q) chopper has the ability to operate in two quadrants of *(v-i)* plane. Therefore, input and output voltages are positive; yet, input and output currents can be positive or negative. Therefore, these converters are also named current reversible choppers. In fact, a 2-Q DC/DC converter is combination of two basic chopper circuits; a step-down chopper (buck mode operation) and a step-up chopper (boost mode operation). Typically in EV/HEV application, the high voltage (HV) side consists of battery modules and the low voltage (LV) side includes of UC modules. Fig. 2-1 shows the 2- Q operation of a half bridge chopper.

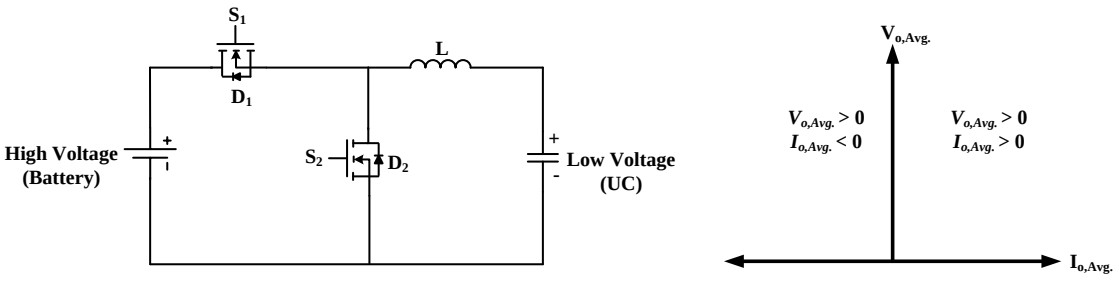

Fig. 2-1. 2- Q bi-directional DC/DC converter.

During the buck mode, switch S_1 is on and D_2 starts conducting; HV side transfers its energy to LV side. During boost mode, switch S_2 is on and D_1 starts conducting. Also, during this interval, LV side supplies its power to HV side. Reversible current choppers can transfer from operating in the power mode to operating in the regenerative mode

smoothly, by changing only the control signals for S_1 and S_2. Fig. 2-2 shows both modes of operation (buck and boost). Fig. 2-3 depicts output current of a 2-Q chopper.

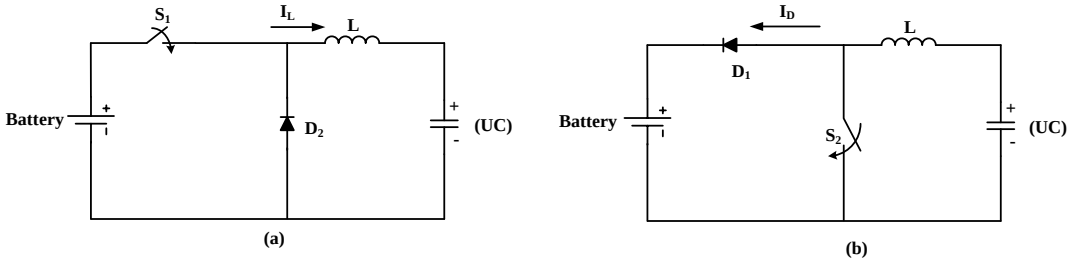

Fig. 2-2. (a) Buck mode operation, (b) Boost mode operation.

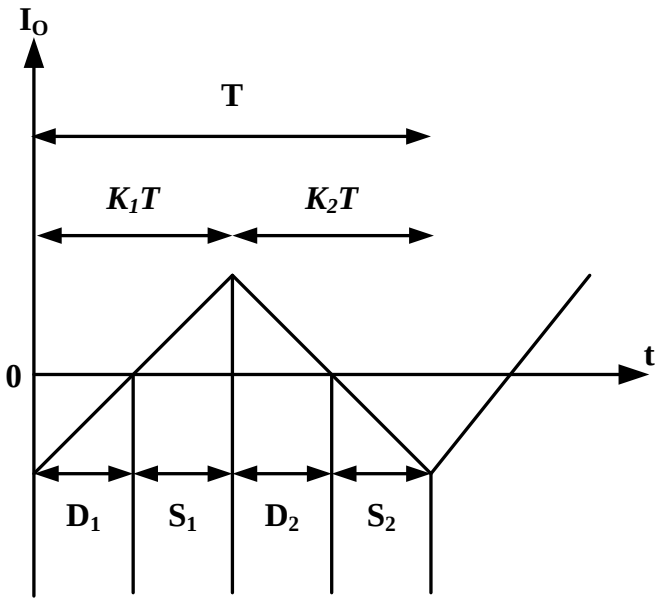

Fig. 2-3. Output current of a 2-Q chopper.

By changing duty cycles of the two switches, K_1 and K_2, not only the amplitude of the average of the output current changes, but also, it can be positive or negative, leading to 2-Q operation [23].

2.2. 2-Q SWITCHED CAPACITOR CONVERTER

2.2.1. CHARGING AND DISCHARGING PROCESS OF THE 2-Q SWITCHED CAPACITOR CONVERTER

A switched capacitor converter (SCC) is simply a combination of switches and capacitors. The different combinations of capacitors and switches result in SCC topologies producing an output voltage that may be higher (boost mode) or lower (buck mode) than the input voltage, in addition to providing polarity reversal. The switches are controlled by a capacitor, *C*, which is charged and discharged through different paths, and transfers its stored energy to HV side or LV side. In addition, the output voltage is proportional to the input voltage. SC bidirectional converters, with their large voltage conversion ratio, possess the potential to be one of the possible solutions for achieving high-efficiency conversion. At the same time, they possess the ability to realize step up/down of voltage [22]. Fig. 2-4 shows a type of SCC that operates in 2 operating modes (buck and boost mode).

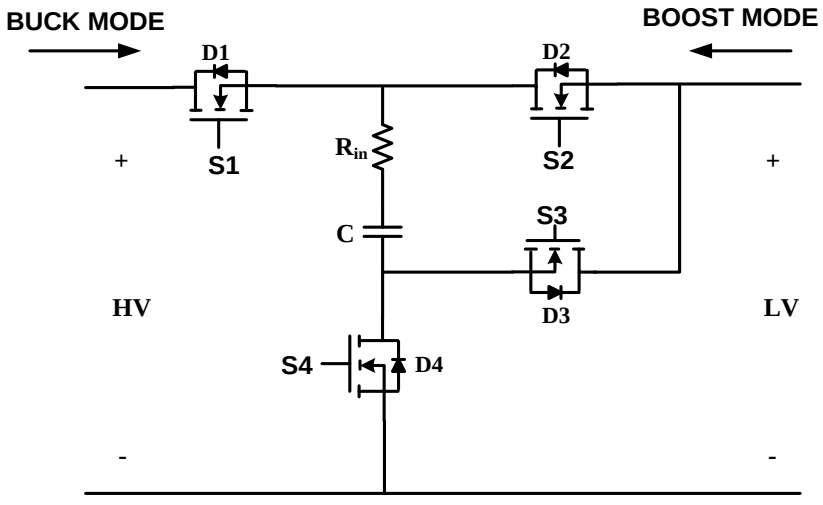

Fig. 2-4. A type of switched capacitor converter.

The typical bidirectional SCC is composed of 4 switches, 4 diodes, and 1 capacitor C. For an HEV application, HV side typically consists of battery modules and LV side could consist of UC modules [25], [26]. In this circuit, the high voltage DC is set at 48V and low voltage side is set at 27 V. There exist 2 modes of operation; mode A (buck mode), where electrical energy is transferred from HV side to LV side, and mode B (boost mode), where electrical energy is transferred from LV side to HV side.

Each mode has 2 states: on and off. Usually, each state is governed by its specific duty ratio, *k*. It is worthwhile mentioning here that there exist some serious control issues related to SCCs. When the circuit works in the generating mode ($P \leq 0$), the capacitor voltage should be compared with battery voltage. In addition, it is critical to observe as to which energy source demands power. If the on-board battery modules need energy and capacitor voltage is less than battery voltage, then as the first step, the battery pack is charged by the load and after that, it charges capacitor *C*. It must be noted that if capacitor voltage is greater than battery voltage, only battery is charged by the load. When UC modules need power, and capacitor voltage is greater than battery voltage, then capacitor *C* transfers its stored energy to the UC modules. If the capacitor voltage is less than the battery voltage, and the battery modules do not need energy, and are fully charged, they can deliver energy to capacitor *C*. Alternatively, when capacitor *C* is charged, it transfers its stored energy to the UC modules. At the same time, if the battery modules are not fully charged, the battery modules get charged by the load. Thereafter, the battery modules charge capacitor *C*.

When the circuit works in the motoring mode ($P \geq 0$), the capacitor voltage is compared with the UC voltage. Close attention is paid as to which energy source should transfer

energy to the load. When the UC modules transfer power to the load, and the UC bank voltage is greater than the voltage of capacitor *C*, they charge capacitor *C*. Thereafter, capacitor *C* transfers its stored energy to the load. At the same time, if capacitor voltage is greater than UC voltage, it directly transfers its stored energy to the load. When the battery modules deliver their energy to the load, it should be established that battery modules are fully charged, after which they can directly transfer their energy to the load. If the battery modules are not fully charged, and if the capacitor voltage is less than UC voltage, then during the first step, UC modules charge capacitor C, followed by capacitor *C* transferring its stored energy to the battery modules. Furthermore, when the battery modules are charged, they deliver their energy to the load. In this state, if the capacitor voltage is greater than UC voltage, capacitor *C* is discharged. Thus, the battery modules are charged by capacitor *C*, followed by the battery modules transferring their energy to the load [27]-[30].

2.2.2. SCC OPERATING CHARACTERISTICS AND MODES

This type converter operates in 2 modes (buck and boost operation). In buck operating mode, S_1 and S_4 are the operating switches, and capacitor C is charged by HV side. After this operating stage, S_2 and D_4 are the operating switches and capacitor C is disconnected from HV and transfers its stored energy to the LV side. The system schematic is shown in Fig. 2-5.

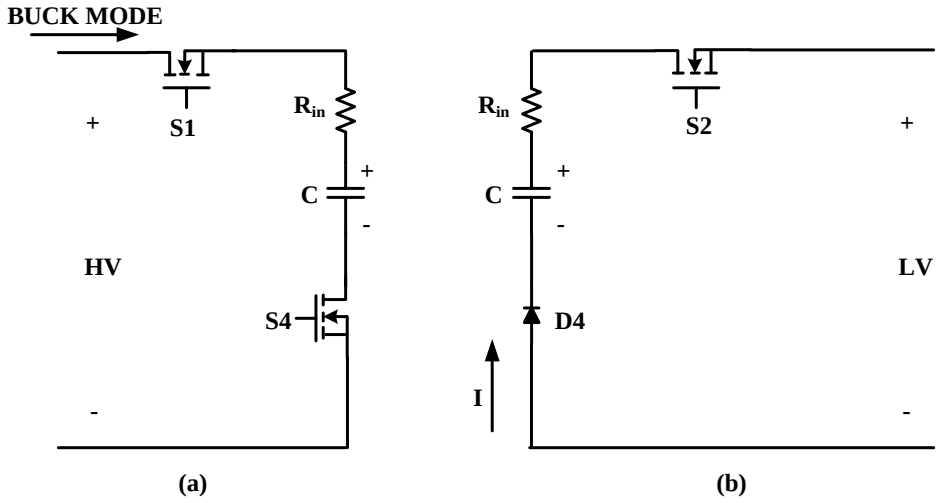

Fig. 2-5. Buck operating mode (a) capacitor *C* is charged and is connected to HV, (b) capacitor *C* discharges and is disconnected from HV.

In boost operating mode, S_4 and D_2 are the operating switches, capacitor C is charged from the LV side, through D_2 and S_4. After this step, S_3 and D_1 are the operating switches and capacitor C is connected in series with the LV side and gets discharged. Thus, capacitor C supplies energy to the HV side. This operation mode is depicted in Fig. 2-6.

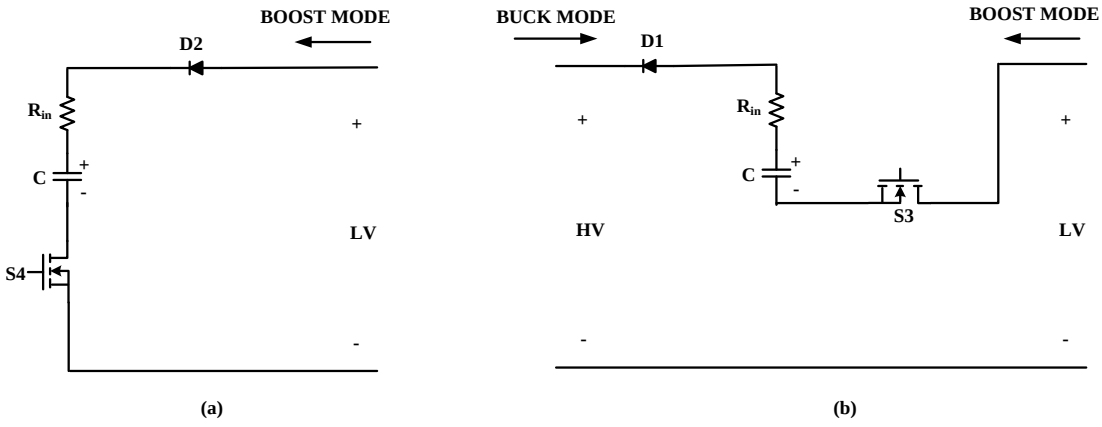

Fig. 2-6. Boost operating mode (a) capacitor C is charged, (b) capacitor C is discharged and is connected in series with the LV side.

2.2.3. CONTROLLER FOR SCC OPERATION

When the circuit operates in the boost mode, the storage systems (UC and battery) supply power to load (motoring mode, P≥0). Conversely, when the circuit operates in the buck mode, load supplies power to the battery and UC modules (generating mode, P≤0). The vehicle model was used from the ADVISOR software (medium sized SUV). A gradient of power on the load side (drive cycle, urban driving mode) is used for the analysis and operation of the converter. The Δ gradient is the mean change or difference between 2 instantaneous power levels on the power profile. In this case, the average power gradient was computed as 3500W, for the chosen city drive cycle. For better understanding of the controller, each operation mode is denoted by a specific code.

When the converter operates in motoring mode, 2 conditions are chosen: If the power gradient on load side is between -3500 and 3500 W; battery modules supply energy to the load, which is denoted by a code number 4. Otherwise, UC modules supply power to load, denoted by codes 2 and 3. During code 4, all of switches are off and only battery connects to load and supplies energy. During code 2, D_2 and S_4 are on and capacitor C charges and in code 3, S_3 and D_1 are on and capacitor C is connected in series with the LV side, after which it discharges and supplies power to the HV side.

Secondly, during motoring mode, capacitor voltage (V_C) is compared with UC voltage. At the same time, close attention is given to the energy source that transfers energy to the load. For this state, $0.8*V_{UC}$ is compared with V_C. When UC modules or LV side transfer power to the load, and $V_C \leq 0.8*V_{UC}$, then they charge capacitor C. Thereafter, capacitor C transfers its stored energy to load. When $V_C > 0.8*V_{UC}$, capacitor C directly transfers its stored energy to the load. When battery modules deliver their

energy to the load, it must be ensured that they are fully charged. Hence, the battery modules can directly transfer their energy to the load. If the battery modules are not fully charged, and $V_C \leq 0.8*V_{UC}$, then during the first step, the UC modules charge capacitor C, followed by capacitor C transferring its stored energy to the battery modules. When the battery modules are charged, they deliver their energy to the load. If in this state, $V_C > 0.8*V_{UC}$, capacitor C is directly discharged and the battery modules are charged by capacitor C. Thereafter, the battery modules transfer their energy to the load.

On the other hand, when the converter operates in generating mode, load supplies energy to the battery (it identifies the state to be under code 4). During this code, all switches are off. When load delivers power to the UC modules, it depicts codes 1 and 5. In this case, battery voltage must be greater than V_C. Hence, V_C is chosen to be less than 0.8*battery voltage so that the battery modules can charge it. If the battery modules need energy, and $V_C \leq 0.8*V_{battery}$, then during the first step, the battery is charged by load and after that, it charges capacitor C. When $V_C > 0.8*V_{battery}$, only battery is charged by load. When UC modules need power, and $V_C > 0.8*V_{battery}$, then capacitor C transfers its stored energy to the UC modules. If $V_C \leq 0.8*V_{battery}$, and battery modules do not need energy (fully charged state), they can deliver energy to capacitor C. When capacitor C is charged, it transfers its stored energy to the UC modules. If the battery modules are not fully charged, then they get charged by the load. Thereafter, the batteries charge capacitor C.

In code 1, S_1 and S_4 are on and capacitor C gets charged. During code 5, D_4 and S_2 are on and capacitor C is disconnected from HV side. During this time, C transfers its stored

energy to LV side. Table 2-1 represents switches and codes-based operation of each mode. Values for the parameters of the equivalent circuit are shown in Table 2-2.

Table 2-1. Switches and codes of operation in each mode.

	Energy storage	CODE	S_1	D_1	S_2	D_2	S_3	S_4	D_4
P>=0	Ultra-capacitor	2	OFF	OFF	OFF	ON	OFF	ON	OFF
		3	OFF	ON	OFF	OFF	ON	OFF	OFF
	Battery	4	OFF	OFF	OFF	OFF	OFF	OFF	OFF
P<0	Ultra-capacitor	1	ON	OFF	OFF	OFF	OFF	ON	OFF
		5	OFF	OFF	ON	OFF	OFF	OFF	ON
	Battery	4	OFF	OFF	OFF	OFF	OFF	OFF	OFF

Table 2-2. Equivalent parameters of battery, UC modules, and capacitor C.

	Nominal Voltage (V)	Internal Resistance (Ohms)	Rated Capacity (Ah)	Initial State-Of-Charge
Battery Modules	48	0.2	6	100
	Capacitor Initial Voltage (V)	Resistance (Ohms)		
Ultra-Capacitor Modules	13.5	0.0001		
	Capacitance (F)	Series Resistance with Capacitor C (Ohms)		
Capacitor C	110 UF	0.004		

The code-based operation is clearly demonstrated by means of a flowchart in Fig. 2-7. As is clear, codes 2 and 3 operate only during motoring mode, because UC modules must deliver power to the load. Also, the power gradient is out of range (-

3500W<gradient<3500W), and hence, $V_C \leq 0.8*V_{UC}$, because the UC bank can charge capacitor C, and then deliver power to load. When code 3 operates, V_C is greater than $0.8*V_{UC}$. Thus, only capacitor C delivers power to load side. In code 4, only battery modules supply energy to the load.

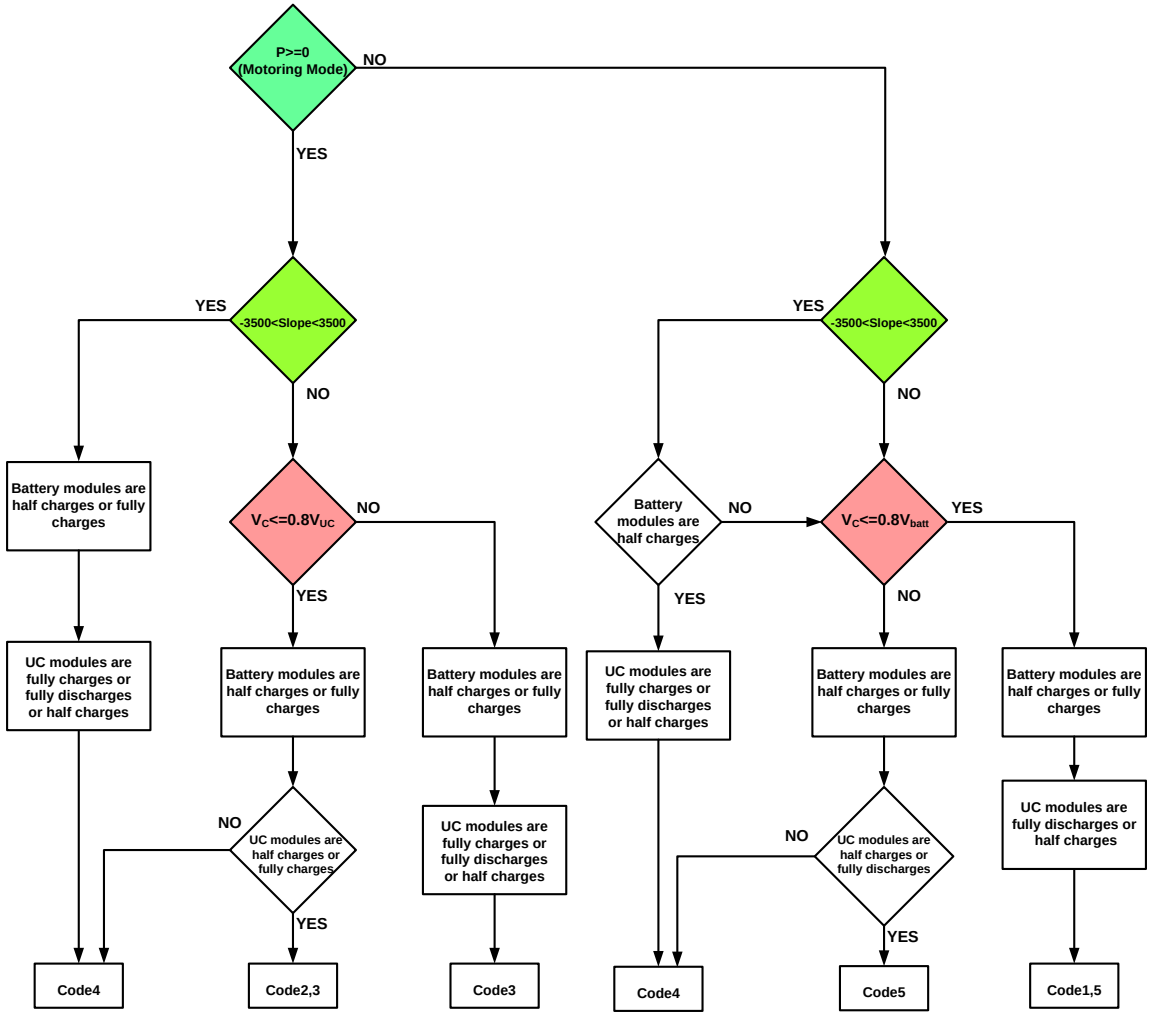

Fig. 2-7. Code operations including charge and discharge routines of UC and battery modules.

During generating mode, codes 1 and 5 operate. Again, this occurs when the power gradient is out of the set range (-3500W<gradient<3500W). UC modules are fully discharged or half-charged and, at the same time $V_C \leq 0.8*V_{battery.}$ Thus, the battery

modules can charge capacitor C. Thereafter, the capacitor C delivers its stored energy to LV side. When code 5 operates, V_C is greater than $0.8*V_{battery}$, and hence, capacitor C transfers energy to the UC side. Thus, when code 4 operates, and when power gradient is between 3500 and -3500 value, and at the same time, when battery modules are half charged or fully discharged, then load feeds back energy to the battery.

2.2.4. SCC MODELING AND SIMULATION RESULTS

This section focuses on the modeling and simulation results and analyzes the overall controller operation. Figs. 2-8 and 2-9 depict power and gradient plots for load side for a portion of the tested drive cycle. When the converter operates in motoring mode, power curve is shown with value = 1, and when it operates in generating mode, it is denoted by value = 0, in Fig. 2-8. Thus, when gradient is between -3500W and 3500W, it is shown with value = 0 (battery supplies energy to the load or load delivers energy to the battery side) and when out of this range, value = 1, in Fig. 2-9. Fig. 2-10 shows the simulation result of capacitor voltage (V_C) during motoring and generating modes.

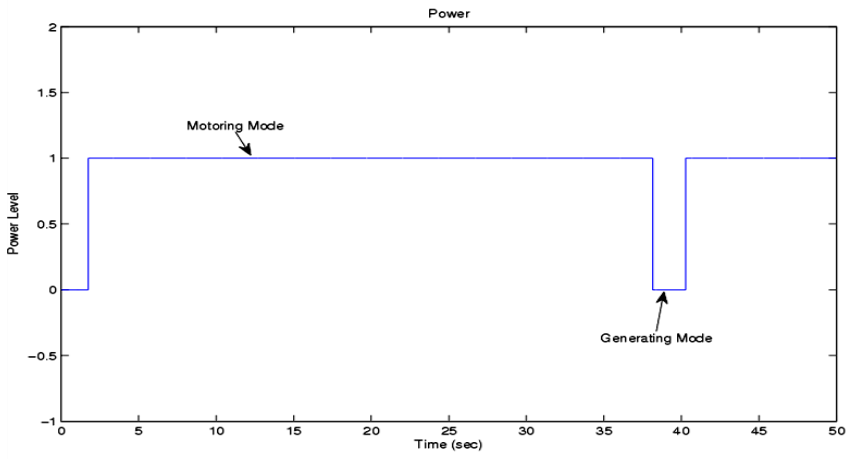

Fig. 2-8. Power status in simulation time.

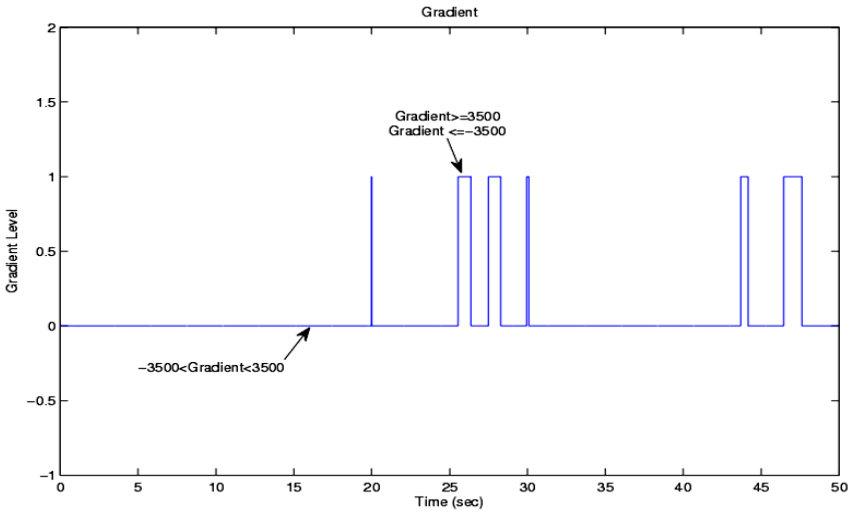

Fig. 2-9. Gradient status in simulation time.

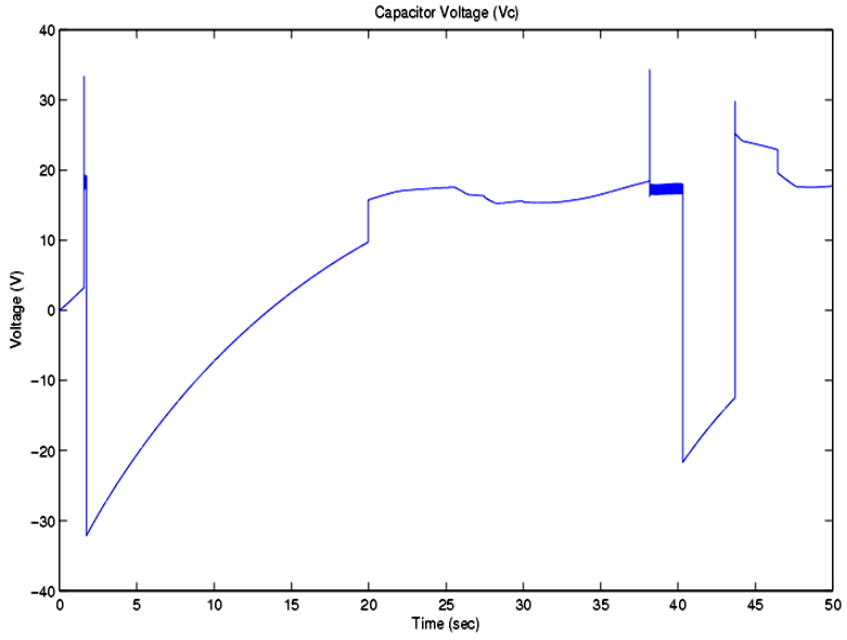

Fig. 2-10. Simulation result of capacitor voltage (V_C).

This represents a just comparison between V_C and $0.8*V_{UC}$ and $0.8*V_{battery}$. When $V_C > 0.8*V_{UC}$, the capacitor voltage enables energy delivery to the load side ($p \geq 0$). This is denoted by value = 0, in Fig. 2-11. When $V_C \leq 0.8*V_{UC}$, UC modules supply power to

HV side (p≥0, with attention given to the status of the UC modules). This is denoted by value = 1, in Fig. 2-11.

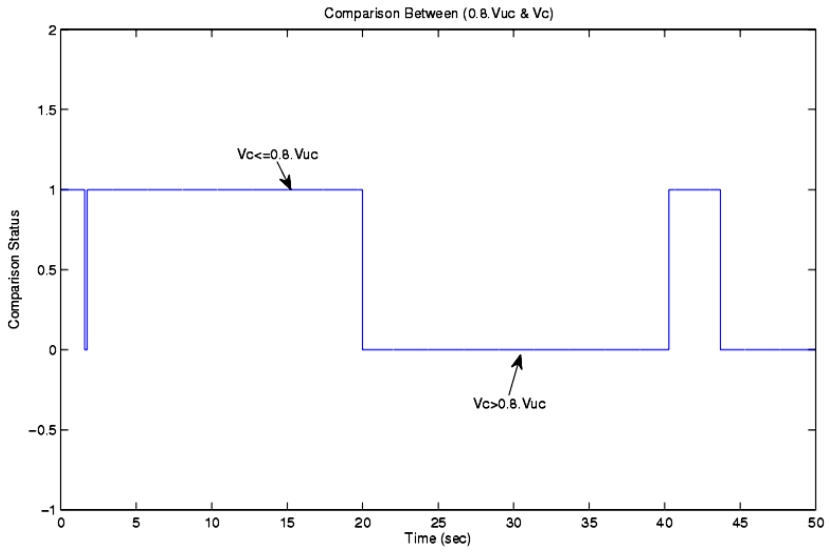

Fig. 2-11. Comparison between 0.8 V_{UC} and V_C.

When $V_C > 0.8*V_{battery}$, capacitor C delivers energy to LV side (p < 0). This is denoted with value = 0. But when $V_C \leq 0.8*V_{battery}$, battery modules supply power to LV side (p<0, with attention given to the state of battery modules). This is denoted by a value = 1, in Fig. 2-12.

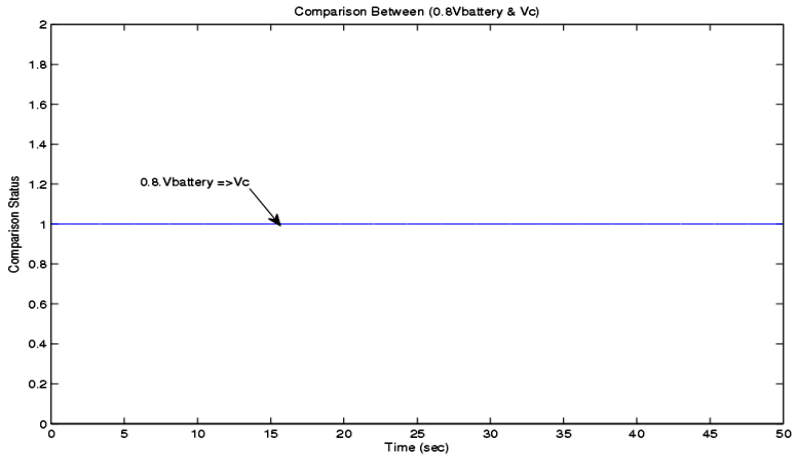

Fig. 2-12. Comparison between $0.8V_{battery}$ and V_C.

Fig. 2-13 shows UC module voltage and current, when it is charged by load or battery modules in generating mode, or when it supplies power to load, in the motoring mode. The UC initial voltage is 13.5V, and the total UC voltage is set at 27 V.

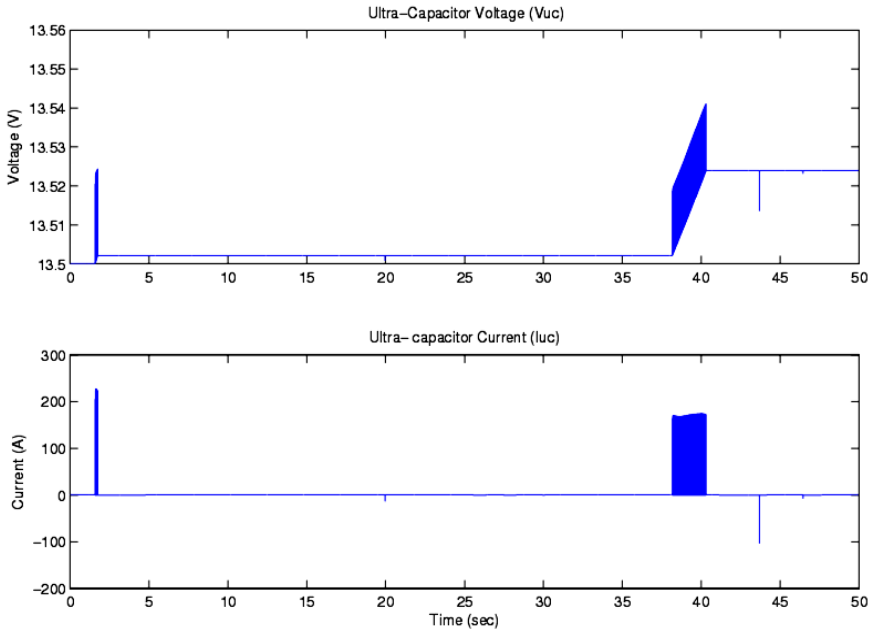

Fig. 2-13. UC modules voltage and current during discharge or charge.

Additional simulation results of load power, state of charge (SOC), current, and voltage of battery are shown in Fig. 2-14. As is clear, current and voltage of battery are proportional with load power, because the battery modules connect directly to load.

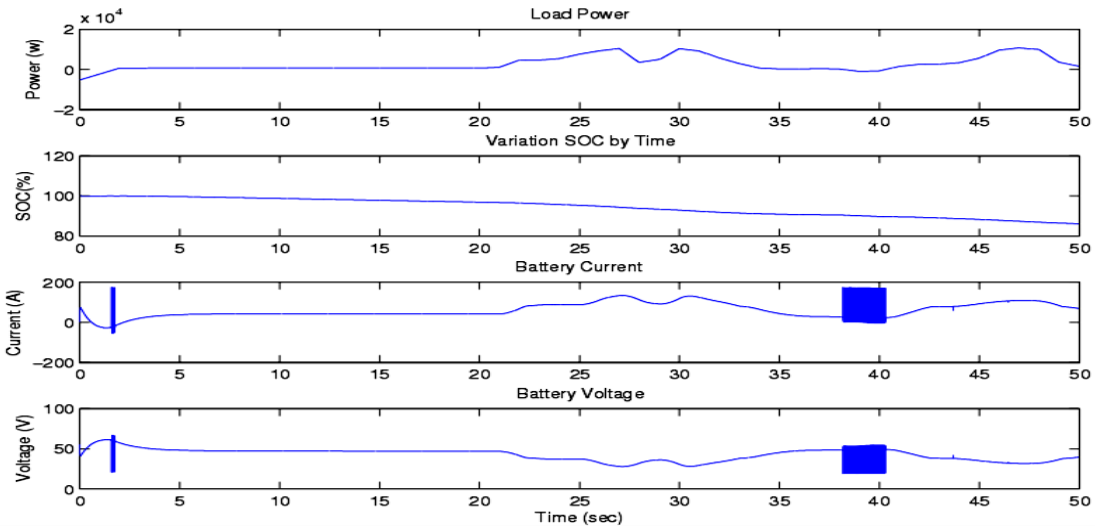

Fig. 2-14. Simulation results of load power, state of charge (SOC), current, and voltage of battery.

According to the above results and flowchart of Fig. 2-7, when capacitor C is charged or discharged, it transfers energy to LV or HV side. In this situation, some switches are on or off. Fig. 2-15 shows capacitor (C) charge and discharge status, with related converter operating codes.

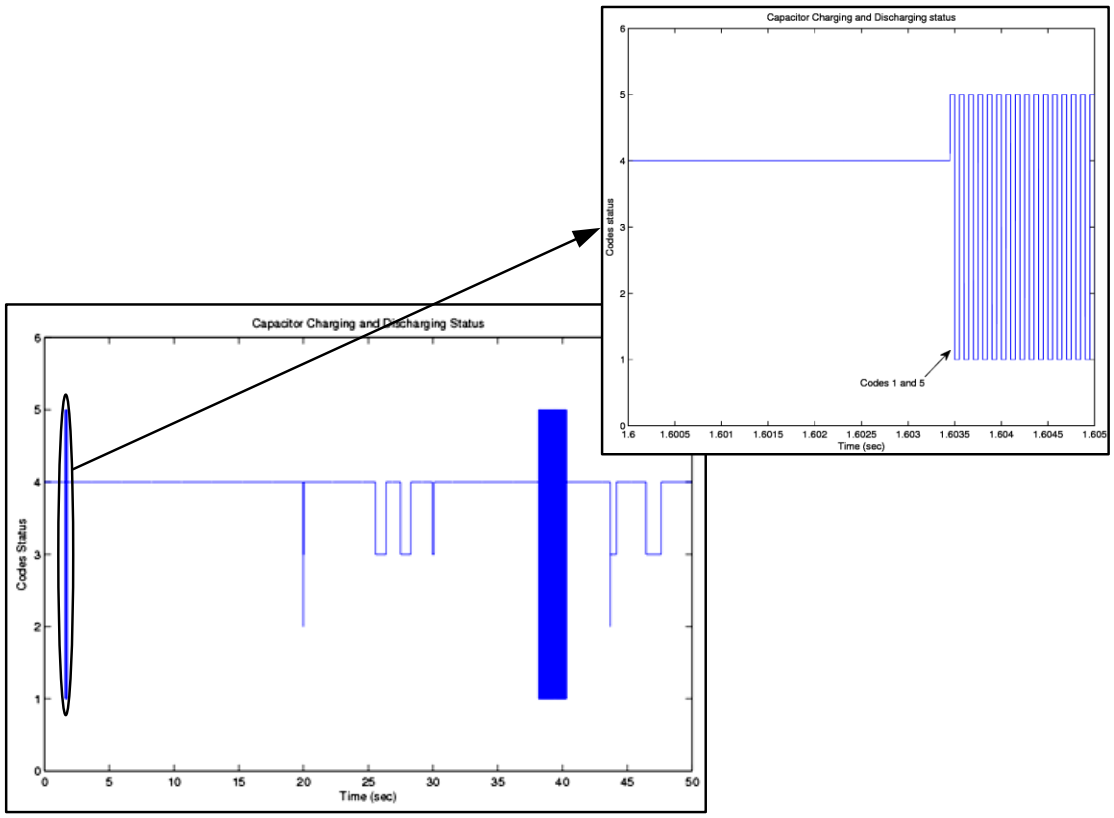

Fig. 2-15. Capacitor charge and discharge status, with codes.

In Fig. 2-15, in the interval between 1.6035s<t<1.7647s, battery modules are fully charged, because SOC depicts 100%, in corresponding battery behavior, shown in Fig. 2-14. Furthermore, the UC modules are half charged, when the power curve is in generating mode (between 0s<t2s). Also, the power gradient curve is shown with value = 0, during this interval, and $V_C \leq 0.8*V_{battery}$. Thus, during this interval, the converter operates with codes 1 and 5, and the battery supplies energy to capacitor C. Thereafter, when C is charged, it transfers its stored energy to the UC modules. When the power curve is in motoring mode, the gradient curve is shown with value = 1, and $V_C \leq 0.8*V_{UC}$. The code status is depicted by 2 and 3 (UC modules supply power to load side). During this interval, when $V_C > 0.8*V_{UC}$, the code status is denoted by 3 (capacitor C directly

supplies power to load side). When the load power curve is in motoring mode, battery and UC modules are half charged, and the gradient curve is shown with value = 0. This means that the battery modules must deliver their energy to load, denoted by code 4. Alternatively, when the power curve is in generating mode, the gradient is shown with value = 0 and the converter operation is denoted by code 4. This indicates that load supplies energy to the battery modules.

Operation of each switch is shown in Fig. 2-16. For example, when converter is operating under code 4, all switches are off and only battery connects to load. Also, when converter is operating under code 1, S_1 and S_4 are on, and capacitor C is charged by HV side. Under code 5, S_2 and D_4 are on, capacitor C is disconnected from HV side, and it transfers its stored energy to LV side. Conversely, when the converter is operating under code 2, D_2 and S_4 are on and capacitor C is charged by LV side. Under code 3 operation, S_3 and D_1 are on and capacitor C is connected in series with the LV side. Thus, capacitor C discharges, and supplies its energy to the HV side.

From the propulsion system point of view, the simulation results of the tested separately excited DC machine are shown in Fig. 2-17.

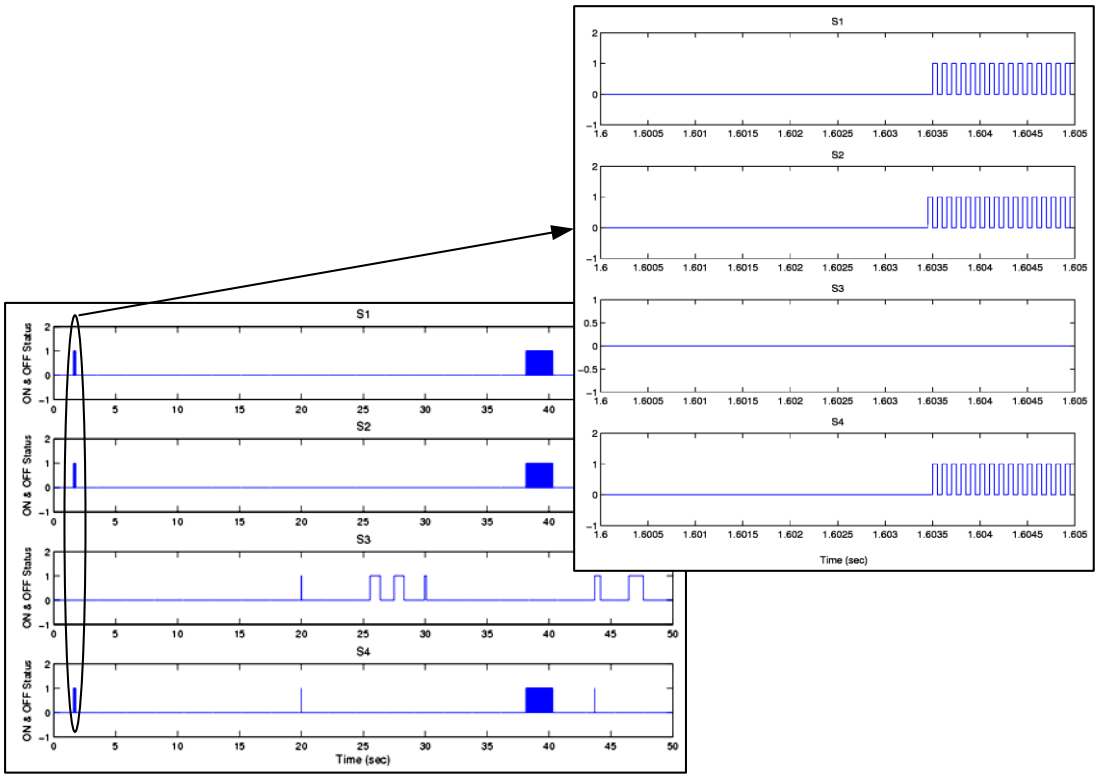

Fig. 2-16**.** Operation of each switch in simulation time.

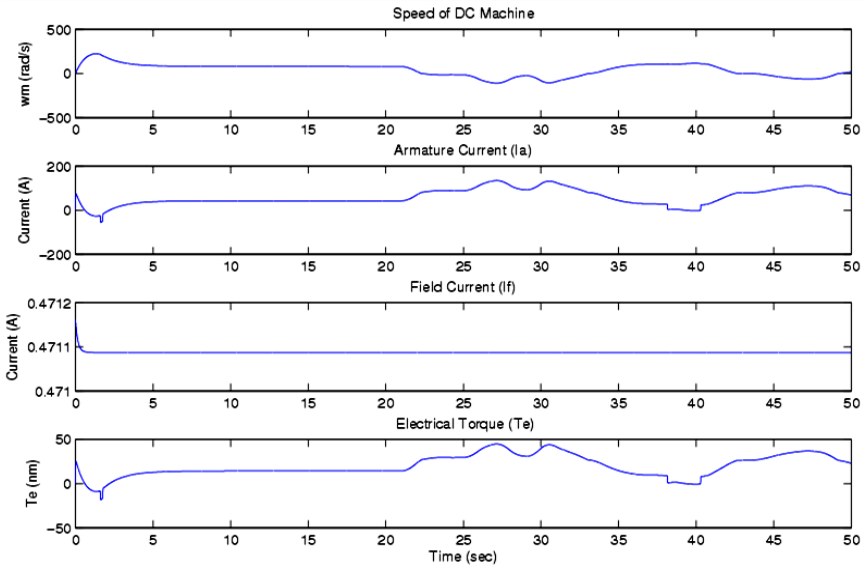

Fig. 2-17. Speed, armature current, field current and electrical torque of DC traction machine.

As is well-known;

$$T \propto I \tag{2-1}$$

$$\omega \propto V \tag{2-2}$$

Thus, load torque is proportional to battery current, and hence, speed of the DC traction machine is proportional to battery voltage.

2.2.5. TRANSFER EFFICIENCY MODELING AND ANALYSIS

The detailed transfer efficiency modeling and analysis of the SCC is explained in this section. As aforementioned, the SCC has 2 main modes of operation, the buck and boost mode. In buck mode, considering switching period *T* is small enough (compared to the circuit time constant), an average current can be used, to replace instantaneous value, for the purpose of integration. Therefore, the voltage across capacitor C can be expressed as:

$$V_C(t) = \begin{cases} V_C(0) + \frac{1}{C}\int_0^t I_C(t)dt \approx V_C(0) + \frac{t}{C}\overline{I_H} & 0 \le t \le kT \\ V_C(kT) + \frac{1}{C}\int_{kT}^t I_C(t)dt \approx V_C(kT) - \frac{t-kT}{C}\overline{I_L} & kT \le t \le T \end{cases} \tag{2-3}$$

In addition, initial values can be used, while ignoring trivial variations. Therefore, the current flowing through capacitor *C* can be written as:

$$Ic(t) = \begin{cases} \frac{V_H - V_{C(0)}}{R_{AN}}\left(1 - e^{\frac{-t}{C*R_{AN}}}\right) = \frac{V_H - V_C}{R_{AN}} = \overline{I_H} & 0 \le t \le kT \\ -\frac{-V_L + V_C(kT) - V_{D4}}{R_{Af}}\left(e^{\frac{-t}{C*R_{Af}}}\right) = -\frac{-V_L + V_C - V_{D4}}{R_{Af}} = -\overline{I_L} & kT \le t \le T \end{cases} \tag{2-4}$$

Here,

$R_{AN} = r_{S1} + r_{S4} + r_C$ $\qquad$ $R_{Af} = r_{S2} + r_C$

Also, r_S represents the parasitic resistance of all switches, r_C is equivalent resistance of capacitor, V_D is voltage drop of all diodes. $\overline{I_H}$ is the average input current during the on-

state period kT and $\overline{I_L}$ is the average output current during the off-state period *(1–k)T*. The variation of the voltage across capacitor *C* is:

$$\Delta \boldsymbol{V_C} = \begin{cases} \frac{\mathbf{1}}{\boldsymbol{C}} \int_{\mathbf{0}}^{\boldsymbol{kT}} \boldsymbol{I_C(t)dt} = \frac{\boldsymbol{kT}}{\boldsymbol{C}} \overline{\boldsymbol{I_H}} & \mathbf{0} \leq \boldsymbol{t} \leq \boldsymbol{kT} \\ \frac{\mathbf{1}}{\boldsymbol{C}} \int_{\boldsymbol{kT}}^{\boldsymbol{T}} \boldsymbol{I_C(t)dt} = \frac{\boldsymbol{(1-k)T}}{\boldsymbol{C}} \overline{\boldsymbol{I_L}} & \boldsymbol{kT} \leq \boldsymbol{t} \leq \boldsymbol{T} \end{cases} \quad (2\text{-}5)$$

Or

$$\Delta V_C = \begin{cases} \frac{k}{Cf} * \frac{V_H - V_C}{R_{AN}} & 0 \leq t \leq kT \\ \frac{(1-k)}{Cf} * \frac{-V_L + V_C - V_{D4}}{R_{Af}} & kT \leq t \leq T \end{cases} \quad (2\text{-}6)$$

Also, voltage across capacitor can be written as:

$$\boldsymbol{V_C} = \frac{\boldsymbol{kR_{Af}V_H + (1-k)R_{AN}(V_L + V_{D4})}}{\boldsymbol{(1-k)R_{AN} + kR_{Af}}} \quad (2\text{-}7)$$

Hence,

$$\Delta \boldsymbol{V_C} = \frac{\boldsymbol{k(1-k)[V_H - (V_L + V_{D4})]}}{\boldsymbol{fC((1-k)R_{AN} + kR_{Af})}} \quad (2\text{-}8)$$

Also,

$V_C - V_C(0) = \frac{\Delta V_C}{2}$ and $V_C(kT) - V_C = \frac{\Delta V_C}{2}$

In addition, the average input current is:

$$\boldsymbol{I_H} = \frac{\mathbf{1}}{\boldsymbol{T}} \int_{\mathbf{0}}^{\boldsymbol{kT}} \boldsymbol{I_C(t)dt} = \boldsymbol{k} \frac{\boldsymbol{V_H - V_C}}{\boldsymbol{R_{AN}}} \quad (2\text{-}9)$$

And the average output current is:

$$\boldsymbol{I_L} = \frac{\mathbf{1}}{\boldsymbol{T}} \int_{\boldsymbol{kT}}^{\boldsymbol{T}} \boldsymbol{I_C(t)dt} = (\mathbf{1} - \boldsymbol{k}) \frac{\boldsymbol{-V_L + V_C - V_{D4}}}{\boldsymbol{R_{Af}}} \quad (2\text{-}10)$$

The total input power is given by:

$$\boldsymbol{P_I} = \boldsymbol{V_H I_H} = \boldsymbol{V_H} * \boldsymbol{k} \frac{\boldsymbol{V_H - V_C}}{\boldsymbol{R_{AN}}} \quad (2\text{-}11)$$

And the output power is expressed as:

$$P_O = V_L I_L = V_L * (1-k)\frac{-V_L+V_C-V_{D4}}{R_{Af}} \tag{2-12}$$

Hence, the overall transfer efficiency can be computed as:

$$\boldsymbol{\eta = \frac{P_O}{P_I} = \frac{V_L*(1-k)(-V_L+V_C-V_{D4})*R_{AN}}{V_H*k*(V_H-V_C)*R_{Af}}} \tag{2-13}$$

In this part focuses on efficiency calculation in boost mode. Thus, the voltage across capacitor *C* can be expressed as:

$$\boldsymbol{V_C(t)} = \begin{cases} \boldsymbol{V_C(0) + \frac{1}{C}\int_0^t I_C(t)dt \approx V_C(0) + \frac{t}{C}\overline{I_L}} & \boldsymbol{0 \le t \le kT} \\ \boldsymbol{V_C(kT) + \frac{1}{C}\int_{kT}^t I_C(t)dt \approx V_C(kT) - \frac{t-kT}{C}\overline{I_H}} & \boldsymbol{kT \le t \le T} \end{cases} \tag{2-14}$$

Also, current flowing through capacitor *C* can be written as:

$$\boldsymbol{Ic(t)} = \begin{cases} \boldsymbol{\frac{V_L-V_C-V_{D2}}{R_{BN}} = \overline{I_L}} & \boldsymbol{0 \le t \le kT} \\ \boldsymbol{-\frac{-V_H+V_C-V_{D1}+V_L}{R_{Bf}} = -\overline{I_H}} & \boldsymbol{kT \le t \le T} \end{cases} \tag{2-15}$$

Here,

$R_{BN} = r_{S4} + r_C$ $\qquad\qquad$ $R_{Bf} = r_{S3} + r_C$

$\overline{\mathrm{I_L}}$ is the average input current during the state-on period *kT* and $\overline{\mathrm{I_H}}$ is the average output current during the state-off period (1 – k)*T*. The variation of the voltage across capacitor *C* is:

$$\boldsymbol{\Delta V_C} = \begin{cases} \boldsymbol{\frac{k}{Cf} * \frac{V_L-V_C-V_{D2}}{R_{BN}}} & \boldsymbol{0 \le t \le kT} \\ \boldsymbol{\frac{(1-k)}{Cf} * \frac{-V_H+V_C-V_{D1}+V_L}{R_{Bf}}} & \boldsymbol{kT \le t \le T} \end{cases} \tag{2-16}$$

Also, the voltage across capacitor can be written as:

$$\boldsymbol{V_C = \frac{kR_{Bf}(V_L-V_{D2})+(1-k)R_{BN}(V_H-V_L+V_{D1})}{(1-k)R_{BN}+kR_{Bf}}} \tag{2-17}$$

Hence,

$$\Delta \boldsymbol{V_C} = \frac{\boldsymbol{k(1-k)[2V_L - V_{D2} - V_{D1} - V_H]}}{\boldsymbol{fC\left((1-k)R_{BN} + kR_{Bf}\right)}} \tag{2-18}$$

In addition, the average input current is:

$$\boldsymbol{I_L} = \frac{\boldsymbol{1}}{\boldsymbol{T}}\left[\int_{\boldsymbol{0}}^{\boldsymbol{kT}} \boldsymbol{I_C(t)dt} + \int_{\boldsymbol{kT}}^{\boldsymbol{T}} \boldsymbol{I_C(t)dt}\right] = \boldsymbol{k}\left(\frac{\boldsymbol{V_L - V_C - V_{D2}}}{\boldsymbol{R_{BN}}}\right) + \boldsymbol{(1-k)}\frac{\boldsymbol{V_L + V_C - V_H - V_{D1}}}{\boldsymbol{R_{Bf}}} \tag{2-19}$$

And the average output current is:

$$\boldsymbol{I_H} = \frac{\boldsymbol{1}}{\boldsymbol{T}}\int_{\boldsymbol{kT}}^{\boldsymbol{T}} \boldsymbol{I_C(t)dt} = \boldsymbol{(1-k)}\frac{\boldsymbol{V_L + V_C - V_H - V_{D1}}}{\boldsymbol{R_{Bf}}} \tag{2-20}$$

Upon determining the total input and output powers, the overall transfer efficiency can be computed as:

$$\boldsymbol{\eta} = \frac{\boldsymbol{P_O}}{\boldsymbol{P_I}} = \frac{\boldsymbol{V_H * [(1-k)(\frac{V_L + V_C - V_H - V_{D1}}{R_{Bf}})]}}{\boldsymbol{V_L * \left[k\left(\frac{V_L - V_C - V_{D2}}{R_{BN}}\right) + (1-k)\frac{V_L + V_C - V_H - V_{D1}}{R_{Bf}}\right]}} \tag{2-21}$$

In steady state, the increase and decrease of the charge across a capacitor should be equal to each other. Therefore, I_I (average input current) should be equal to I_O(average output current) [31]-[34]. Hence, another easy method to calculate transfer efficiency of the 2-Q SCC with one capacitor, *C*, is:

$$\boldsymbol{\eta} = \frac{\boldsymbol{P_O}}{\boldsymbol{P_I}} = \frac{\boldsymbol{V_O I_O}}{\boldsymbol{V_I I_I}} = \frac{\boldsymbol{V_O}}{\boldsymbol{V_I}} \tag{2-22}$$

From above analysis, it can be seen that transfer efficiency only dependent to the ratio of source and load voltage and it is independent of *C*, *f*, and *k*.

2.3. INTERLEAVED 2-Q SWITCHED CAPACITOR CONVERTER

2.3.1. INTERLEAVED 2-Q SCC OPERATING CHARACTERISTICS AND MODES

In this section the SCC is compared with the interleaved SCC. As a first step, the interleaved SCC operating characteristics and modes are explained. The interleaved SCC encompasses 10 switches, 10 diodes, and 3 capacitors. The operating conditions are the same as an SCC. The high voltage DC side (battery modules) represents the 48V DC bus, while the low voltage side (UC modules) represents the 27 V bus. The schematic of an interleaved SCC is shown in Fig. 2-18.

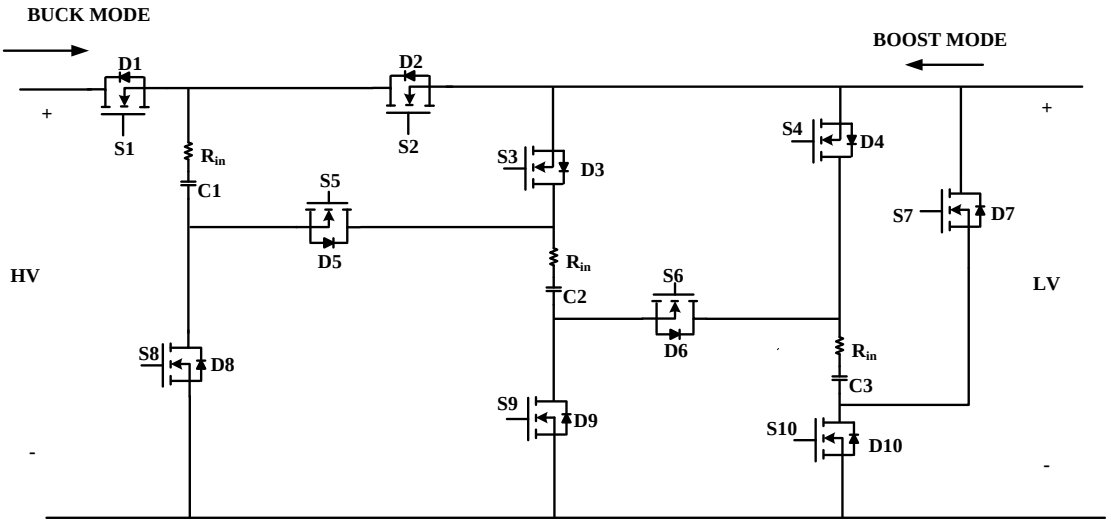

Fig. 2-18. Interleaved 2-Q SC bidirectional DC/DC converter.

In boost operating mode, switches S_{10}, S_9, S_8 and diodes D_4, D_3, D_2 conduct, while other switches and diodes are off. In this case, the 3 capacitors are charged through S_{10}, S_9, S_8, D_4, D_3, and D_2. Also, voltage across the 3 capacitors increase, and this situation is denoted by codes 5, 6, and 7. This operation mode is depicted in Fig. 2-19 (a). After this

step, switches S_7, S_6, S_5 and diode D_1 conduct, while other switches and diodes are off. In this state, the 3 capacitors are discharged through S_7, S_6, S_5, and D_1 and the voltage across the 3 capacitors starts decreasing. In this mode, capacitors directly transfer their stored energy to HV side, denoted by code 8. This operation mode is represented in Fig. 2-19 (b).

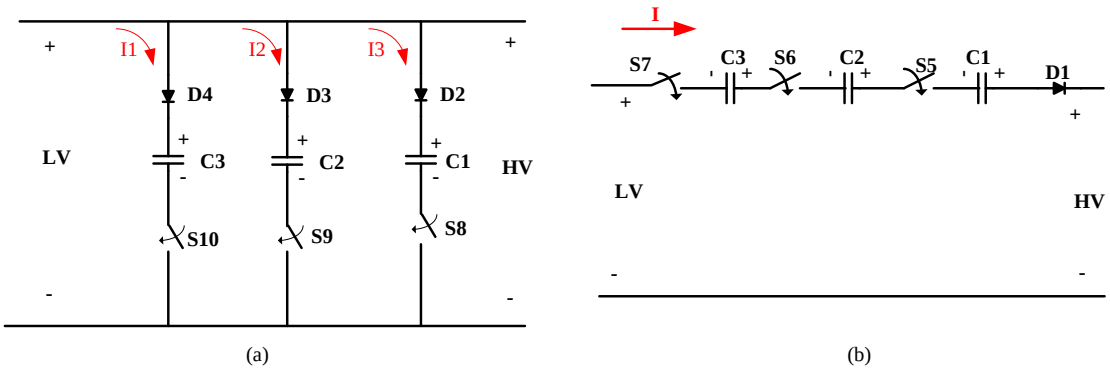

Fig. 2-19. Boost mode, (a) Capacitors are charged by LV side, (b) Capacitors are discharged and transfer their stored energy to HV side.

In buck operating mode, S_1 and S_{10} are closed and D_5 and D_6 conduct. Other switches and diodes are off. In this case, the 3 capacitors are charged through S_1, S_{10}, D_5, and D_6, while the voltage across the 3 capacitors starts increasing. This state is denoted by code 1. This operation mode is depicted in Fig. 2-20 (a).

After this step, S_2, S_3 and S_4 are closed and D_8, D_9 and D_{10} start conducting, while other switches and diodes are off [24], [31]-[34]. In this state, the 3 capacitors are discharged through S_2, S_3, S_4, D_8, D_9, and D_{10}, and the voltage across the 3 capacitors starts decreasing. In this case, capacitors directly transfer their stored energy to the LV side, denoted by codes 2, 3, and 4. This operation mode is represented in Fig. 2-20 (b).

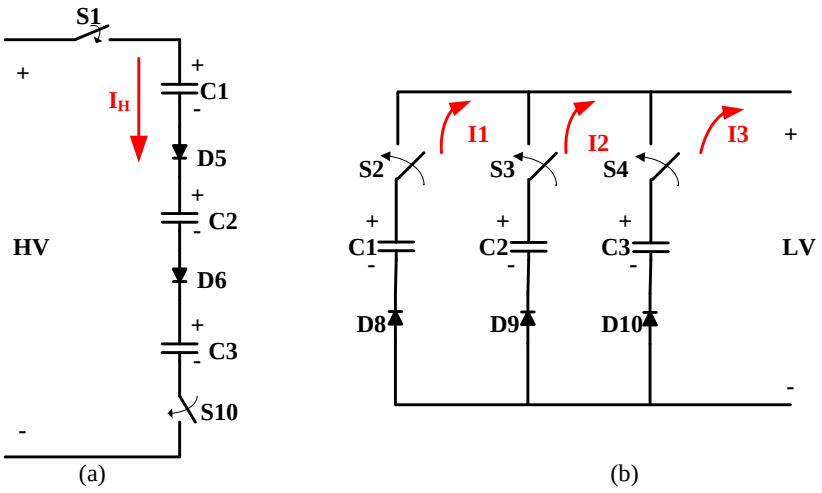

Fig. 2-20. Buck mode, (a) Capacitors are charged by HV side, (b) Capacitors are discharged and transfer their stored energy to LV side.

Also, when battery modules supply energy to load (motoring mode) or load supplies energy to battery side (generating mode), the operation is denoted by code 9. Table 2-3 represents switches and code-based operation of each mode for the interleaved SCC.

Table 2-3. Switches and codes of operation in each mode.

	Hybrid Energy Sources	Codes	Switches & Diodes	States
Motoring or Boost Mode (P>=0)	Ultra-Capacitor (UC)	5	S_{10}	ON
			D_4	ON
		6	S_9	ON
			D_3	ON
		7	S_8	ON
			D_2	ON
		8	S_5	ON
			S_6	ON
			S_7	ON
			D_1	ON
Buck & Boost Mode	Battery	9	$S_{1,2,3,4,5,6,7,8,9,10}$	OFF
			$D_{1,2,3,4,5,6,7,8,9,10}$	OFF
Generating or Buck Mode (P<0)	Ultra-Capacitor (UC)	1	S_1	ON
			S_{10}	ON
			D_5	ON
			D_6	ON
		2	S_2	ON
			D_8	ON
		3	S_3	ON
			D_9	ON
		4	S_4	ON
			D_{10}	ON

The ensuing section focuses on the simulation results of the interleaved SCC with the proposed novel control logic and similar conditions of operation for the SCC, as presented in the previous section.

2.3.2. INTERLEAVED SCC MODELING AND SIMULATION RESULTS

For modeling and simulation purposes, the load power and gradient plots are tested on a portion of the city drive cycle, similar to Figs. 2-8 and 2-9, in section 2.2.4. It must be noted that the 3 capacitors in the interleaved SCC possess the same capacitance and

voltage across them. Figs. 2-21 and 2-22 depict a comparison between V_{C1}, 0.8*V_{UC}, and 0.8 $V_{battery}$, respectively.

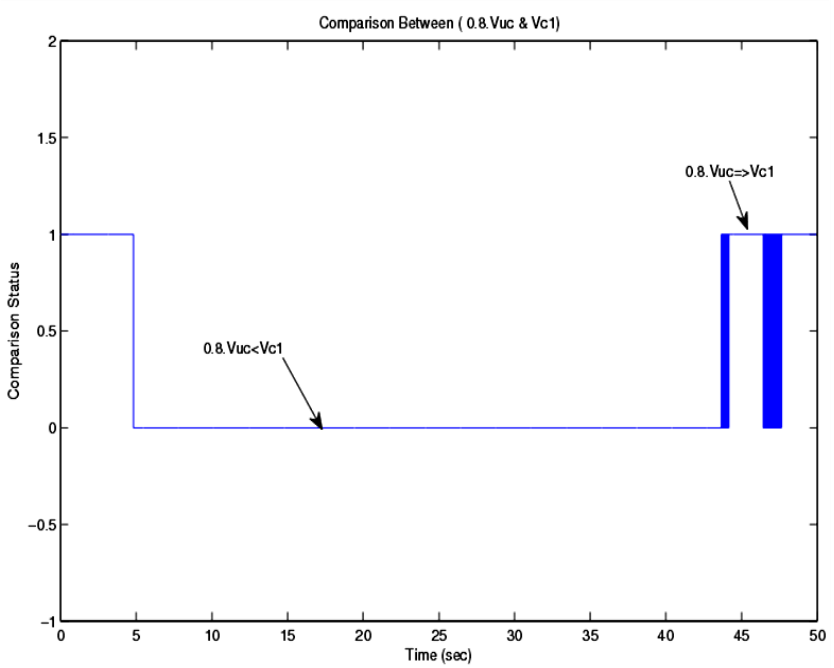

Fig. 2-21. Comparison between 0.8*V_{UC} and V_{C1}.

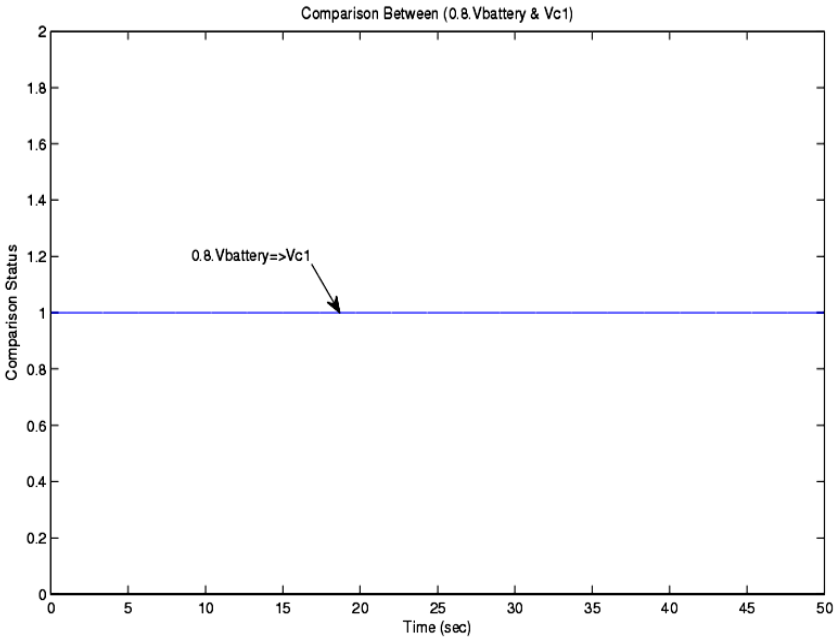

Fig. 2-22. Comparison between 0.8*$V_{battery}$ and V_{C1}.

Fig. 2-23 shows UC modules voltage and current, when they are charged by load or battery modules (in generating mode), or when they supply power to load (in motoring mode).

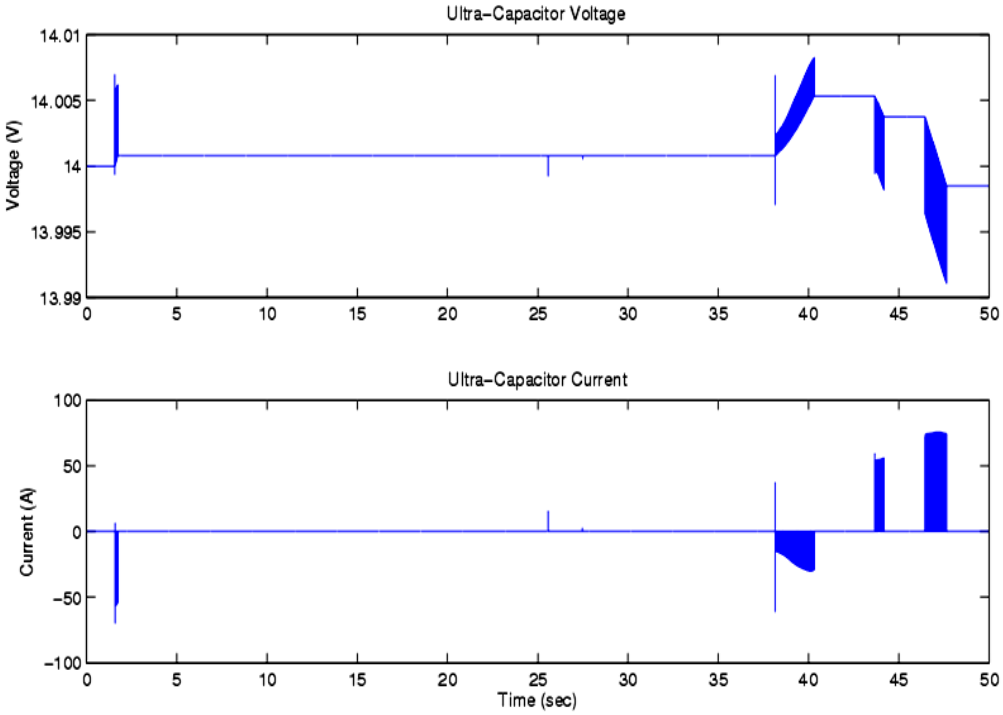

Fig. 2-23. UC modules voltage and current during discharge or charge.

Additional simulation results of load power, state of charge (SOC), current, and voltage of battery modules are depicted in Fig. 2-24. Furthermore, Fig. 2-25 depicts the charge and discharge status of each of the 3 capacitors, with related converter operating codes.

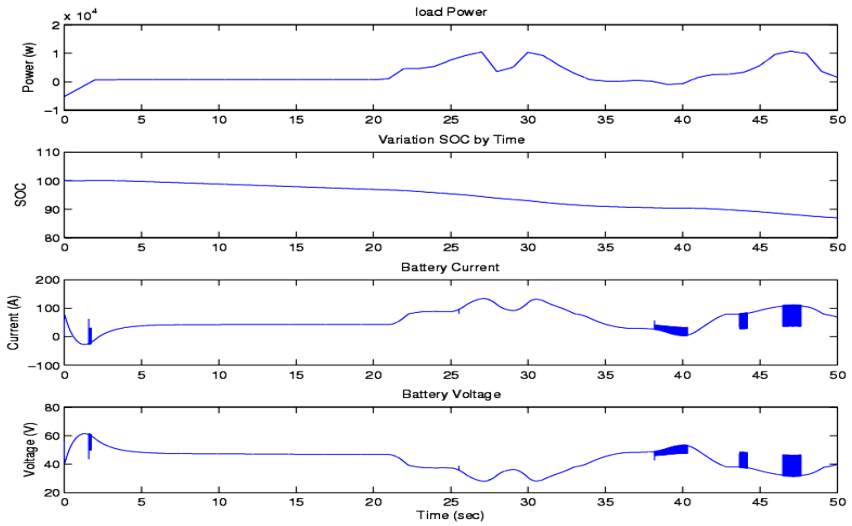

Fig. 2-24. Simulation results of load power, state of charge, current, and battery voltage.

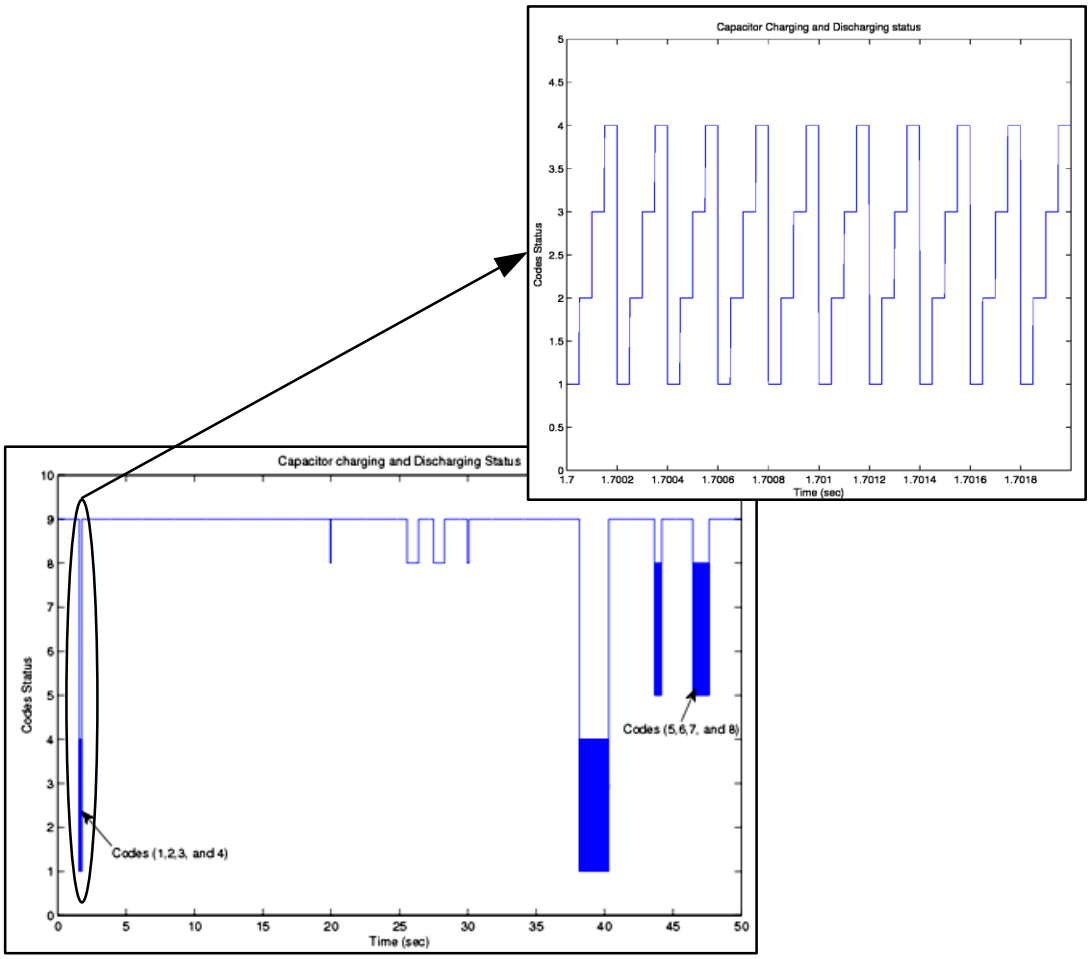

Fig. 2-25. Capacitor charge and discharge status, with codes.

In Fig. 2-25, in the interval 1.6035s ≤ *t* ≤ 1.7647s, battery modules are fully charged, UC modules are half charged, the power curve is in generating mode (between 0s ≤ t ≤ 2s), gradient curve is shown with value = 0, and $V_{C1} \leq 0.8*V_{battery}$. Thus, this interval is represented by codes 1, 2, 3, and 4, and battery modules supply energy to the capacitors. When the battery modules are fully charged, they transfer their stored energy to UC modules. However, when the power curve is in motoring mode, the gradient curve is shown with value = 1, UC and battery modules are half charged, and $V_{C1} \leq 0.8*V_{UC}$. The codes status are denoted by 5, 6, 7, and 8 (UC modules supply power to load side). During this interval, when $V_{C1} > 0.8*V_{UC}$, the code status is denoted by 8 (capacitors supply power to load). On the other hand, when the load power curve depicts motoring mode, the battery and UC modules are half charged, and the gradient curve has value = 0. This means that the battery modules must deliver their energy to load, denoted by code 9, or when power curve is in generating mode and gradient curve shows a value = 0. Thus, this mode of operation is denoted by code 9, which means load supplies energy to the battery modules and they start charging. The related simulation results of the tested separately excited DC machine are shown in Fig. 2-26. As is evident, battery current and voltage are proportional with current and speed of DC machine, respectively. This is because the battery modules connect directly to load (or motor side).

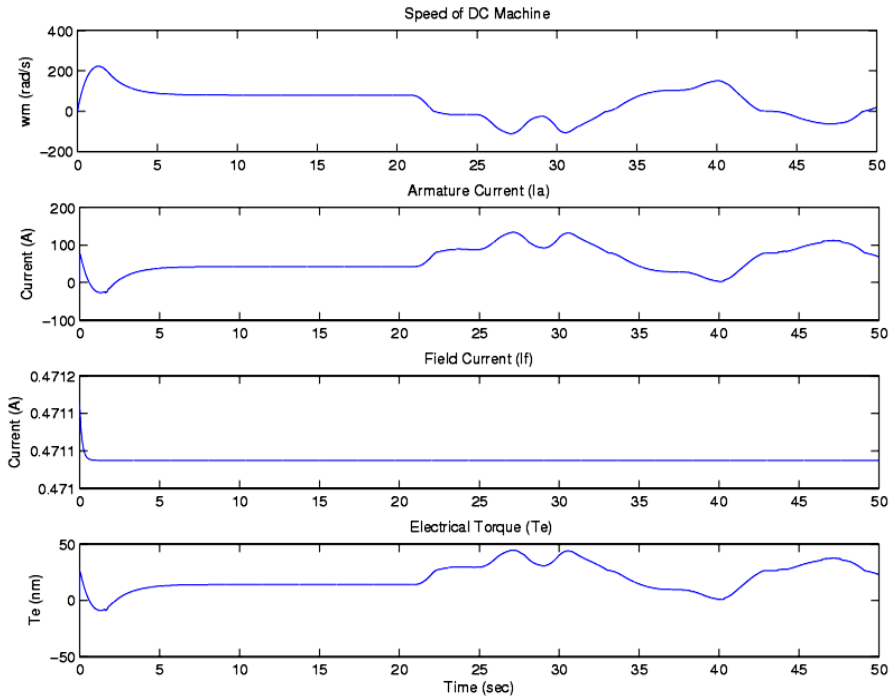

Fig. 2-26. Speed, armature current, field current and electrical torque of DC traction machine.

Operation of each switch is shown in Fig. 2-27. For example, when the converter is operating under code 9, all switches are off, and only battery connects to load. Also, when converter is operating under code 1, S_1 and S_{10} are closed and D_5 and D_6 conduct. The 3 capacitors (C_1, C_2, and C_3) are charged by HV side. Under codes 2, 3, and 4, S_2, S_3 and S_4 are closed and D_8, D_9, and D_{10} conduct. Here, the 3 capacitors are disconnected from HV, and they transfer their stored energy to LV side.

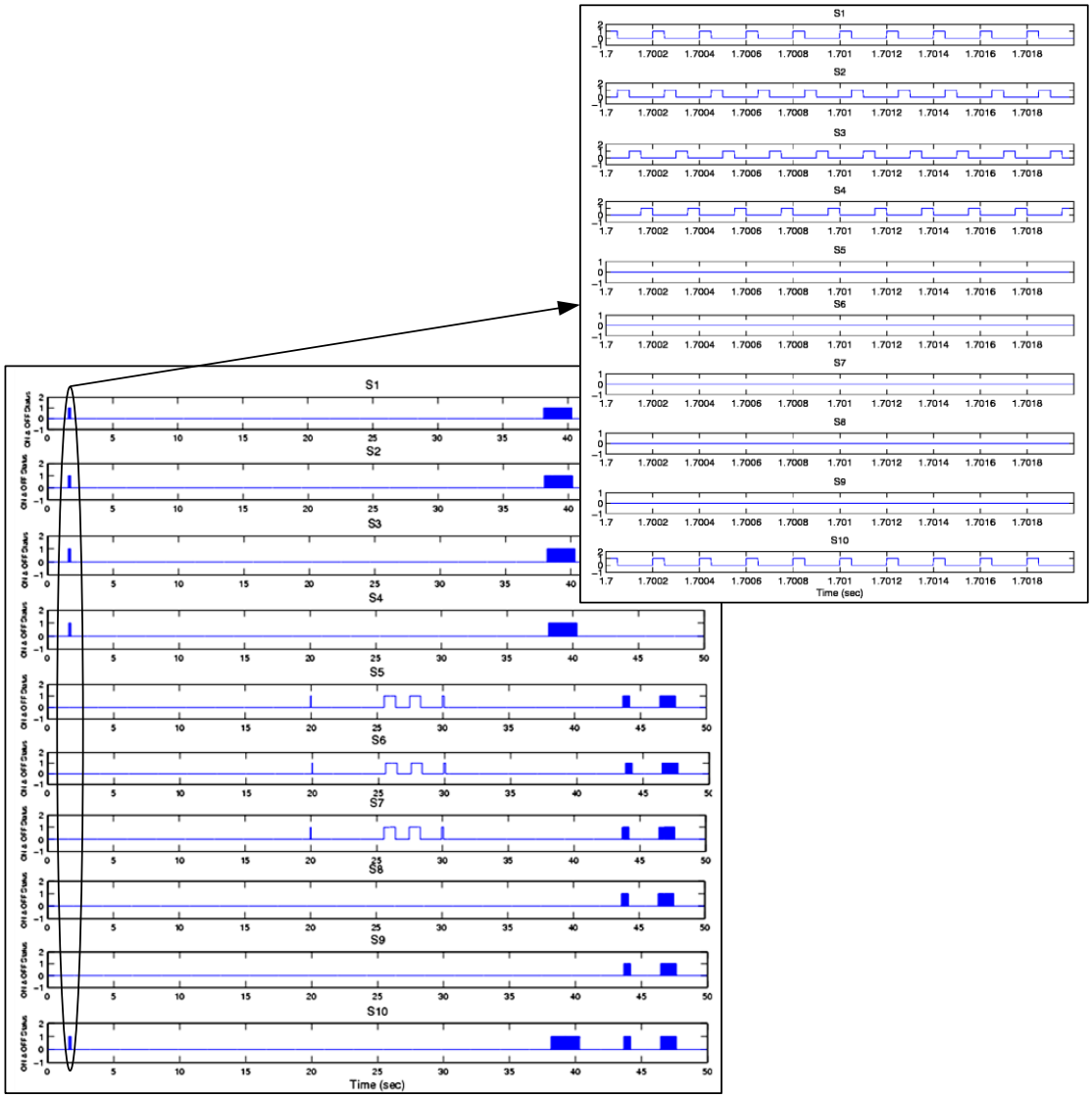

Fig. 2-27**.** Operation of each switch in simulation time.

Conversely, when the converter is operating under codes 5, 6, and 7, switches S_{10}, S_9, and S_8 are closed and D_4, D_3, and D_2 conduct. At this point, the 3 capacitors start charging. Under code 8 operation, S_7, S_6, and S_5 are closed and D_1 conducts, and the 3 capacitors are connected in series with the LV side. At this point, the 3 capacitors start discharging, and supply their energy to the HV side.

2.3.3. TRANSFER EFFICIENCY MODELING AND ANALYSIS

This section deals with the derivation of the transfer efficiency computation process, for the interleaved 2-Q SCC. The buck mode uses the *current-amplification technique*. The 3 capacitors are charged in series during on-state and the input current that flows through them are equal. These capacitors are discharged in parallel during off-state. Therefore, in essence, the output current is amplified by these capacitors. Therefore the voltage across capacitor C_1 can be written as:

$$\boldsymbol{V_{C1}(t)} = \begin{cases} \boldsymbol{V_C(0) + \frac{1}{C}\int_0^t I_C(t)dt \approx V_C(0) + \frac{t}{C}\overline{I_H}} & \boldsymbol{0 \le t \le kT} \\ \boldsymbol{V_C(kT) + \frac{1}{C}\int_{kT}^t I_C(t)dt \approx V_C(kT) - \frac{t-kT}{3C}\overline{I_L}} & \boldsymbol{kT \le t \le T} \end{cases} \quad (2\text{-}23)$$

Therefore the current flowing through capacitor C_1 is:

$$I_{C1}(t) = \begin{cases} \frac{V_H - 2V_D - 3V_{C1}}{R_{AN}} = \overline{I_H} & 0 \le t \le kT \\ -\frac{-V_L + V_{C1} - V_D}{R_{Af}} = -\frac{\overline{I_L}}{3} & kT \le t \le T \end{cases} \quad (2\text{-}24)$$

$$R_{AN} = r_{S1} + r_{S10} + 3r_C = 2r_S + 3r_C \qquad R_{AF} = r_S + r_C$$

Here, $\overline{I_H}$ is the average input current during on-state period kT and $\overline{I_L}$ is the average output current during off-state period (1–k) *T*. The variation of the voltage across capacitor C_1 is:

$$\Delta V_{C1} = \begin{cases} \frac{1}{C}\int_0^{kT} I_{C1}(t)dt = \frac{k}{Cf} * \frac{V_H - 2V_D - 3V_{C1}}{R_{AN}} & 0 \le t \le kT \\ \frac{1}{C}\int_{kT}^{T} I_{C1}(t)dt = \frac{(1-k)}{Cf} * \frac{-V_L + V_{C1} - V_D}{3R_{Af}} & kT \le t < T \end{cases} \quad (2\text{-}25)$$

Also, voltage across capacitor C_1, after calculation is:

$$V_{C1} = \frac{3 * kR_{Af}(V_H - 2V_D) + (1-k)R_{AN}(V_L + V_D)}{(1-k)R_{AN} + 9kR_{Af}} \quad (2\text{-}26)$$

Hence,

$$\Delta V_{C1} = \frac{k(1-k)[V_H-(3V_L+5V_D)]}{fC[(1-k)R_{AN}+9kR_{Af}]} \quad (2\text{-}27)$$

The average input current is:

$$\boldsymbol{I_H = \frac{1}{T}\int_0^{kT} I_C(t)dt = k\frac{V_H-2V_D-3V_{C1}}{R_{AN}}} \quad (2\text{-}28)$$

The average output current is:

$$\boldsymbol{I_L = \frac{1}{T}\int_{kT}^{T} I_C(t)dt = (1-k)\frac{-V_L+V_{C1}-V_D}{R_{Af}}} \quad (2\text{-}29)$$

Hence, the transfer efficiency can be expressed as:

$$\eta = \frac{P_O}{P_I} = \frac{V_L*(1-k)(-V_L+V_{C1}-V_D)*R_{AN}}{V_H*k*(V_H-2V_D-3V_{C1})*R_{Af}} \quad (2\text{-}30)$$

The boost mode principally employs the *voltage-lift technique*. The 3 capacitors are charged in parallel during on-state. The input voltage is applied to the 3 capacitors and the voltage across them is equal. The capacitors are discharged in series with LV side during the off-state. Therefore, in essence, the output voltage is lifted by the 3 capacitors. The voltage across capacitor C_1 in boost mode is:

$$\boldsymbol{V_{C1}(t)} = \begin{cases} \boldsymbol{V_{C1}(0) + \frac{1}{C}\int_0^t I_C(t)dt \approx V_{C1}(0) + \frac{t}{3C}\overline{I_L}} & \boldsymbol{0 \le t \le kT} \\ \boldsymbol{V_{C1}(kT) + \frac{1}{C}\int_{kT}^t I_C(t)dt \approx V_{C1}(kT) - \frac{t-kT}{C}\overline{I_H}} & \boldsymbol{kT \le t \le T} \end{cases}$$

(2-31)

Also, current flowing through capacitor C_1 is:

$$\boldsymbol{I_{C1}(t)} = \begin{cases} \boldsymbol{\frac{V_L-V_{C1}-V_D}{R_{BN}} = \frac{\overline{I_L}}{3}} & \boldsymbol{0 \le t \le kT} \\ \boldsymbol{-\frac{-V_H+3V_{C1}-V_D+V_L}{R_{Bf}} = -\overline{I_H}} & \boldsymbol{kT \le t \le T} \end{cases} \quad (2\text{-}32)$$

$$R_{BN} = r_S + r_C \qquad R_{BF} = r_{S5} + r_{S6} + r_{S7} + 3r_C = 3(r_S + r_C)$$

Here, $\overline{I_L}$ is the average input current during on-state period kT and $\overline{I_H}$ is the average output current during off-state period (1 – k)*T*. The variation of the voltage across capacitor C_1 is:

$$\Delta V_{C1} = \begin{cases} \frac{k}{Cf} * \frac{V_L - V_{C1} - V_D}{3R_{BN}} & 0 \le t \le kT \\ \frac{(1-k)}{Cf} * \frac{-V_H + 3V_{C1} - V_D + V_L}{R_{Bf}} & kT \le t < T \end{cases} \quad (2\text{-}33)$$

Also, voltage across capacitor C_1, after calculation, can be expressed as:

$$\boldsymbol{V_{C1} = \frac{kR_{Bf}(V_L - V_D) + 3(1-k)R_{BN}(V_H - V_L + V_D)}{9(1-k)R_{BN} + kR_{Bf}}} \quad (2\text{-}34)$$

Hence,

$$\boldsymbol{\Delta V_{C1} = \frac{k(1-k)[4V_L - 4V_D - V_H]}{fC(9(1-k)R_{BN} + kR_{Bf})}} \quad (2\text{-}35)$$

The average input current is:

$$\boldsymbol{I_L = \frac{1}{T}\left[\int_0^{kT} I_C(t)dt + \int_{kT}^{T} I_C(t)dt\right] = k\left(\frac{V_L - V_{C1} - V_D}{R_{BN}}\right) + (1-k)\frac{-V_H + 3V_{C1} - V_D + V_L}{R_{Bf}}} \quad (2\text{-}36)$$

The average output current is:

$$\boldsymbol{I_H = \frac{1}{T}\int_{kT}^{T} I_C(t)dt = (1-k)\frac{-V_H + 3V_{C1} - V_D + V_L}{R_{Bf}}} \quad (2\text{-}37)$$

Hence, the transfer efficiency can be expressed as:

$$\boldsymbol{\eta = \frac{P_O}{P_I} = \frac{V_H * [(1-k)(\frac{-V_H + 3V_{C1} - V_D + V_L}{R_{Bf}})]}{V_L * \left[k\left(\frac{V_L - V_{C1} - V_D}{R_{BN}}\right) + (1-k)\frac{-V_H + 3V_{C1} - V_D + V_L}{R_{Bf}}\right]}} \quad (2\text{-}38)$$

It is clear that the transfer efficiency is independent of *C* and *f*. The conduction duty, *k*, does not affect the transfer efficiency. However, *k* does affect P_I (input power) and P_o (output power) in a diminutive region.

2.4. 2-Q SC *LUO* CONVERTER

2.4.1. SC *LUO* CONVERTER OPERATING CHARACTERISTICS AND MODES

As aforementioned, the *voltage lift technique* represents an excellent method to boost output voltage. Hence, by using a suitable combination of the SCC and the *voltage lift technique*, a converter with high voltage gain, high power density, high efficiency, low EMI, ease of control, and small size can be constructed [35]-[40]. A typical system schematic for a 2- Q SC *Luo* converter, operating between HEV energy storage systems, is shown in Fig. 2-28.

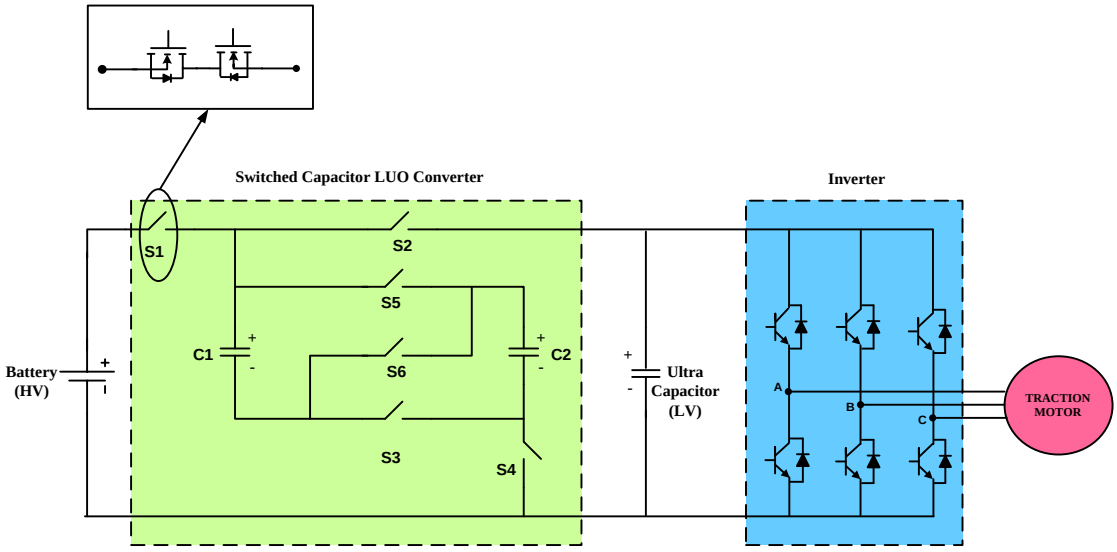

Fig. 2-28. A typical system schematic with energy storage system and SC- *Luo* converter.

This type converter utilizes 6 switches and 2 capacitors. Each switch consists of 2 back-to-back MOSFETs in series, except S_6 (1 MOSFET). It must be pointed out here that the 2 capacitors have same capacitance and voltage. Again, the idea is to operate this converter in 2 operating modes; buck and boost mode.

In the buck operating mode (when load power P≤0), S_1, S_3, S_5, and S_4 are on and D_1, D_3, D_5, and D_4 start conducting. Capacitors C_1 and C_2 are charged in parallel through S_1, S_3, S_5, S_4, D_1, D_3, D_5, and D_4. Also, the voltage across the 2 capacitors starts increasing. This operation is denoted by codes 1 and 2. This operation mode is depicted in Fig. 2-29 (a). After this step, S_4, S_3, S_5, and S_2 are on and D_4, D_3, D_5, and D_2 start conducting. Capacitors C_1 and C_2 are discharged in parallel and transfer their stored energy to LV side. Also, the voltage across the 2 capacitors starts decreasing. This operation is denoted by codes 3 and 4. This operation mode is shown in Fig. 2-29 (b).

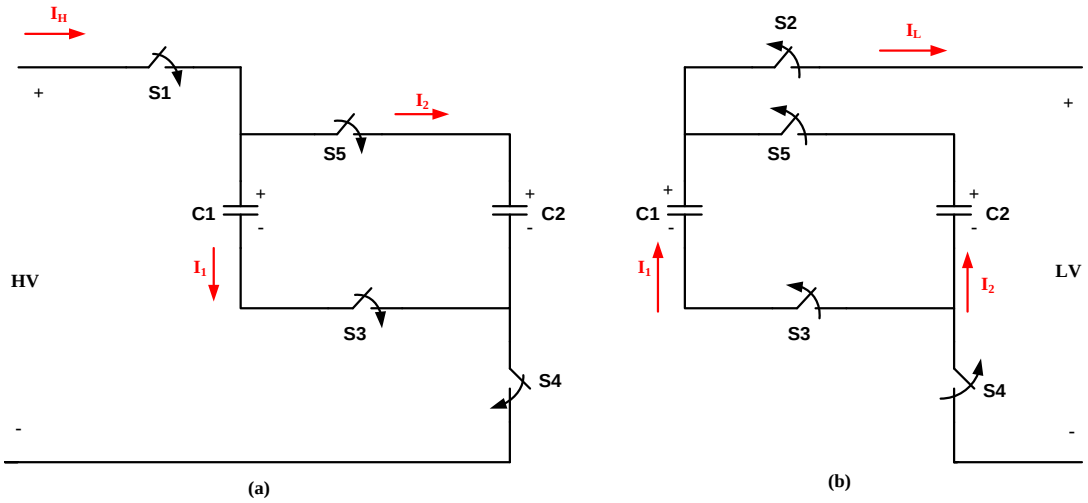

Fig. 2-29. Buck operation mode (a) capacitors C_1 and C_2 are charged and are connected to HV side; (b) capacitors are discharged and are disconnected from HV side.

In the boost operating mode (when load power P≥0), S_2, S_5, S_3, and S_4 are on and D_2, D_5, D_3, and D_4 start conducting. Capacitors C_1 and C_2 are charged in parallel by LV side. Also, the voltage across the 2 capacitors starts increasing. This operation is denoted by codes 5 and 6. This operation mode is depicted in Fig. 2-30 (a). After this step, S_4, S_6, and S_1 are on and D_4, D_6, and D_1 start conducting. Capacitors C_1 and C_2 are discharged in

series through S_4, S_6, S_1, D_4, D_6, and D_1. Also, the voltage across the 2 capacitors starts decreasing and this operation is denoted by code 7. This operation mode is represented in Fig. 2-30 (b).

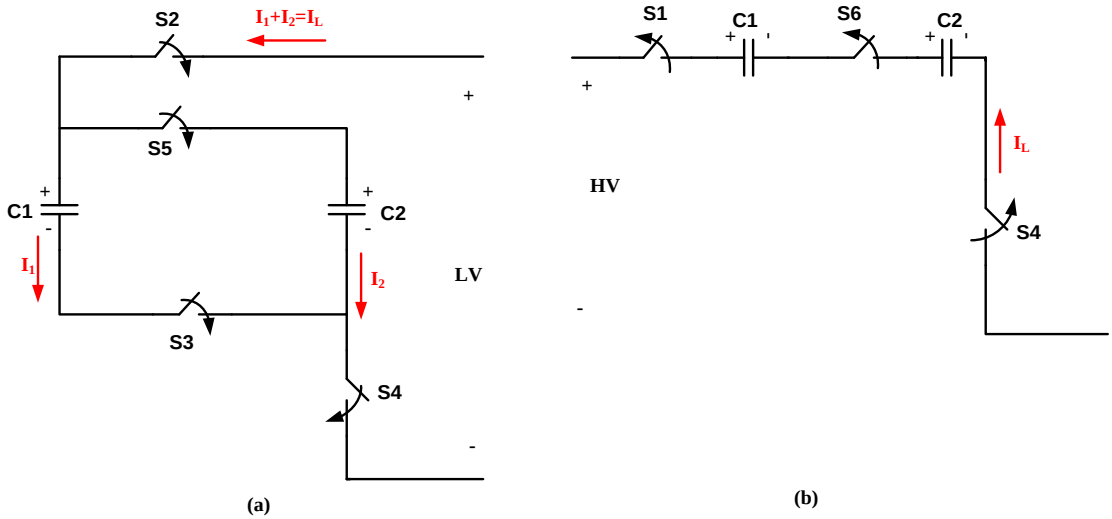

Fig. 2-30. Boost operation mode (a) capacitors are charged and are connected to the LV side; (b) Capacitors are discharged and transfer their stored energy to HV side.

Boost mode implements the *voltage-lift technique*, because the capacitors are charged in parallel during the on-state. The capacitors are discharged in series during the off-state. Hence, through this straightforward method, output voltage can be boosted by the capacitors [31], [41]-[45].

2.5. SUMMARY

Comparison between a hybrid switched capacitor converter (SCC) and interleaved SCC are proposed that can offer features of voltage step-down, voltage step-up, and bidirectional power flow, associated with two or more HEV energy storage devices. Furthermore, detailed transfer efficiency modeling and analyses are conducted for each topology, for each operating mode, using the developed novel SCC control strategy. It is

found that the interleaved SCC has higher energy transfer efficiency, due to the fact that the buck mode uses the *current-amplification technique* and boost mode implements the *voltage-lift technique*, which elevates output current and voltage, respectively.

This chapter also proposed a novel SCC control strategy. The control algorithm was tested for city driving load conditions, which depicts the following major advantages: (a) lower source current ripple, (b) simpler dynamics than the typical buck converter, (c) control simplicity, (d) continuous input current waveform in both modes of operation (buck and boost).

CHAPTER 3

MODELING AND DESIGN OF AN ADVANCED *LUO* CONVERTER

3.1. 4-Q SWITCHED CAPACITOR *LUO* CONVERTER

3.1.1. CONTROLLER DESIGN FOR 4-Q SC *LUO* CONVERTER OPERATION

The typical bidirectional SC *Luo* Converter consists of 6 switches and 2 capacitors, C_1 and C_2. Fig. 3-1 shows a type of SC *Luo* Converter that operates in four quadrants (forward and reverse mode).

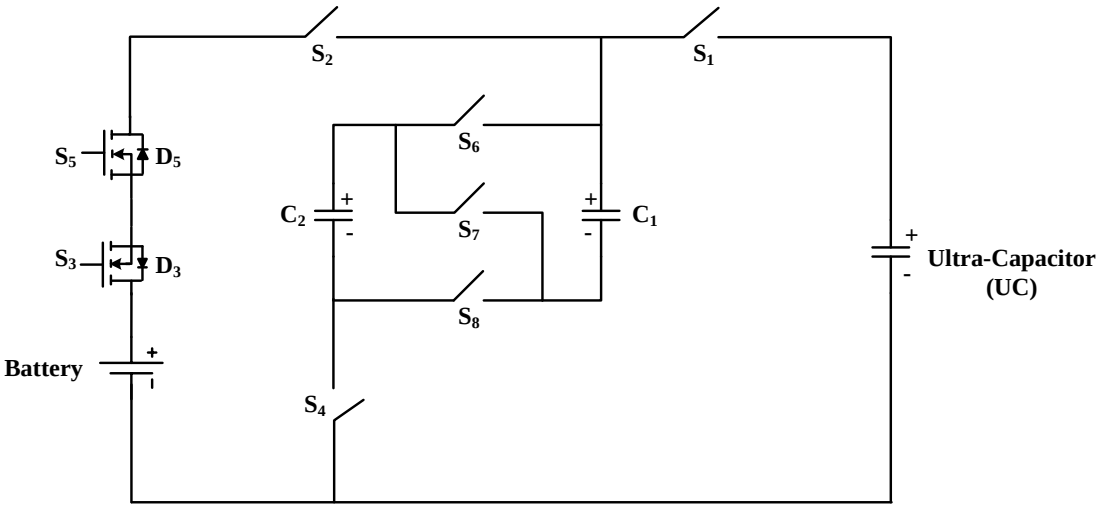

Fig. 3-1. A typical system schematic with hybrid energy sources and SC converter.

Each switch consists of two MOSFETs for current flow in both directions. For an HEV application, the high voltage (HV) side typically consists of battery modules and the low voltage (LV) side could consist of UC modules. In this case, the high voltage DC is

at 86V, low voltage side is set at 43V, and UC initial voltage is at 22V. Fig. 3-2 shows the complete system schematic.

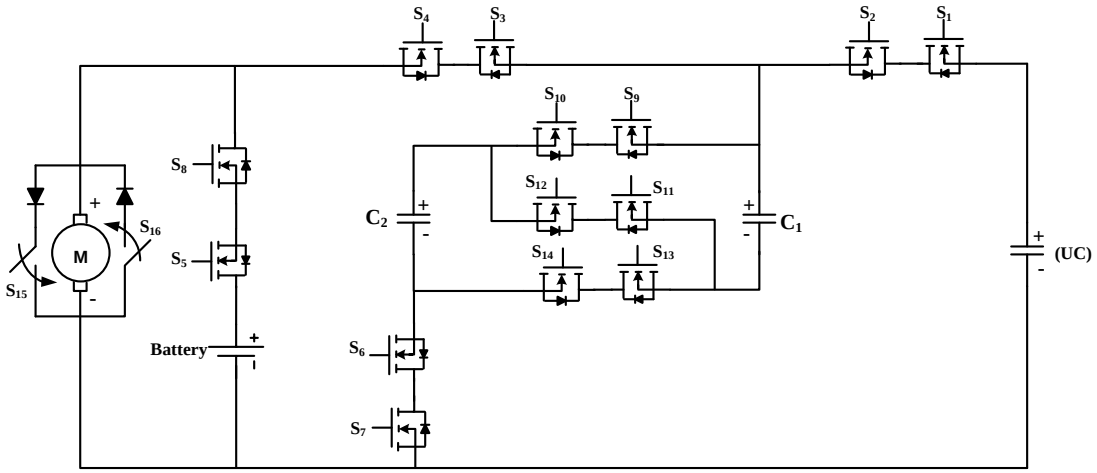

Fig. 3-2. Circuit schematic with hybrid energy sources and traction motor.

When the converter operates in motoring mode ($P \geq 0$), two conditions are chosen: If the battery current gradient is between -2mA/sec and 2mA/sec, battery modules supply their energy to the load and motor side. Otherwise, UC modules supply their power to load and motor side. Secondly, during motoring mode, output power of motor (P_{out}) is compared with load power (P_L). If $P_{out} < P_L$, with attention given to battery current gradient, UC or battery modules supply their power to the motor. Otherwise, if the battery modules need energy and fully discharge, the UC modules transfer their energy to battery or HV side. If the UC modules need energy and fully discharge, the battery modules deliver their energy to UC or LV side. On the other hand, when the converter operates in generating mode ($P < 0$), only the first condition is considered. In generating mode, the motor tends to give up its power; thus it is not compared with load power. The SC *Luo* and its modes of operation are explained in the next section.

3.1.2. SC *LUO* CONVERTER OPERATING CHARACTERISTIC AND MODES

In forward motoring or quadrant I operation, voltage and current are positive. At the same time, if $P_{out} < P_L$, the UC or battery modules supply their power to motor side with attention given to the gradient of battery current. Otherwise, battery or UC modules deliver their energy between each other. For better understanding of the controller, each operation mode is denoted by a specific code.

When $P_{out} < P_L$, and UC modules transfer their power to motor side. As a first step, switches S_2, S_{10}, S_{14}, and S_7 are on, and D_1, D_9, D_{13}, and D_6 start conducting. Capacitors C_1 and C_2 are charged by the LV side. Also, the voltage across the 2 capacitors increases. Also, in this operation mode, S_{16} is on, because motor does not stop and current flows through the armature. This mode is represented by code 3. The operation mode is shown in Fig. 3-3.

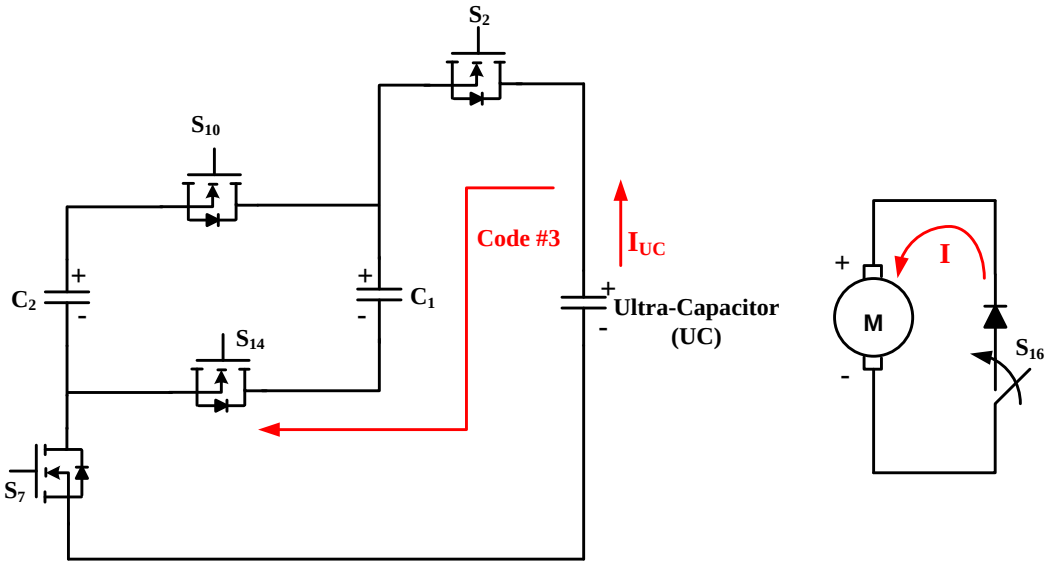

Fig. 3-3. Forward motoring; Capacitors C_1 and C_2 are charged by LV side (S_{16} is on and current flows in motor).

After this operating stage, S_6, S_{11} and S_4 are on, and D_7, D_{12}, and D_3 start conducting. Capacitors C_1 and C_2 are disconnected from LV side and transfer their stored energy to motor side. Also, the voltage across the 2 capacitors decreases. This mode is shown by code 1. This operation mode is depicted in Fig. 3-4.

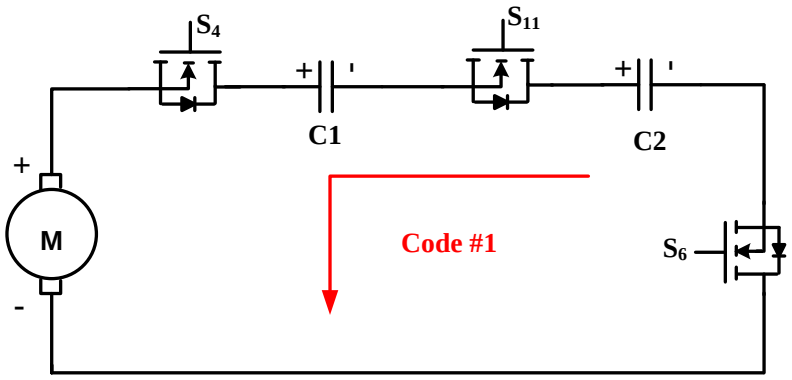

Fig. 3-4. Forward motoring; Capacitors are discharged and are disconnected from LV side.

However, when battery modules deliver their energy to motor side, switch S_5 is closed and D_8 starts conducting. This mode is shown by code 2, and is depicted in Fig. 3-5.

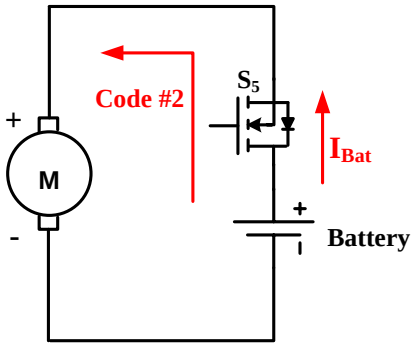

Fig. 3-5. Forward motoring; Battery modules supply energy to motor side.

Now, if $P_{out} \geq P_L$, and battery modules are fully discharged, LV side or UC modules transfer their energy to HV side. As a first step, switches S_2, S_{10}, S_{14}, and S_7 are on, and

D_1, D_9, D_{13}, and D_6 start conducting. This mode is represented by code 3 and shown in Fig. 3-3. Also, in both operation modes (buck and boost modes), S_{16} is on, because motor does not stop and current flows through the armature.

After this operating stage, S_6, S_{11}, S_4 and S_8 are on, and D_7, D_{12}, D_3, and D_5 start conducting. Capacitors C_1 and C_2 are disconnected from LV side and transfer their stored energy to the HV side. Also, the voltage across the 2 capacitors decreases. This mode is shown by code 4.

The boost mode implements the *voltage-lift technique*, because the capacitors are charged in parallel during the on-state. The input voltage (LV) appears across to the capacitors. The capacitors are discharged in series during the off-state. Hence, through this straightforward method, output voltage can be boosted by the capacitors. This operation mode is depicted in Fig. 3-6.

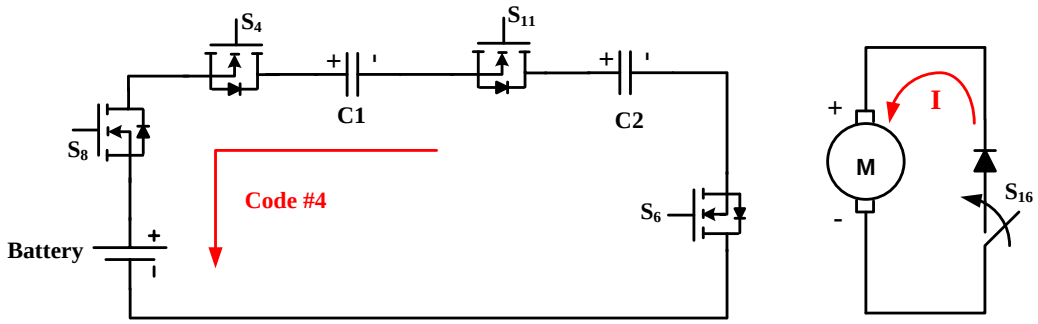

Fig. 3-6. Capacitors are discharged and are disconnected from LV side (S_{16} is on and current flows in motor).

Now, if $P_{out} \geq P_L$, and UC modules are fully discharged, battery modules transfer their energy to the LV side. As a first step, switches S_5, S_3, S_{12}, and S_7 are on, and D_8, D_4, D_{11}, and D_6 start conducting. Capacitors C_1 and C_2 are charged by HV side. Also, the voltage

across the 2 capacitors increases. This mode is represented by code 10. This operation mode is shown in Fig. 3-7.

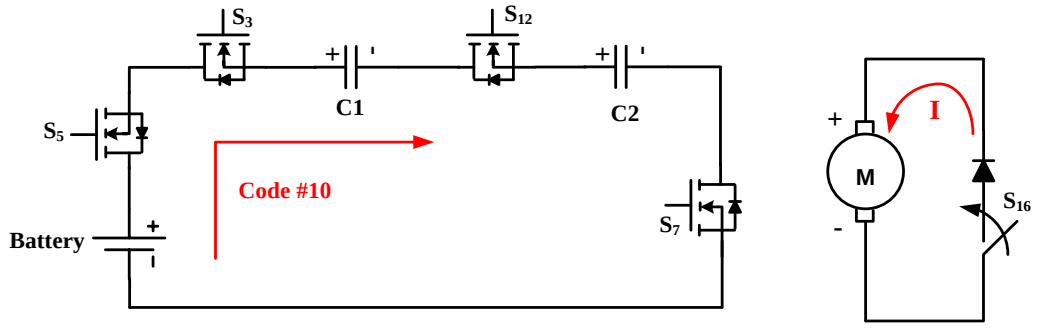

Fig. 3-7. Capacitors C_1 and C_2 are charged by HV side (S_{16} is on and current flows in motor).

After this operating stage, switches S_6, S_9, S_{13} and S_1 are on, and D_7, D_{10}, D_{14}, and D_2 start conducting. Capacitors C_1 and C_2 are disconnected from HV side and transfer their stored energy to the LV side. Also, the voltage across the 2 capacitors decreases. This mode is shown by code 11. The buck mode uses the *current-amplification technique*, because the capacitors are charged in series during on-state. The input current flows through capacitors. These capacitors are discharged in parallel during off-state. Therefore, the output current is amplified by these capacitors [31], [35]-[41], [46]-[50]. This operation mode is depicted in Fig. 3-8.

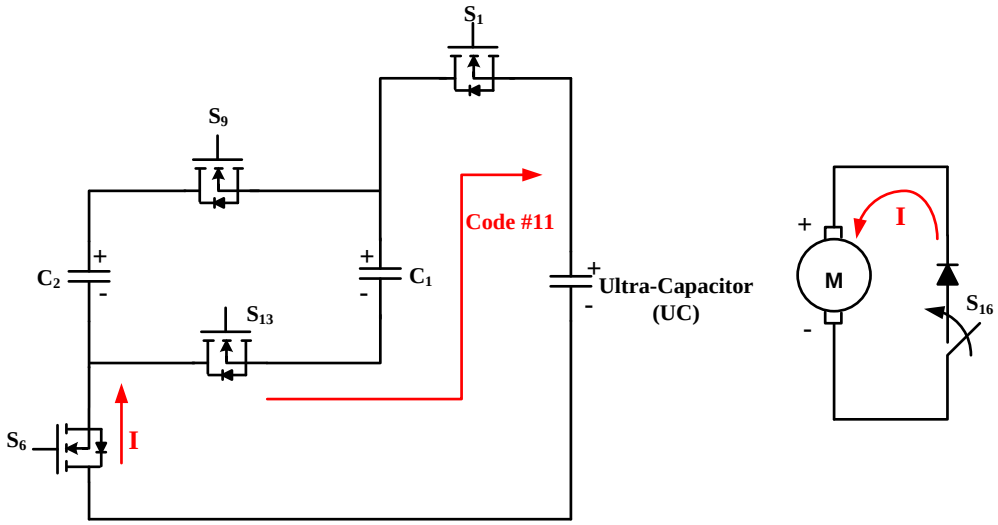

Fig. 3-8. Capacitors are discharged and are disconnected from HV side (S_{16} is on and current flows in motor).

If UC or battery modules are fully discharged, and $P_{out} \geq P_L$, then S_{16} turns on, because current flows through the motor. This mode is represented by code 9. This operation mode is shown in Fig. 3-9.

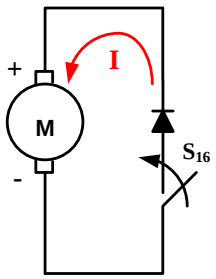

Fig. 3-9. Forward motoring; hybrid energy sources are fully discharged ($P_{out} \geq P_L$ and S_{16} is on).

In forward regenerative (forward braking) or quadrant II operation, voltage is positive but current is negative. In this operating mode, only battery current gradient is considered. When motor supplies power to the UC side and UC modules are fully

discharged (or half charged), then motor transfer its power to LV side. As a first step, switches S_3, S_{12}, and S_7 are on, and D_4, D_{11}, and D_6 start conducting. Capacitors C_1 and C_2 are charged by motor. Also, the voltage across the 2 capacitors increases. This mode is represented by code zero, and is shown in Fig. 3-10.

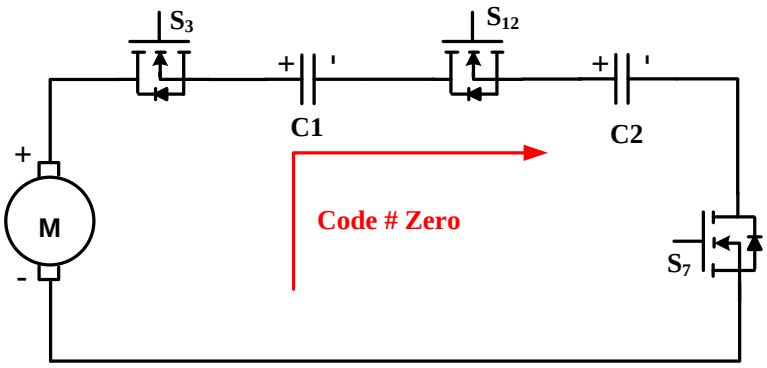

Fig. 3-10. Forward regenerative operation; Capacitors C_1 and C_2 are charged by motor.

After this operating stage, switches S_6, S_9, S_{13} and S_1 are on, and D_7, D_{10}, D_{14}, and D_2 start conducting. Capacitors C_1 and C_2 are disconnected from motor side and transfer their stored energy to the LV side. Also, the voltage across the 2 capacitors decreases. Also, at the same time, switch S_{15} is on because motor does not stop. This mode is shown by code 12, and is depicted in Fig. 3-11.

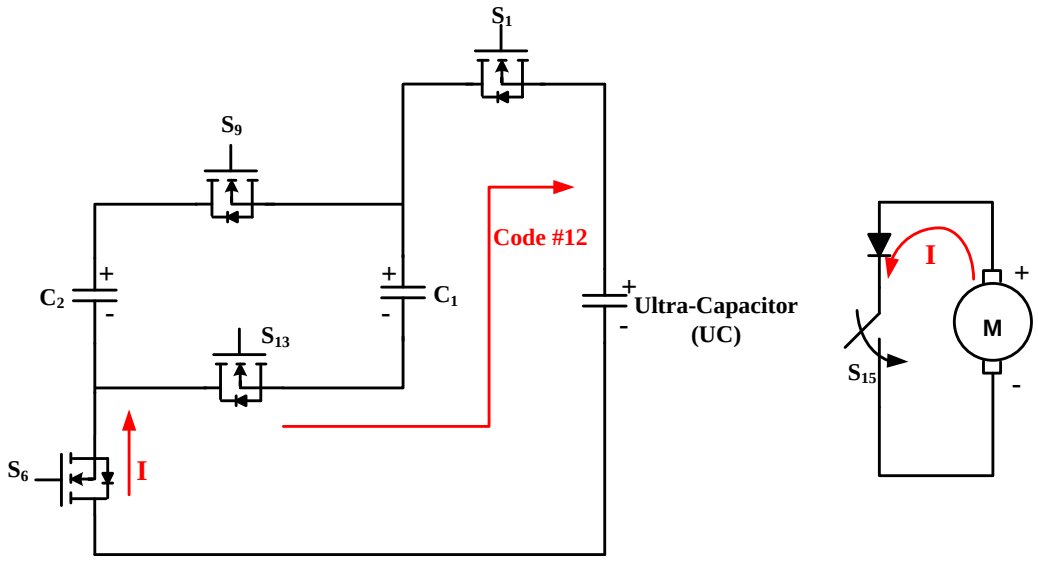

Fig. 3-11. Forward regenerative operation; Capacitors C_1 and C_2 are disconnected from motor side and transfer their stored energy to the LV side (S_{15} is on and current flows in motor).

When the motor supplies power to battery side, and also, battery modules are fully discharged (or half charged), motor transfers its power to HV side, and switch S_8 turns on. D_5 starts conducting, and this mode is represented by code 5, as shown in Fig. 3-12.

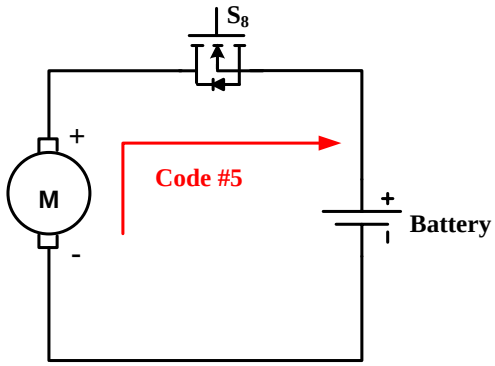

Fig. 3-12. Forward regenerative operation; Battery modules are fully discharged or half charged.

However, if UC or battery modules are fully charged, switch S_{15} is on, because current flows through the motor. This mode is shown by code 8, and is depicted in Fig. 3-13.

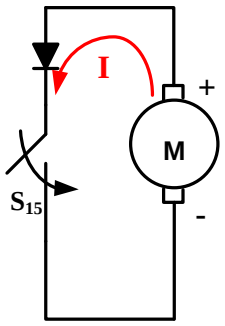

Fig. 3-13. Forward regenerative operation; UC or Battery modules are fully charged and current flows in motor.

In reverse motoring (quadrant III) operation, voltage and current are negative. This operation mode and its codes are same as forward motoring. In reverse regenerative (reverse braking or quadrant IV) operation, voltage is negative but current is positive. This operation mode and its codes are same as forward regenerative.

The next section focuses on modeling and simulation results and analyzes the overall controller operation.

3.1.3. SC *LUO* CONVERTER MODELING AND SIMULATION RESULTS

Fig. 3-14 depicts a comparison between P_{out} and P_L, load torque (T_L), battery current gradient, and voltage across of DC motor (armature voltage). In the first plot, when $P_{out} \geq P_L$, power curve is shown with value = 1. When $P_{out} < P_L$, it is denoted by value = 0. When $T_L \geq 0$, the converter operates in motoring mode (otherwise converter operates in generating mode). The third plot shows battery current gradient. As is clear, when this value is out of range (-2mA/sec and 2mA/sec), the UC modules supply their power to the

load and motor side, in motoring mode (or motor and load must transfer their power to UC or LV side, in generating mode). As is clear from the final plot, when $V_a \geq 0$, converter operates in forward mode. When $V_a < 0$, converter operates in reverse mode.

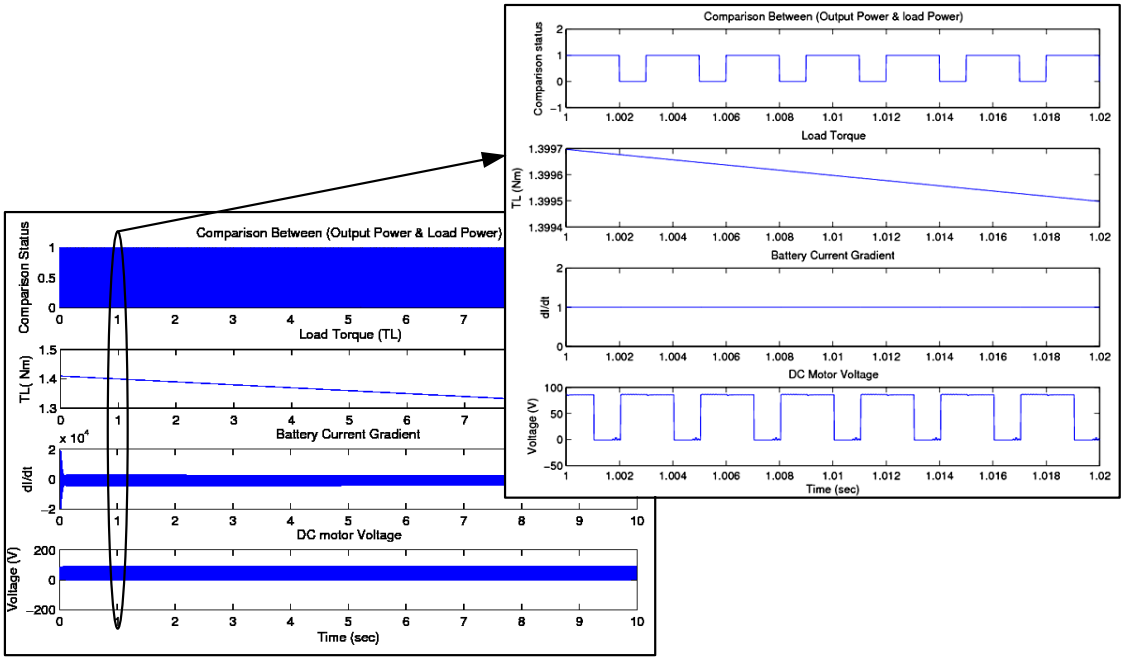

Fig. 3-14. Comparison between P_{out} and P_L, load torque (T_L), battery current gradient, and voltage across DC motor (armature voltage).

UC voltage is 21.5V (fully discharged) and battery voltage is 87V (fully charged). Considering the scenario when battery modules are fully charged, UC modules are fully discharged, power curve is shown with value = 1 and converter operates in motoring mode. During this interval, battery modules supply their power to the LV side. This is shown by codes 10 and 11 in both operating modes (forward motoring and reverse motoring).

However, when the power curve is shown with value = 0, with same conditions, whereby the motor needs power, battery modules supply their power to motor side, and

LV side is fully discharged. In this case, battery modules, instead of the LV side, supply their energy to the motor side in both operating modes (forward motoring and reverse motoring). This mode is shown by code 2. Fig. 3-15 shows the charge and discharge status of the hybrid energy sources, with related converter operating codes.

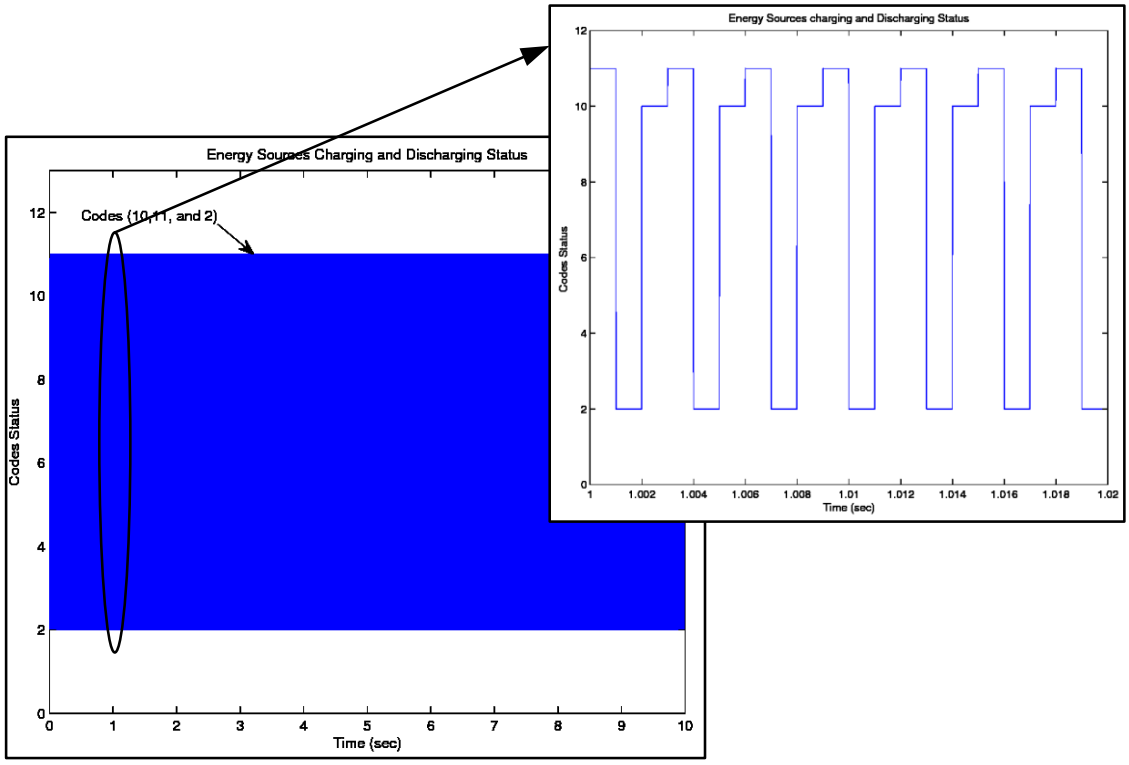

Fig. 3-15. Charge and discharge status of the hybrid energy sources, with codes.

Fig. 3-16 shows UC modules voltage and current during operation in codes 10, 11, and 2, when UC modules are charged by battery side (or when UC modules are disconnected from HV side).

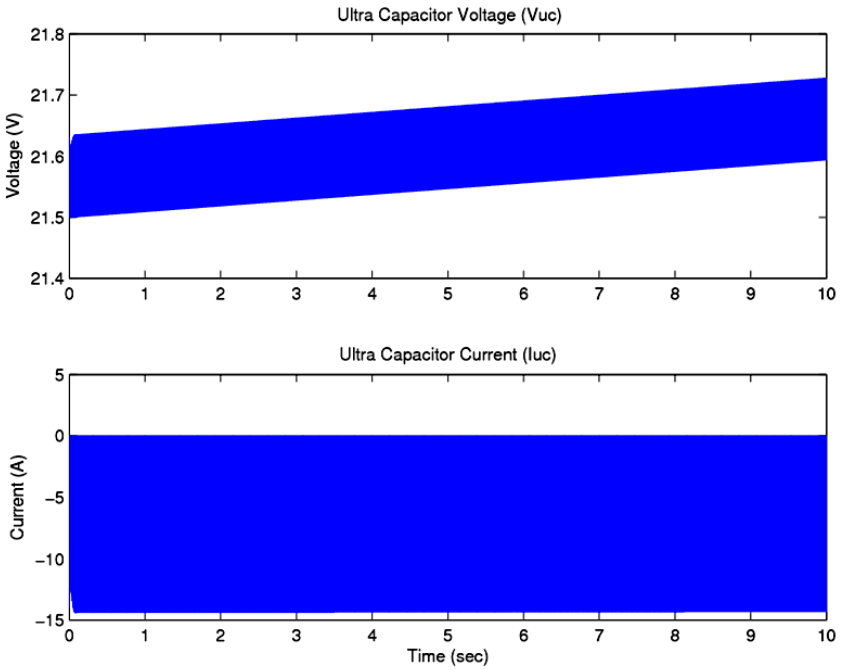

Fig. 3-16. UC modules voltage and current during charge (or when disconnected from HV side).

Additional simulation results of state of charge (SOC), current, and voltage of battery are shown in Fig. 3-17. As is evident, battery voltage gradually decreases, because battery modules supply their energy to motor side, during operation in code 2, as well as they transfer their energy to LV side, or UC modules, during operation in codes 10 and 11. Only during operation in code 11, battery voltage does not decrease, and it is constant, because they are disconnected from the converter.

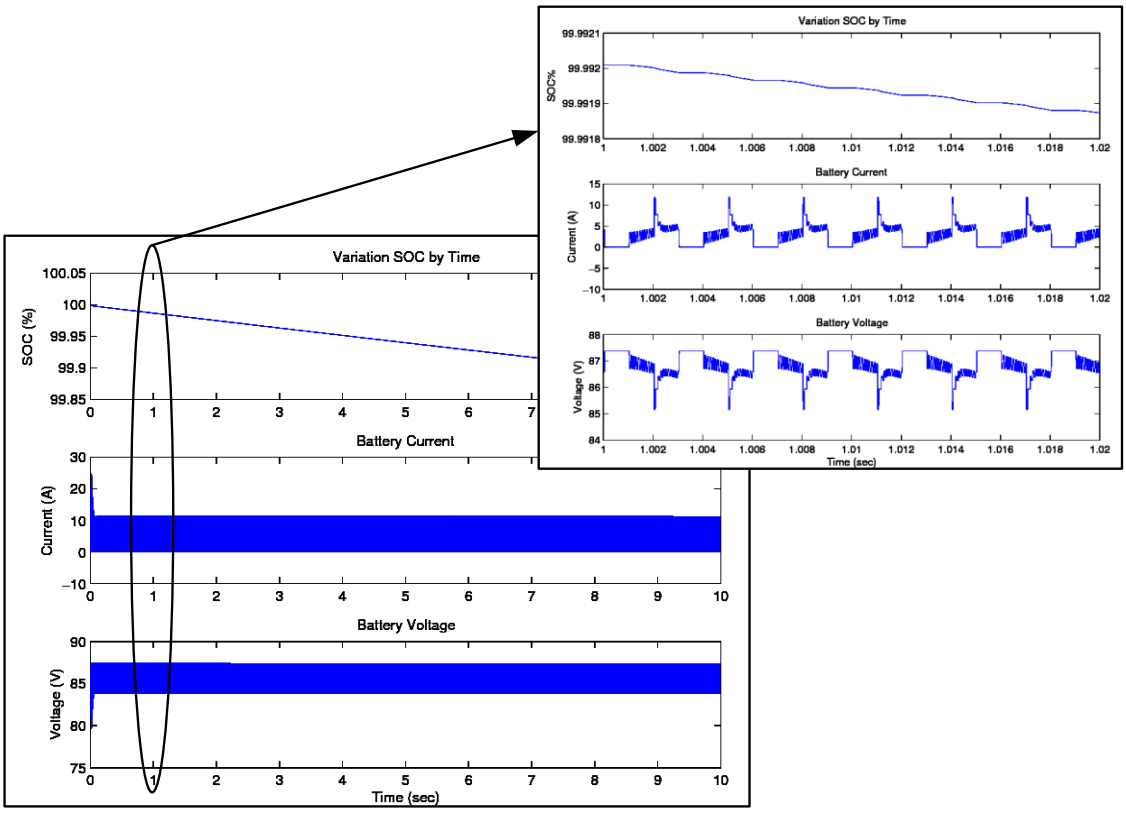

Fig. 3-17. Simulation results of state of charge (SOC), current, and battery voltage.

Furthermore, the simulation results of the tested separately excited DC machine are summarized in Fig. 3-18.

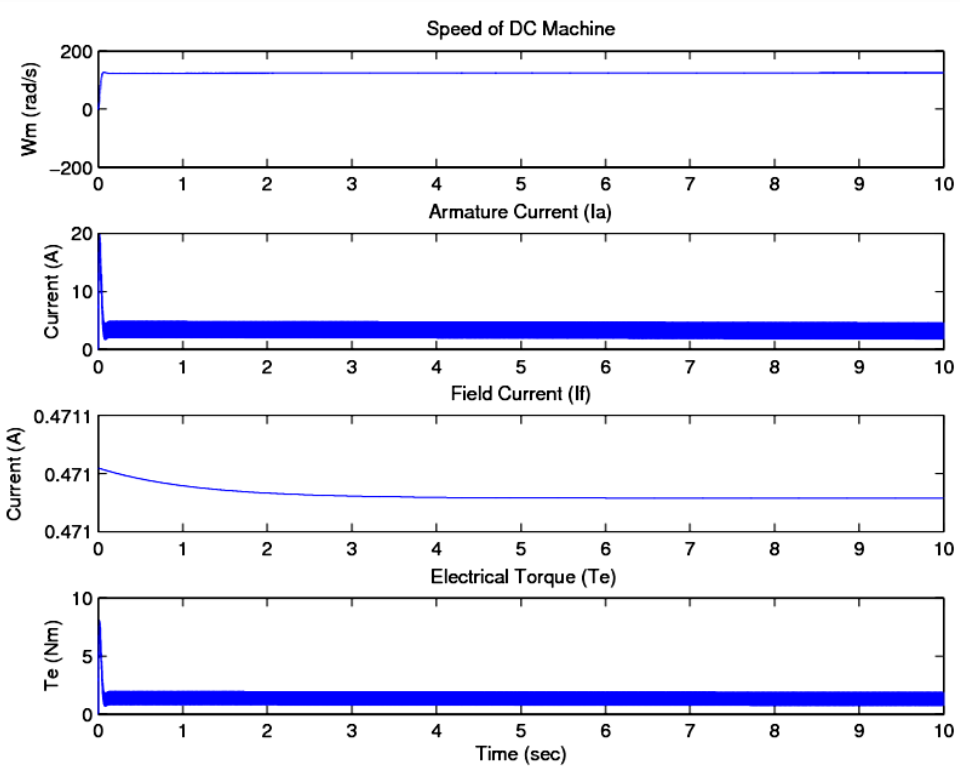

Fig. 3-18. Speed, armature current, field current and electrical torque of the tested DC machine.

Operation of switch numbers 1 through 8 and switches 9 through 16 are shown in Figs. 3-19 and 3-20, respectively. For example, when the converter is operating under code 10, S_5, S_3, S_{12}, and S_7 are on and D_8, D_4, D_{11}, and D_6 start conducting (capacitors C_1 and C_2 are charged by the HV side).

Under code 11 operation, S_6, S_9, S_{13} and S_1 are on and D_7, D_{10}, D_{14}, and D_2 start conducting. Capacitors C_1 and C_2 are disconnected from HV side and transfer their stored energy to the LV side. In both codes (10 and 11) operation, S_{16} is on, because motor does not stop and current flows in it. Also, under code 2 operation, switch S_5 is on and D_8 starts conducting.

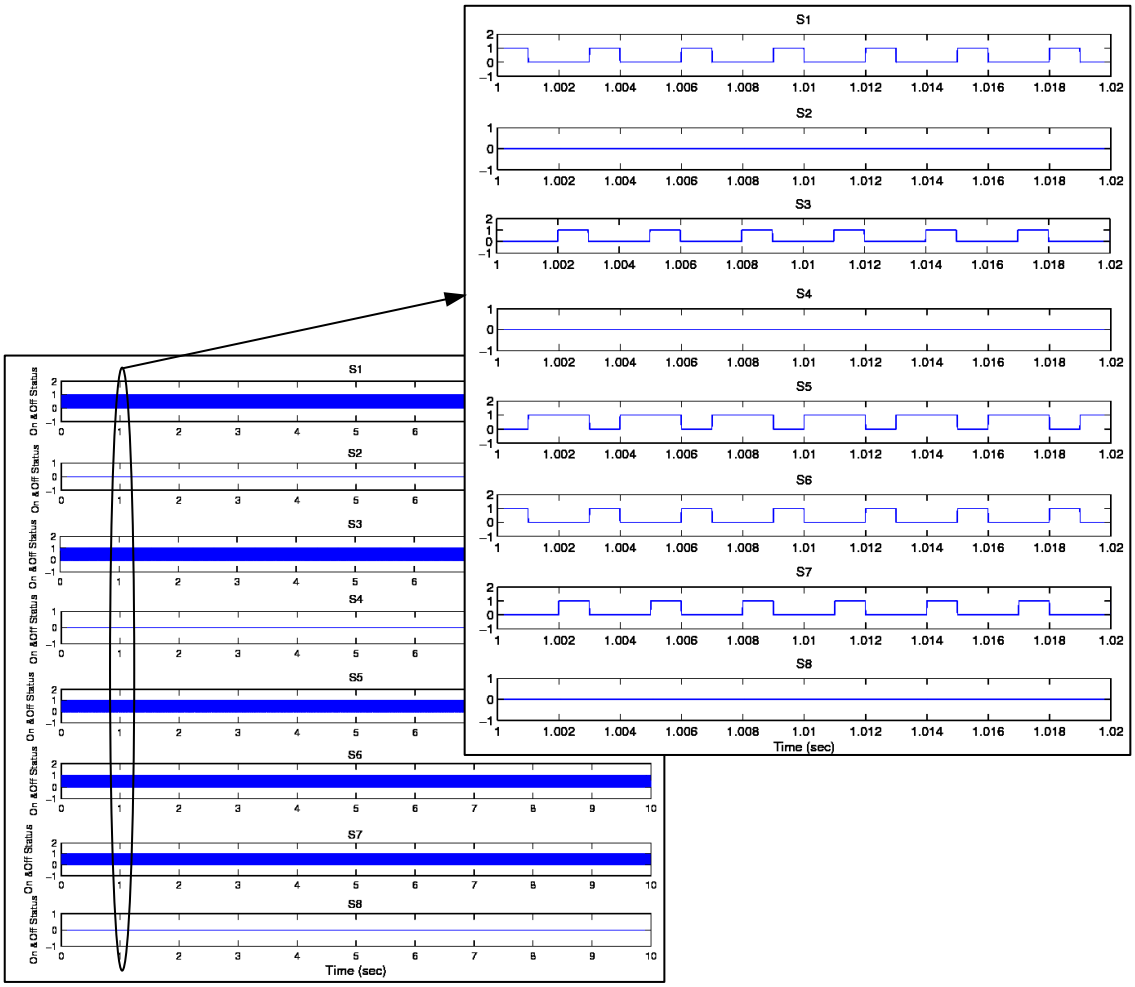

Fig. 3-19. Operation of each switch in simulation time.

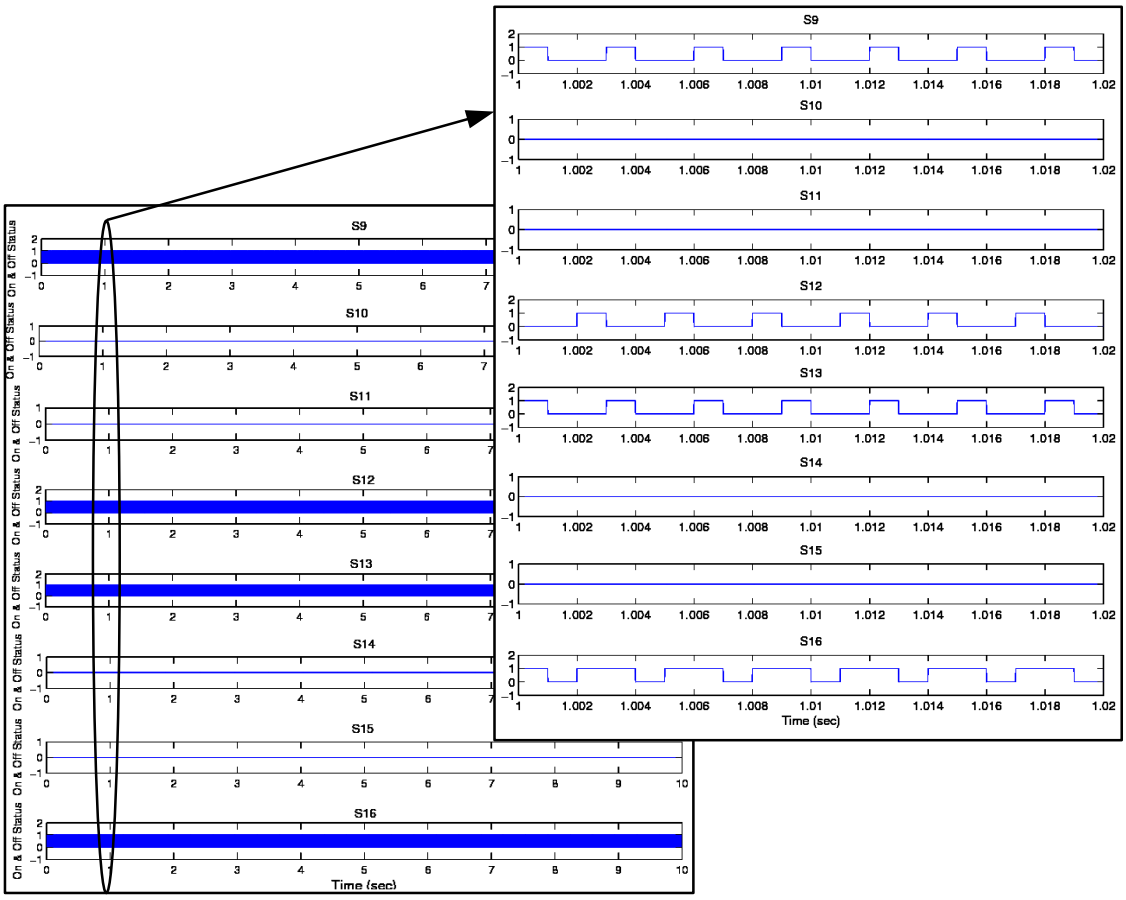

Fig. 3-20. Operation of each switch in simulation time.

The next section focuses on transfer efficiency modeling and analysis of the SC *Luo* converter.

3.1.4. TRANSFER EFFICIENCY MODELING AND ANALYSIS

The detailed transfer efficiency modeling and analysis of the SC *Luo* converter are explained in this section. As aforementioned, the SC *Luo* converter has 2 main modes of operation, the buck mode and boost mode. The buck mode uses the *current-amplification technique.* Capacitors C_1 and C_2 are charged during on-state in series and input current flows through them. These capacitors are discharged during off-state in parallel. Therefore, the output current is amplified by these capacitors. If the switching period, *T*,

is small enough (compared to the circuit time constant), an average current can be used, to replace its instantaneous value, for the purpose of integration. Also, capacitors C_1 and C_2 are of equal sizes, so that the voltage across each of them is equal. Therefore, the voltage across capacitor C_1 can be expressed as:

$$V_{C1}(t) = \begin{cases} V_C(0) + \frac{1}{C}\int_0^t I_C(t)dt \approx V_C(0) + \frac{t}{C}\overline{I_{Bat}} & 0 \le t \le kT \\ V_C(kT) + \frac{1}{C}\int_{kT}^t I_C(t)dt \approx V_C(kT) - \frac{t-kT}{2C}\overline{I_{UC}} & kT \le t \le T \end{cases} \quad (39)$$

If the switching period, T, is small enough (compared to the circuit time constant), initial values can be used, while ignoring trivial variations. Therefore, the current flowing through capacitor C_1 can be written as:

$$I_{C1}(t) = \begin{cases} \frac{V_{Bat}-4V_D-2V_{C(0)}}{R_{AN}}\left(1 - e^{\frac{-t}{C*R_{AN}}}\right) & 0 \le t \le kT \\ -\frac{-V_{UC}+V_C(kT)-3V_D}{R_{Af}}\left(e^{\frac{-t}{C*R_{Af}}}\right) & kT \le t \le T \end{cases} \quad (40)$$

Here,

$R_{AN} = 4\mathrm{r_S} + 2\mathrm{r_C}$ $\qquad$ $R_{Af} = 3\mathrm{r_S} + \mathrm{r_C}$

In fact, the capacitor C_1 current in buck mode is:

$$I_{C1}(t) = \begin{cases} \frac{V_{Bat}-4V_D-2V_C}{R_{AN}} = \overline{I_{Bat}} & 0 \le t \le kT \\ -\frac{-V_{UC}+V_C-3V_D}{R_{Af}} = -\frac{\overline{I_{UC}}}{2} & kT \le t \le T \end{cases} \quad (3\text{-}3)$$

$\overline{\mathrm{I_{Bat}}}$ is the average input current during the switch-on period, kT, and $\overline{\mathrm{I_{UC}}}$ is the average output current during the switch-off period, $(1–k)T$. The variation of the voltage across capacitor C_1 is:

$$\Delta V_{C1} = \begin{cases} \frac{1}{C}\int_0^{kT} I_C(t)dt = \frac{kT}{C}\overline{I_{Bat}} & 0 \le t \le kT \\ \frac{1}{C}\int_{kT}^{T} I_C(t)dt = \frac{(1-k)T}{2C}\overline{I_{UC}} & kT \le t \le T \end{cases} \quad (3\text{-}4)$$

Or

$$\Delta V_{C1} = \begin{cases} \frac{k}{Cf} * \frac{V_{Bat}-4V_D-2V_C}{R_{AN}} & 0 \le t \le kT \\ \frac{(1-k)}{Cf} * \frac{-V_{UC}+V_C-3V_D}{2R_{Af}} & kT \le t \le T \end{cases} \quad (3\text{-}5)$$

Also, voltage across capacitor C_1 can be written as:

$$V_{C1} = \frac{2kR_{Af}(V_{Bat}-4V_D)+(1-k)R_{AN}(V_{UC}+3V_D)}{(1-k)R_{AN}+4kR_{Af}} \quad (3\text{-}6)$$

Hence,

$$\Delta V_{C1} = \frac{k(1-k)[V_{Bat}-(2V_{UC}+10V_D)]}{fC((1-k)R_{AN}+4kR_{Af})} \quad (3\text{-}7)$$

Then capacitor C can be expressed as:

$$C = \frac{k(1-k)[V_{Bat}-(2V_{UC}+10V_D)]}{2f(V_C-V_C(0))((1-k)R_{AN}+4kR_{Af})} \quad (3\text{-}8)$$

In addition, the average input current is:

$$I_{Bat} = \frac{1}{T}\int_0^{kT} I_C(t)dt = k\frac{V_{Bat}-4V_D-2V_C}{R_{AN}} \quad (3\text{-}9)$$

And the average output current is:

$$I_{UC} = \frac{1}{T}\int_{kT}^{T} I_C(t)dt = (1-k)\frac{-V_{UC}+V_C-3V_D}{R_{Af}} \quad (3\text{-}10)$$

The total input power is given by:

$$\boldsymbol{P_I = V_{Bat} * I_{Bat} = V_{Bat} * k\frac{V_{Bat}-4V_D-2V_C}{R_{AN}}} \quad (3\text{-}11)$$

And the output power is expressed as:

$$P_O = V_{UC} * I_{UC} = V_{UC} * (1-k)\frac{-V_{UC}+V_C-3V_D}{R_{Af}} \quad (3\text{-}12)$$

Hence, the overall transfer efficiency can be computed as:

$$\boldsymbol{\eta = \frac{P_O}{P_I} = \frac{V_{UC}*(1-k)(-V_{UC}+V_C-3V_D)*R_{AN}}{V_{Bat}*k*(V_{Bat}-4V_D-2V_C)*R_{Af}}} \quad (3\text{-}13)$$

During buck mode (or codes 10 and 11), the battery modules are half charged (or fully charged), and UC modules are fully discharged.

As aforementioned, the boost mode implements the *voltage-lift technique.* The capacitors C_1 and C_2 are charged in parallel during on-state and input voltage is applied across them. The capacitors are discharged in series during off-state. Therefore, the output voltage is lifted by the capacitors. Thus, the voltage across capacitor C_1 can be expressed as:

$$V_{C1}(t) = \begin{cases} V_C(0) + \frac{1}{C}\int_0^t I_C(t)dt \approx V_C(0) + \frac{t}{2C}\overline{I_{Uc}} & 0 \le t \le kT \\ V_C(kT) + \frac{1}{C}\int_{kT}^t I_C(t)dt \approx V_C(kT) - \frac{t-kT}{C}\overline{I_{Bat}} & kT \le t \le T \end{cases} \quad (3\text{-}14)$$

Also, current flowing through capacitor C_1 can be written as:

$$I_{C1}(t) = \begin{cases} \frac{V_{UC}-V_C(0)-3V_D}{R_{BN}}\left(1 - e^{\frac{-t}{C*R_{BN}}}\right) & 0 \le t \le kT \\ -\frac{-V_{Bat}+2V_C(kT)-4V_D}{R_{Bf}}\left(e^{\frac{-t}{C*R_{Bf}}}\right) & kT \le t \le T \end{cases} \quad (3\text{-}15)$$

Here,

$R_{BN} = 3\mathrm{r_S} + \mathrm{r_C} \qquad R_{Bf} = 4\mathrm{r_S} + 2\mathrm{r_C}$

In fact, the capacitor C_1 current in boost mode is:

$$\boldsymbol{I_{C1}(t) = \begin{cases} \frac{V_{UC}-V_C-3V_D}{R_{BN}} = \frac{\overline{I_{UC}}}{2} & 0 \le t \le kT \\ -\frac{-V_{Bat}+2V_C-4V_D}{R_{Bf}} = -\overline{I_{Bat}} & kT \le t \le T \end{cases}} \quad (3\text{-}16)$$

$\overline{\mathrm{I_{UC}}}$ is the average input current during the switch-on period, kT, and $\overline{\mathrm{I_{Bat}}}$ is the average output current during the switch-off period, $(1 - k)T$. The variation of the voltage across capacitor C_1 is:

$$\Delta V_{C1} = \begin{cases} \frac{k}{Cf} * \frac{V_{UC}-V_C-3V_D}{2R_{BN}} & 0 \le t \le kT \\ \frac{(1-k)}{Cf} * \frac{-V_{Bat}+2V_C-4V_D}{R_{Bf}} & kT \le t \le T \end{cases} \quad (3\text{-}17)$$

Also, the voltage across capacitor C_1 can be written as:

$$\boldsymbol{V_{C1} = \frac{kR_{Bf}(V_{UC}-3V_D)+2(1-k)R_{BN}(V_{Bat}+4V_D)}{4(1-k)R_{BN}+kR_{Bf}}} \quad (3\text{-}18)$$

Hence,

$$\Delta V_{C1} = \frac{k(1-k)[2V_{UC}-10V_D-V_{Bat}]}{fC(4(1-k)R_{BN}+kR_{Bf})} \quad (3\text{-}19)$$

In addition, the average input current is:

$$\boldsymbol{I_{UC} = \frac{1}{T}\int_0^{kT} I_C(t)dt = k\left(\frac{V_{UC}-V_C-3V_D}{R_{BN}}\right)} \quad (3\text{-}20)$$

And the average output current is:

$$\boldsymbol{I_{Bat} = \frac{1}{T}\int_{kT}^{T} I_C(t)dt = (1-k)\frac{-V_{Bat}+2V_C-4V_D}{R_{Bf}}} \quad (3\text{-}21)$$

Upon determining the total input and output power, the overall transfer efficiency can be computed as:

$$\eta = \frac{P_O}{P_I} = \frac{V_{Bat}*[(1-k)(\frac{-V_{Bat}+2V_C-4V_D}{R_{Bf}})]}{V_{UC}*k*(\frac{V_{UC}-V_C-3V_D}{R_{BN}})} \quad (3\text{-}22)$$

In boost mode (or codes 3 and 4), the battery modules are fully discharged and the UC modules are half charged (or fully charged).

3.2. SUMMARY

This chapter presented a novel control technique for a hybrid 4-Q SC *Luo* bi-directional DC/DC converter applicable for HEV energy storage system applications. Table 3-1 below shows the transfer efficiency comparison between three types of converters (SCC, interleaved SCC, and SC *Luo* converter).

Table 3-1. Transfer efficiency comparison between three type converters.

	Transfer Efficiency	
Converter Characteristic	**Buck Mode**	**Boost Mode**
Switched Capacitor Converter (SCC)	**40%**	**68%**
Interleaved Switched Capacitor Converter	**73%**	**70%**
4-Q Switched Capacitor *Luo* Converter	**97%**	**70%**

It is clear, that for HEV energy storage applications, the 4-Q SC *Luo* converter has transfer efficiencies higher than those compared to the SCC and interleaved SCC. This is due to the fact that, during both operation modes (buck and boost) of the SC *Luo* converter, the converter equivalent resistance (especially the resistances of capacitors C_1 and C_2) are in parallel. As a result, reduced overall losses can be experienced, and the resulting efficiency is enhanced.

CHAPTER 4

EXPERIMENTAL SETUP AND CONTROLLER IMPLEMENTATION

4.1. EXPERIMENTAL TEST SETUP

This section focuses on the experimental implementation and controller verification for the proposed 4-Q SC *Luo* converter. Fig. 4-1 shows the experimental set-up, which is used for practical implementation of the SC *Luo* converter. The experimental test set-up consists of 24 cells Li-ion polymer battery (10Ah), 16 cells ultra capacitor (BCAP 1200 P270) and a 1 HP permanent-magnet DC machine (PMDC).

A digital signal processor (*eZdsp*^{TM} F2812) is used to implement the control strategy. The *eZdsp*^{TM} F2812 is a digital controller for rapid prototyping, which can be directly programmed with the Simulink file used for simulation runs. This setup is accompanied with a user interface for operating, managing, and monitoring the experimental results. A schematic representation of the experimental set-up is shown in Fig. 4-1, while the specifications of key components of the setup are shown in Table 4-1.

Table 4-1. Specifications of circuit parameters.

Parameters Characteristics	Nominal Capacity	Internal Resistance (ESR)	Nominal Voltage
Li-Ion polymer Battery	10Ah	≤10 mΩ	3.75 V
BCAP 1200P270T04	1200 F	0.58 mΩ	2.7 V
Prime mover DC machine (PMDC)	-	0.12368 Ω	150 V
Capacitors (C_1, C_2)	1mF	0.216 Ω	450 V

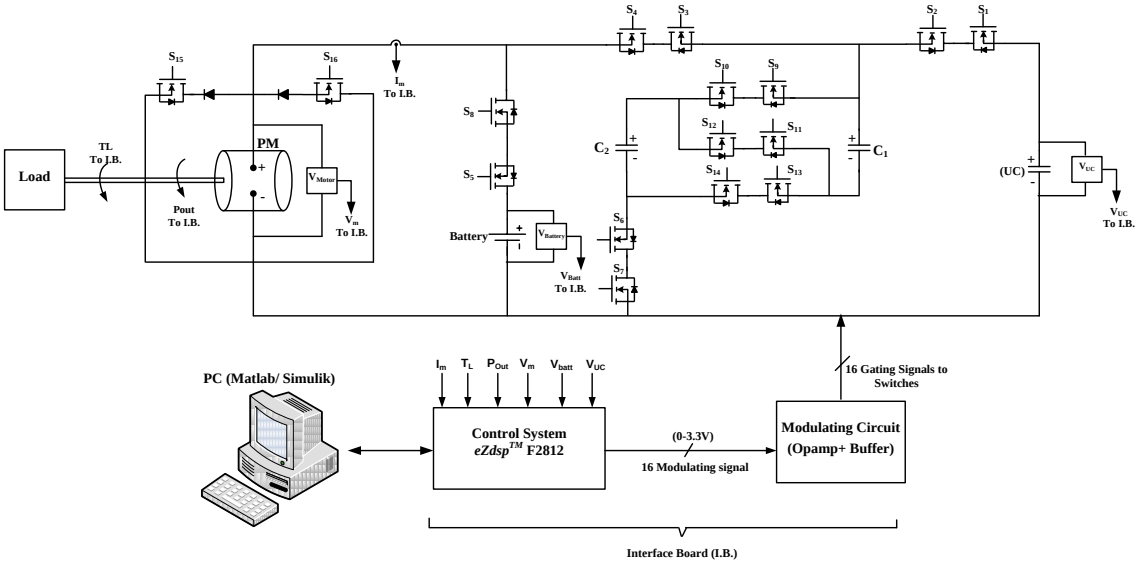

Fig. 4-1. Experimental set-up for implementing the SC *Luo* converter.

4.2. DSP CONTROLLER IMPLEMENTATION

The *eZdsp*^{TM} F2812 is a multi-layered printed circuit board (PCB), which includes four major logic blocks; 1) Analog interface connector (ADC connector), 2) I/O interface connector (DAC connector), 3) JTAG interface, and 4) Parallel port/JTAG controller interface. Fig. 4-2 shows the input/output signals to and from DSP F2812 control board.

The main advantage of this setup is the provision of additional block-set libraries in Matlab/Simulink, which include analog-to-digital converter (ADC) as well as digital-to-analog converter (DAC) blocks. The output values of ADC are in the range (0 to 4095), because the ADC is 12-bit converter. The voltage level for the *eZdsp*^{TM} F2812, which can receive input signals and send output signals to individual switch gating circuitry, varies from 0 V to 3.3 V.

The maximum current that the controller can supply to the output signals is around 307 mA. An electronic board was used to provide the required current for the drive circuit of the switches, which is around 25 mA.

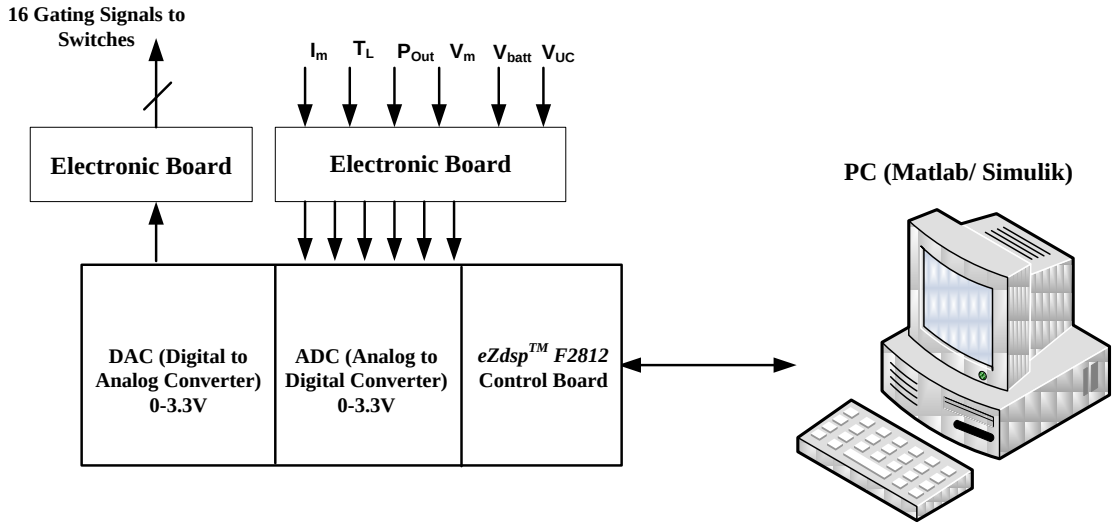

Fig. 4-2. Input/output signals to and from DSP control board.

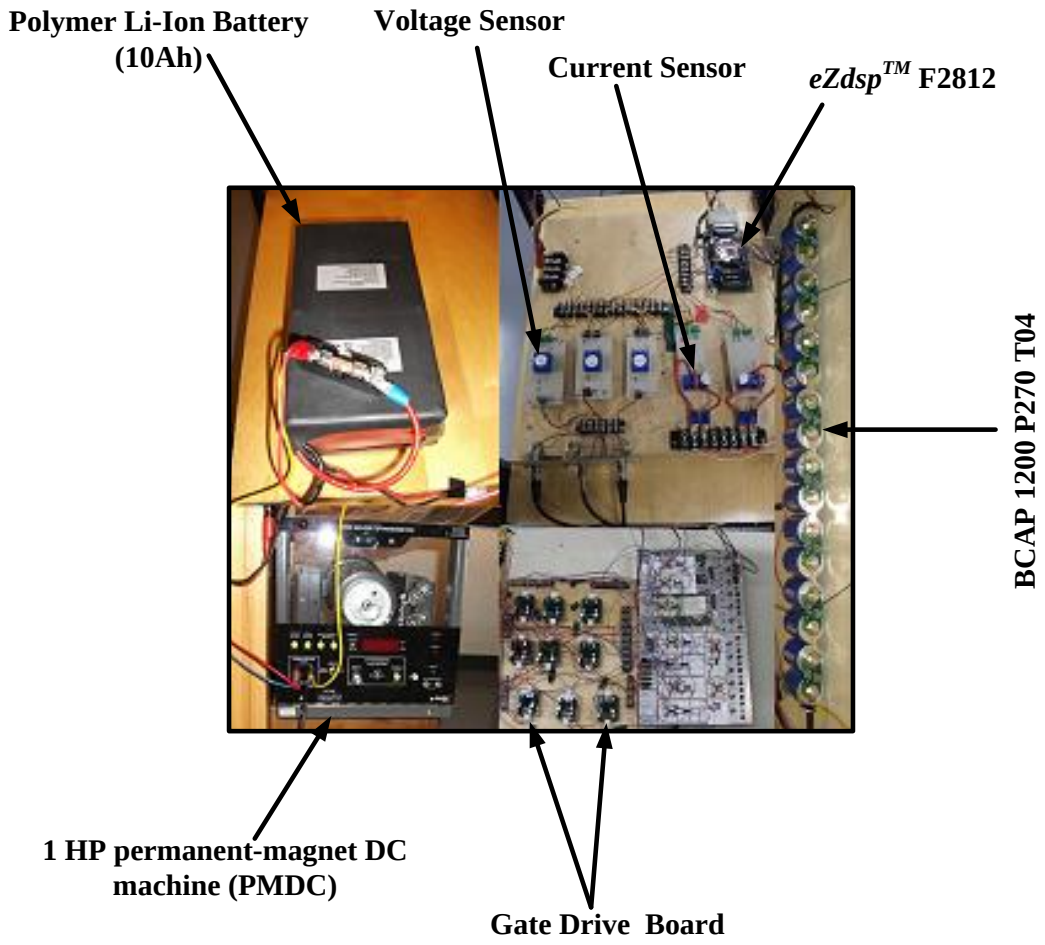

Fig. 4-3. Experimental set- up consisting of battery, UC modules, voltage and current sensor, PMDC, DSP, and gate drive.

Fig. 4-3 shows the experimental set-up for the implementation of the SC *Luo* converter and testing of the proposed control strategy. The experimental set-up consists of lithium-polymer battery modules (24 cells in series), 16 cells of ultra capacitors in series, with voltage management board, 1 HP permanent-magnet DC machine, current and voltage sensors, gate drive board, and the *eZdsp*^{TM} F2812 controller.

4.3. EXPERIMENTAL TEST RESULTS

This section focuses on experimental results of buck mode (codes 10 and 11), codes 3 and 1, code 2 (when the battery modules supply energy to motor), and the case when the converter operates in generating mode ($P < 0$).

Considering buck mode, when $P_{out} \geq P_L$, high voltage DC (battery modules) are fully charged and low voltage side (UC modules) are fully discharged. Fig. 4-4 shows voltage across of each capacitor, voltage across of DC motor (armature voltage), and operation of switches S_3 and S_9 during operation in codes 10 and 11, respectively.

As is clear, under code 10 operation, when switches S_5, S_3, S_{12}, and S_7 are on, Capacitors C_1 and C_2 are charged by HV side, and the voltage across of each capacitor increases. Also, the battery modules supply their energy to motor side and during buck operation mode, S_{16} is on. This is due to the fact that the motor does not stop.

After this operating stage, during operation in code 11, when switches S_6, S_9, S_{13} and S_1 are on, Capacitors C_1 and C_2 are disconnected from HV side, and transfer their stored energy to the LV side. At this time, as is evident from Fig. 4-4, voltage across of each capacitor decreases.

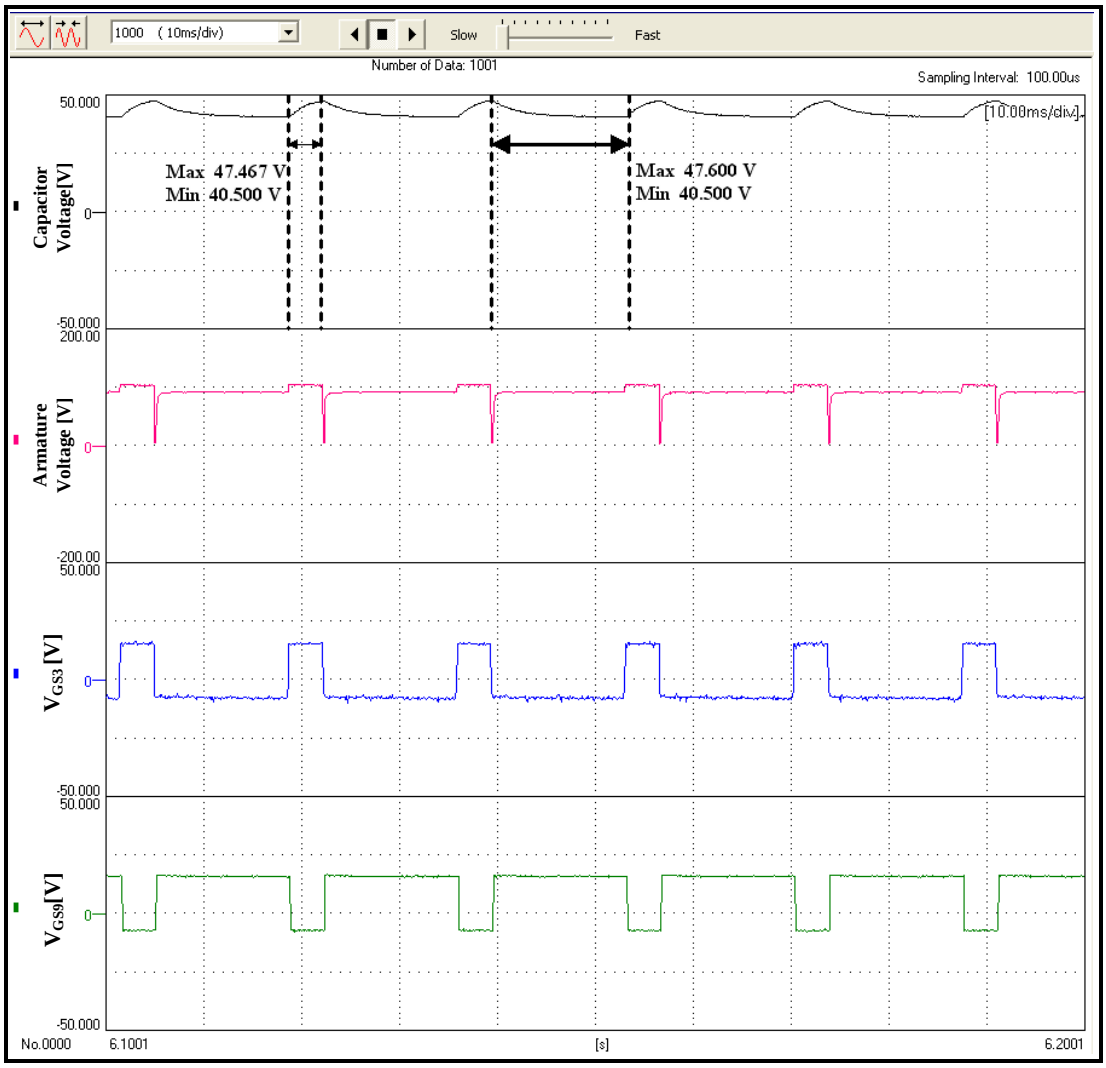

Fig. 4-4. Capacitor voltage (V_{C1} or V_{C2}), armature voltage, operation of switches S_3 (V_{GS3}) and S_9 (V_{GS9}).

Fig. 4-5 shows the voltage of the UC modules, current, and the operation of switch S_9, when UC modules are charged by capacitors (or when UC modules are disconnected from capacitors). Fig. 4-6 shows the motor voltage, current, and operation of switch S_3, respectively.

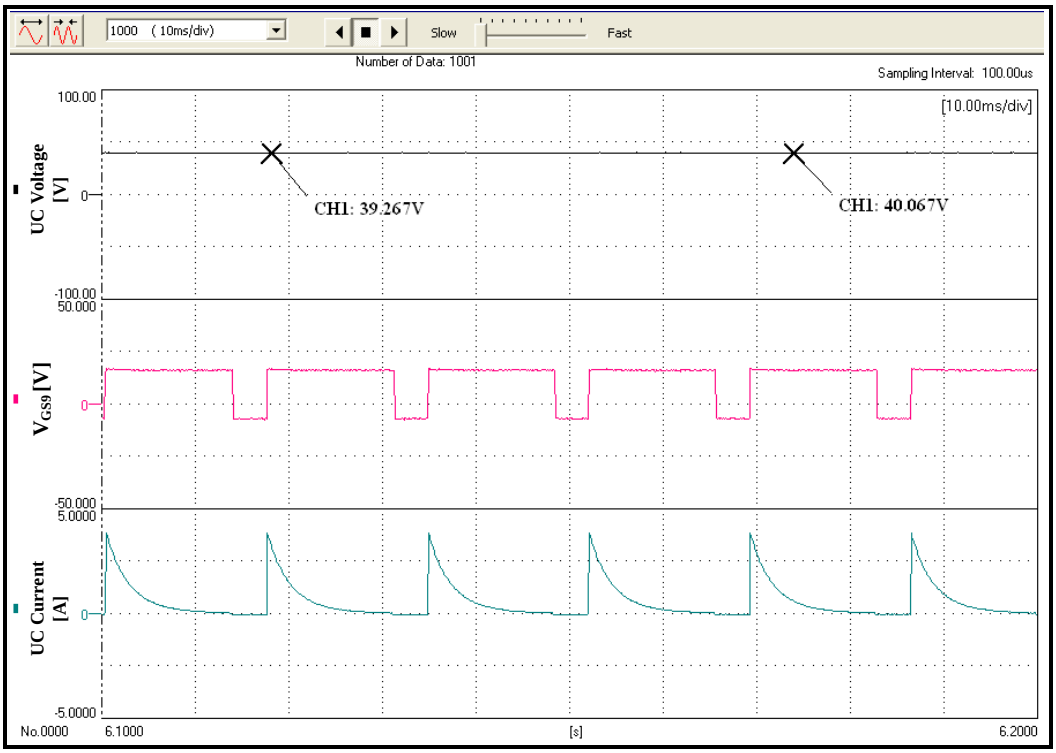

Fig. 4-5. Voltage of UC module, operation of switch S_9 (V_{GS9}), and UC module current.

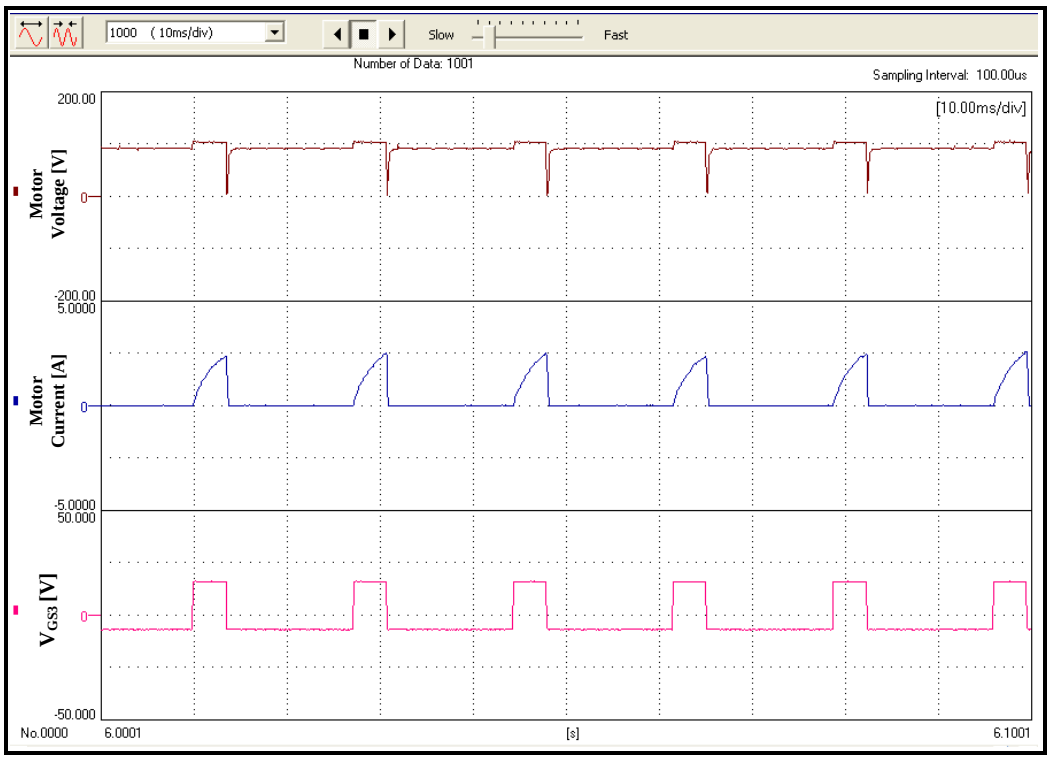

Fig. 4-6. Motor voltage, current, and operation of switch S_3 (V_{GS3}).

Fig. 4-7 depicts the operation of switches S_5, S_{12}, S_7, S_9, S_1, and S_{16}. As is clear, when the converter is operating under code 10, S_5, S_3, S_{12}, and S_7 are on, and D_8, D_4, D_{11}, and D_6 start conducting (capacitors C_1 and C_2 are charged by HV side).

Under code 11 operation, S_6, S_9, S_{13}, and S_1 are on, and D_7, D_{10}, D_{14}, and D_2 start conducting. Capacitors C_1 and C_2 are discharged and transfer their stored energy to the LV side. In both codes (10 and 11), S_{16} is on, because motor does not stop, and current flows through the armature.

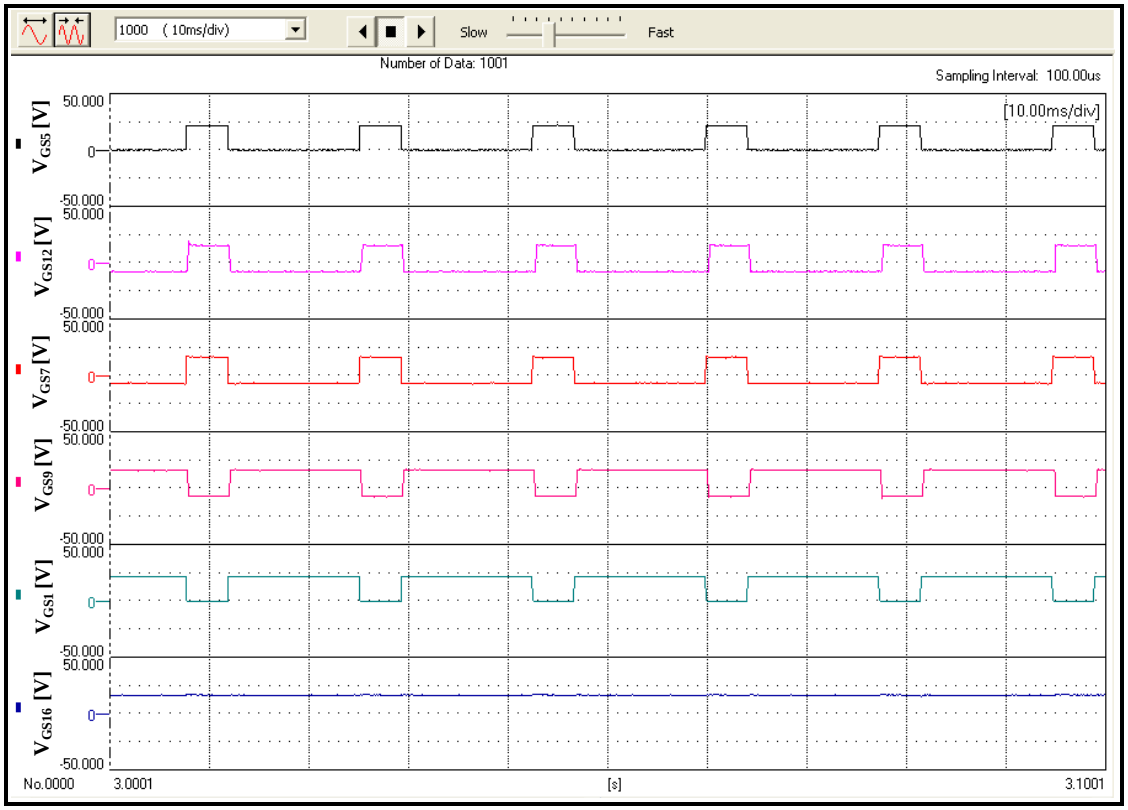

Fig. 4-7. V_{GS} (gate-to-source voltage) of switches S_5, S_{12}, S_7, S_9, S_1, and S_{16}.

Fig. 4-8 shows the overall converter transfer efficiency (η) for varying duty cycle, *k*, under codes 10 and 11. Average transfer efficiency in buck mode is computed to be around 88%.

It is evident from Fig. 4-8 that conduction duty does not influence transfer efficiency significantly. However, k does affect P_I (input power) and P_o (output power) in a diminutive region.

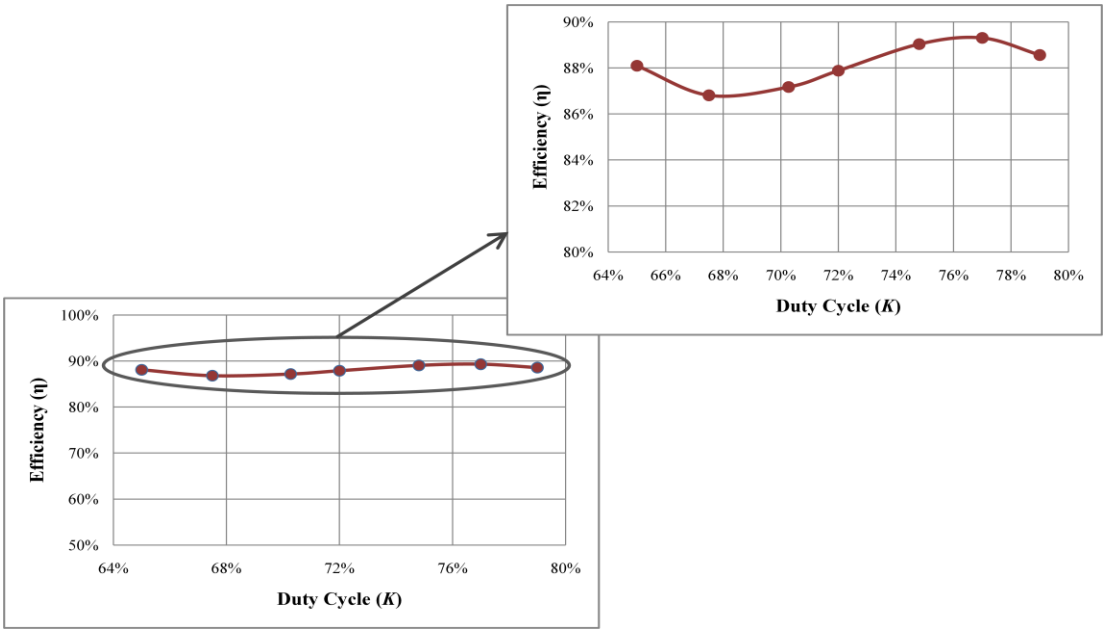

Fig. 4-8. Overall transfer efficiency vs. varying converter duty cycle.

Consider codes 3 and 1, $P_{out} < P_L$, and UC modules transfer their power to motor side. Fig. 4-9 depicts the voltage across of each capacitor, voltage across the DC motor (armature voltage), and operation (gate-to-source voltage) of switches S_2 and S_4 during codes 3 and 1, respectively.

As shown in Fig. 4-9, under code 3 operation, when switches S_2, S_{10}, S_{14}, and S_7 are on, capacitors C_1 and C_2 are charged by LV side in parallel, and voltage across of each capacitor increases. Also during this interval, S_{16} is on, because motor does not stop.

After this operating stage, during operation in code 1, when switches S_6, S_{11}, and S_4 are on, capacitors C_1 and C_2 are disconnected from LV side, and transfer their stored energy to motor side. At this time, the voltage across each capacitor decreases.

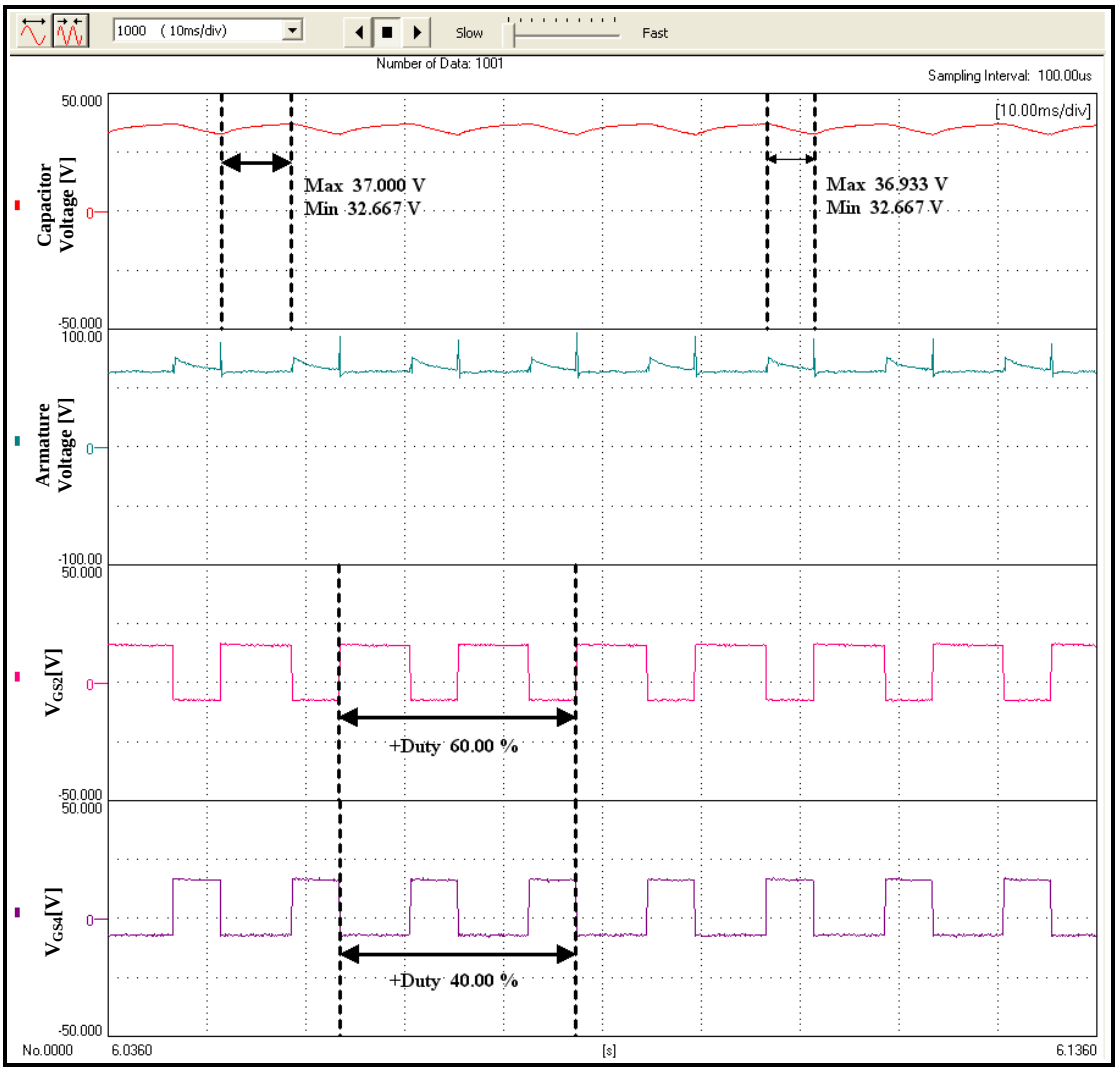

Fig. 4-9. Capacitor voltage (V_{C1} or V_{C2}), armature voltage, operation of switches S_2 (V_{GS2}) and S_4 (V_{GS4}).

Fig. 4-10 shows UC module voltage that gradually decreases and supplies power to motor. Fig. 4-11 represents UC module current and gate-to-source voltage of S_2. Fig. 4-12 depicts motor voltage, current, and operation of switch S_4.

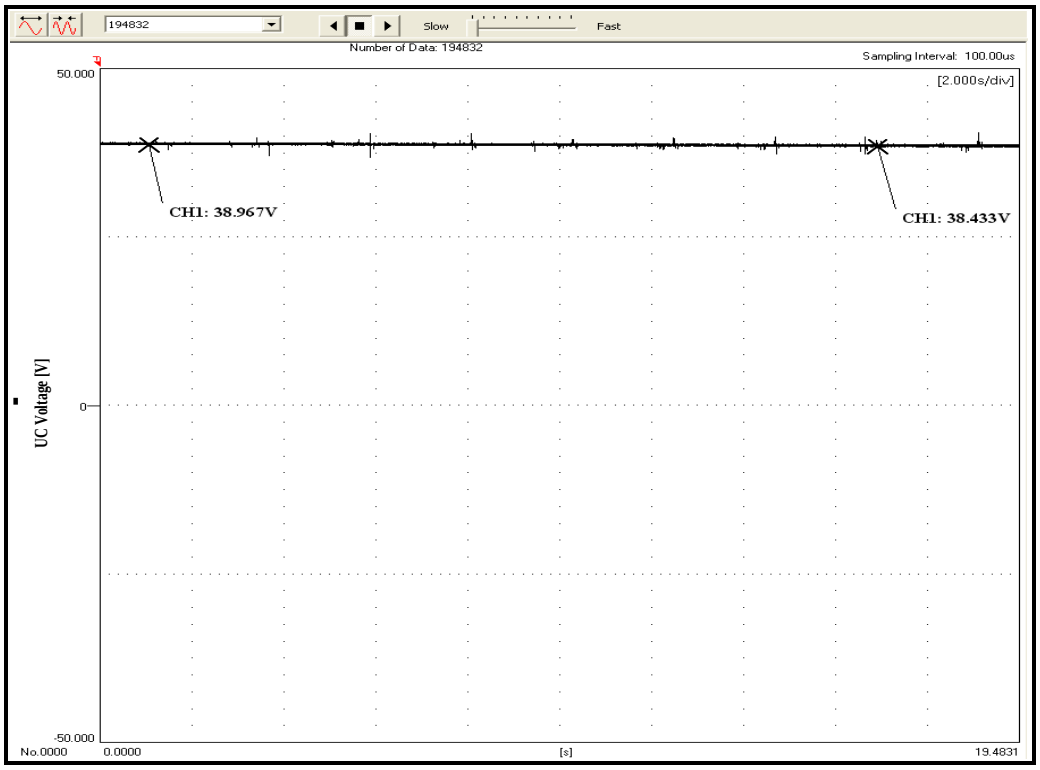

Fig. 4-10. Voltage across UC module.

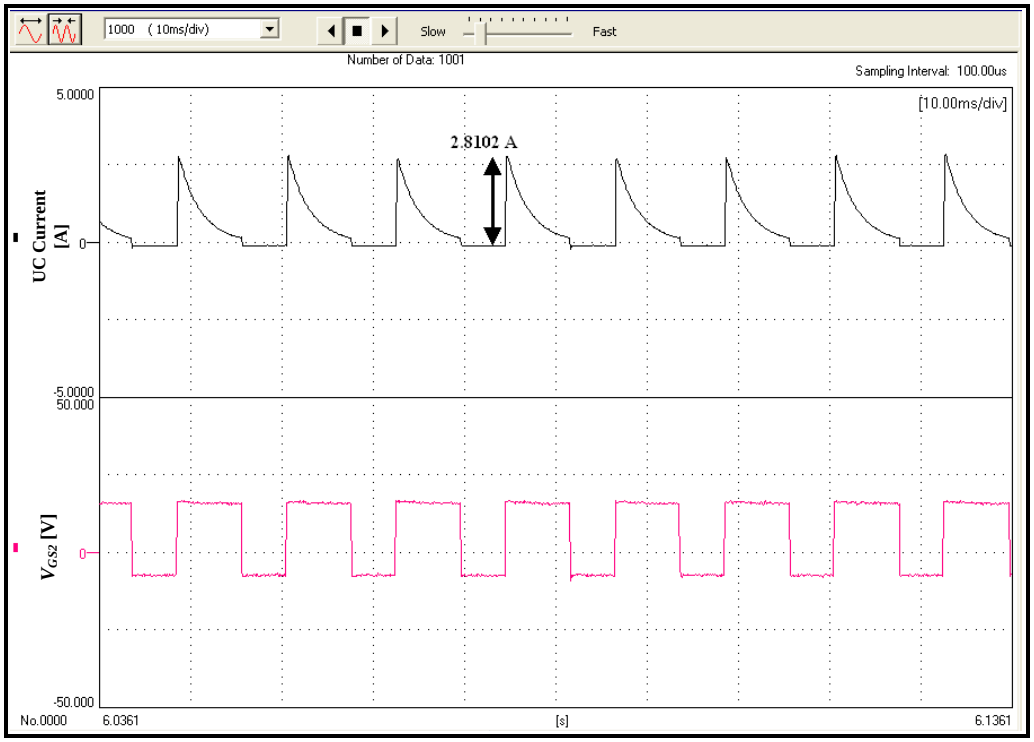

Fig. 4-11. UC module current and operation of switch S_2 (V_{GS2}).

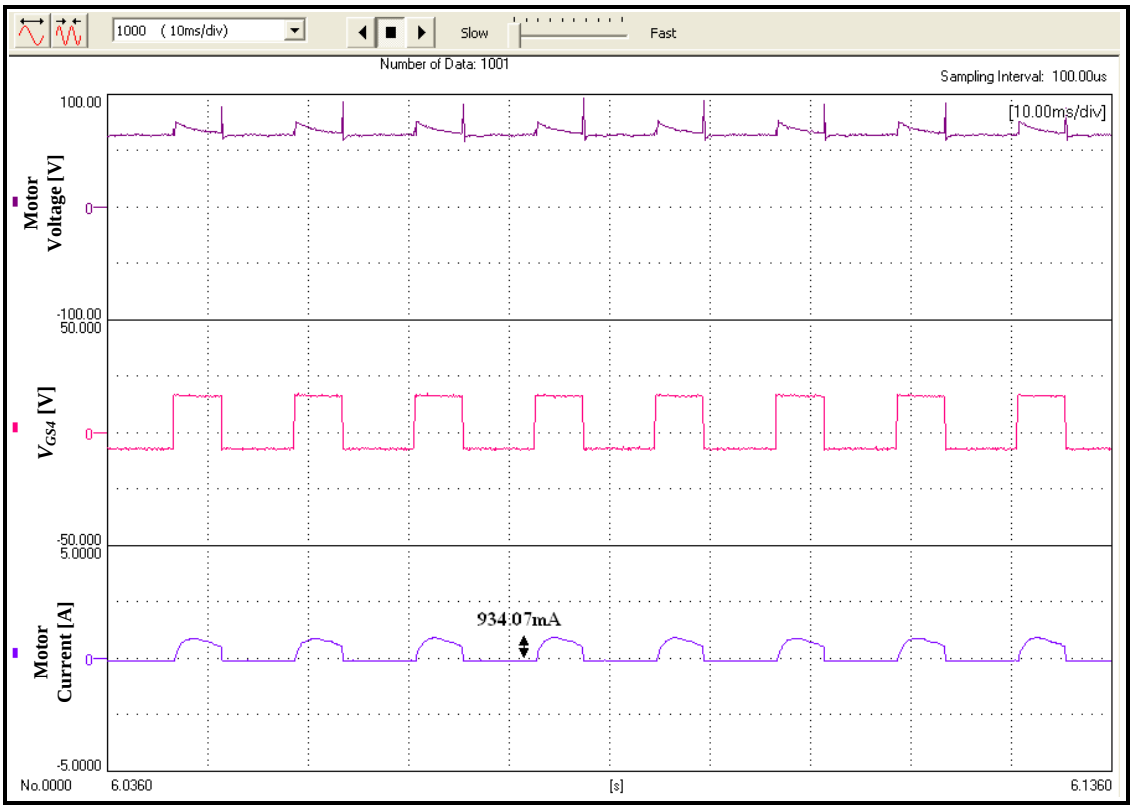

Fig. 4-12. Motor voltage, operation of switch S_4 (V_{GS4}), and motor current.

Operation of switches S_2, S_{10}, S_7, S_{11}, S_4, and S_{16} are shown in Fig. 4-13. As is clear, when the converter is operated under code 3, S_2, S_{10}, S_{14} ,S_7, and S_{16} are on, and D_1, D_9, D_{13}, and D_6 start conducting (capacitors C_1 and C_2 are charged by the LV side). Under code 1 operation, S_6, S_{11}, and S_4 are on, and D_7, D_{12}, and D_3 start conducting. Capacitors C_1 and C_2 are discharged and transfer their stored energy to motor side.

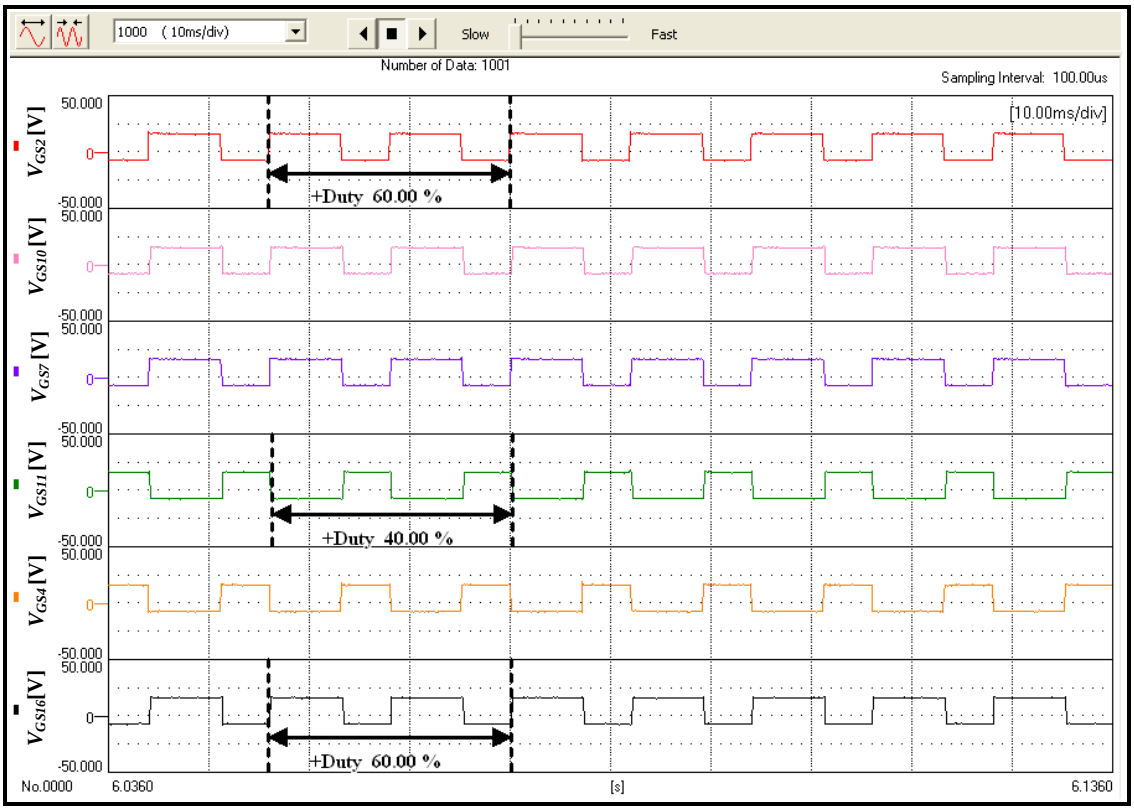

Fig. 4-13. Operation of switches S_2, S_{10}, S_7, S_{11}, S_4, and S_{16}.

Fig. 4-14 shows the overall computed energy transfer efficiency (η) versus varying conduction duty cycle, *k*, under codes 3 and 1.

Average transfer efficiency in this mode is calculated to be about 87%. Thus, it is evident that conduction duty does not affect the transfer efficiency significantly. However, *k* does affect P_I (input power) and P_o (output power) in a diminutive region.

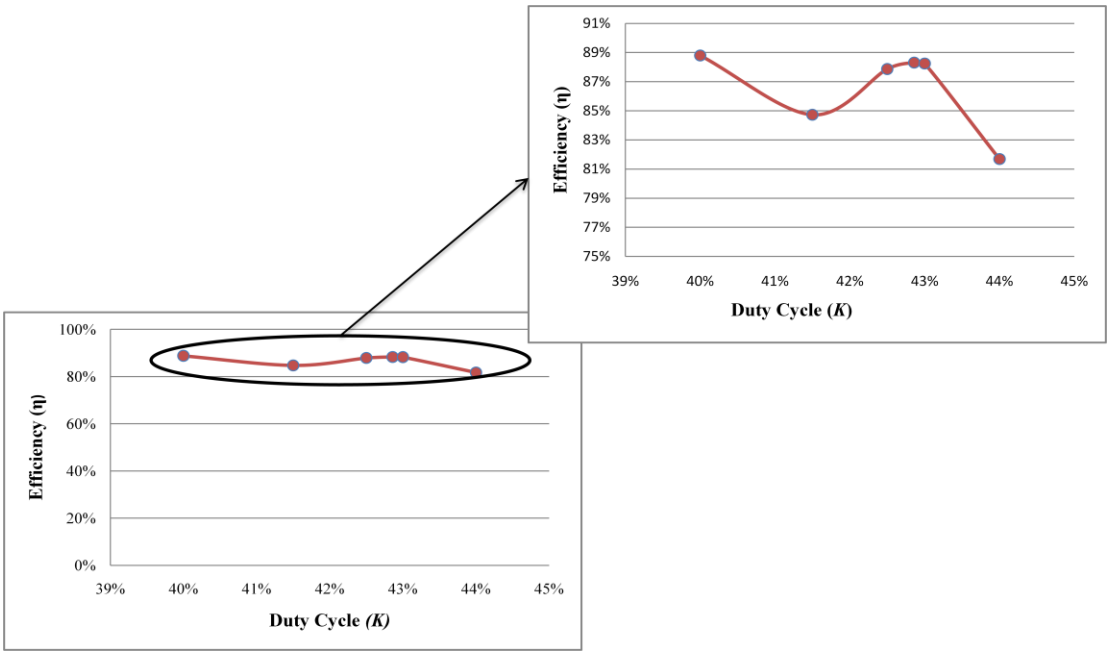

Fig. 4-14. Overall transfer efficiency versus varying duty cycle.

Now, consider code 2, when the battery modules are fully charged, UC modules are fully discharged, and $P_{out} < P_L$. When the motor needs power, battery modules supply their power to motor side, and LV side is fully discharged.

In this specific case, the battery modules, instead of the LV side (UC modules), supply their energy to the motor, in both operating modes (forward motoring as well as reverse motoring).

Figs. 4-15 and 4-16 depict motor and battery voltage as well as current, respectively. Fig. 4-17 shows the gate-to-source voltage of switch S_5 (V_{GS5}), which conducts throughout the duration of this mode (code 2).

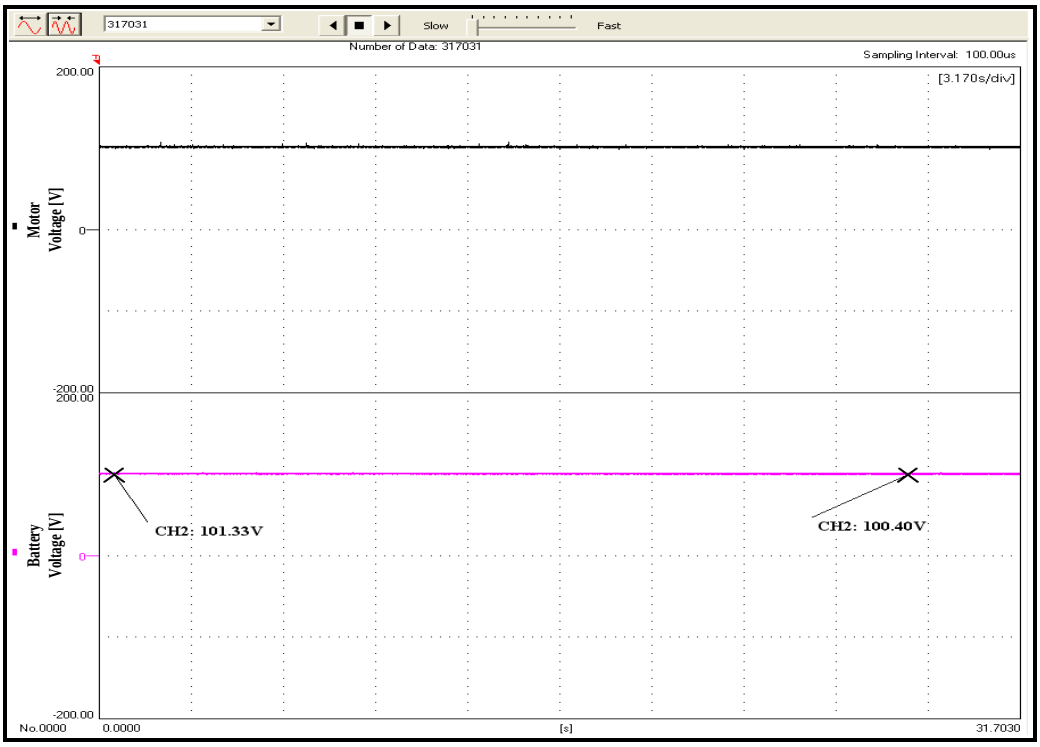

Fig. 4-15. Motor armature and battery voltage.

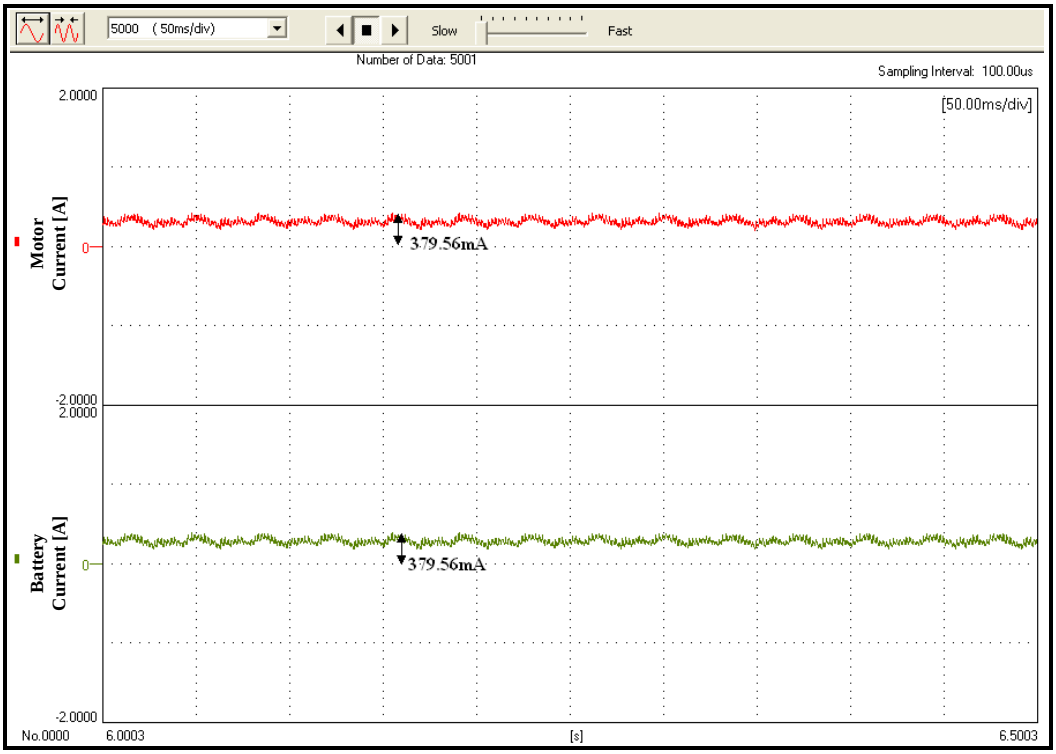

Fig. 4-16. Motor armature and battery current.

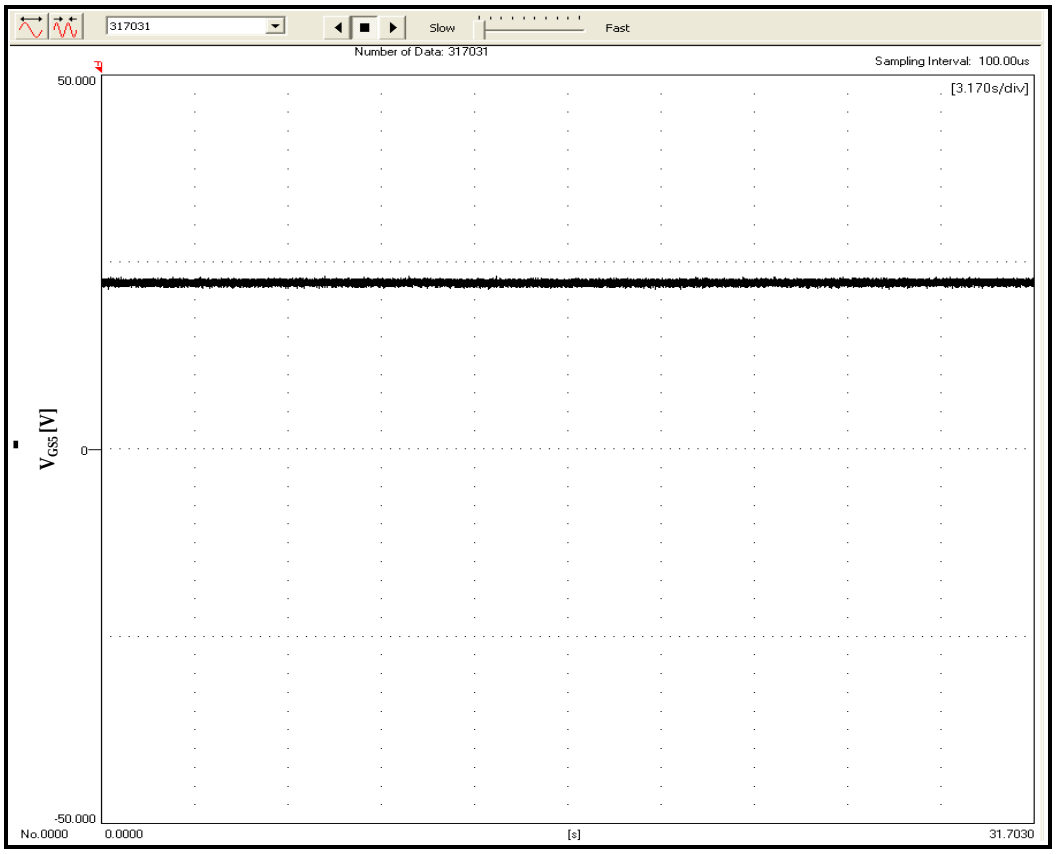

Fig. 4-17. Operation of switch S_5 (V_{GS5}).

In the generating mode, the motor tends to give up its power; thus, it is not compared with load power. In this operating mode, only battery current gradient is considered. In codes zero and 12, low voltage side (UC modules) are fully discharged or half charged. Fig. 4-18 shows voltage across each capacitor, voltage across DC motor (armature voltage), and operation of switches S_{12} and S_9 during operation in codes zero and 12, respectively.

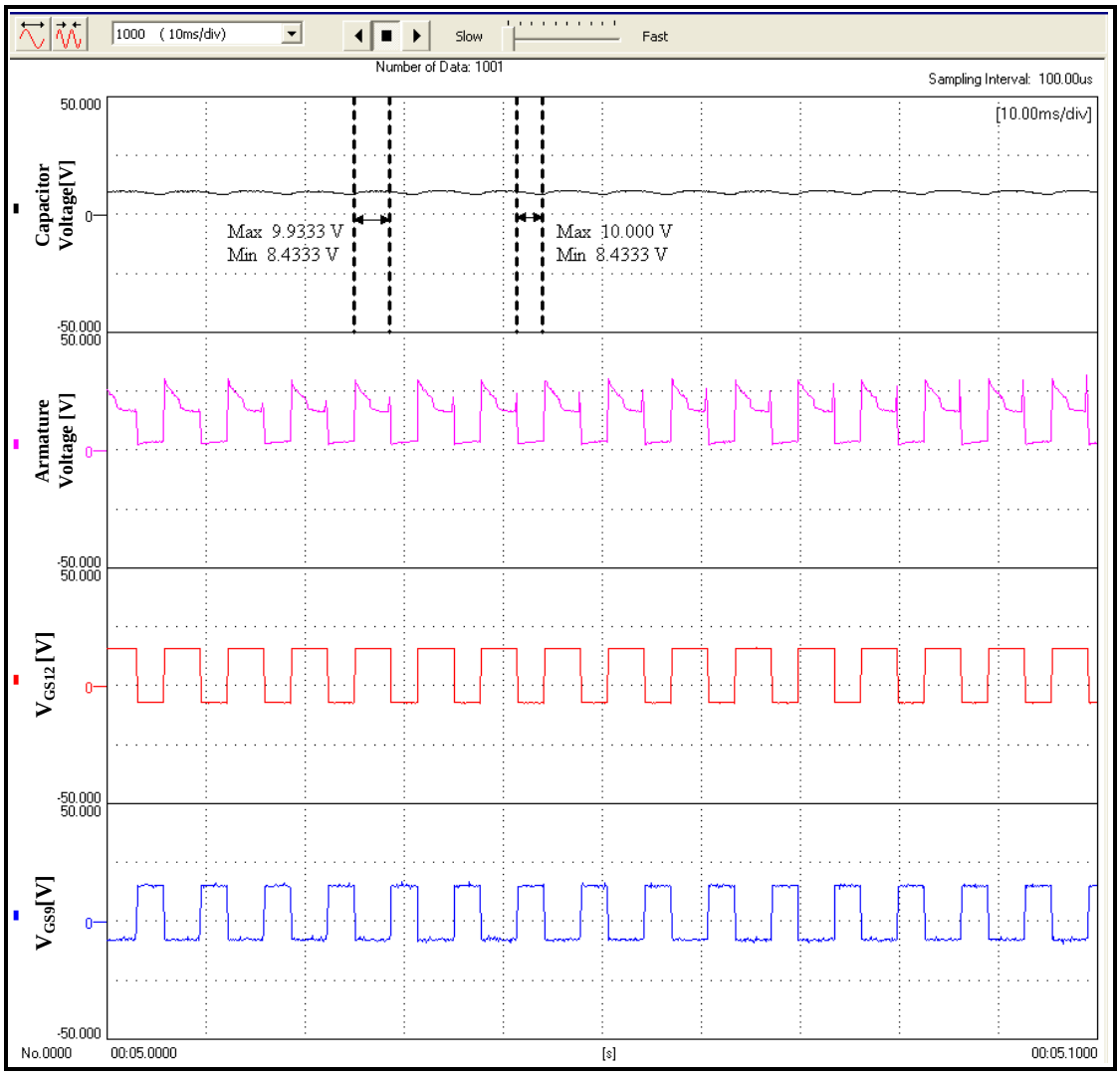

Fig. 4-18. Capacitor voltage (V_{C1} or V_{C2}), armature voltage, and operation of switches S_{12} (V_{GS12}) and S_9 (V_{GS9}).

As is clear, under code zero operation, when switch S_{12} is on, Capacitors C_1 and C_2 are charged by motor side in series, and the voltage across each capacitor increases. After this operating stage, during operation in code 12, when switch S_9 is on, Capacitors C_1 and C_2 are disconnected from motor side, and transfer their stored energy to the LV side. At this time, as is evident from Fig. 4-18, voltage across each capacitor decreases. Also, during this interval, S_{15} is on, because motor does not stop.

Fig. 4-19 shows voltage across of the two capacitors and voltage across DC motor, during operation in codes zero and 12, respectively. As is evident from Fig. 4-19, both voltages (voltage across the two capacitors and armature voltage) have same shape, because the two capacitors are connected to the motor in parallel. Also, when capacitors C_1 and C_2 are disconnected from motor side, voltage across of the two capacitors decreases.

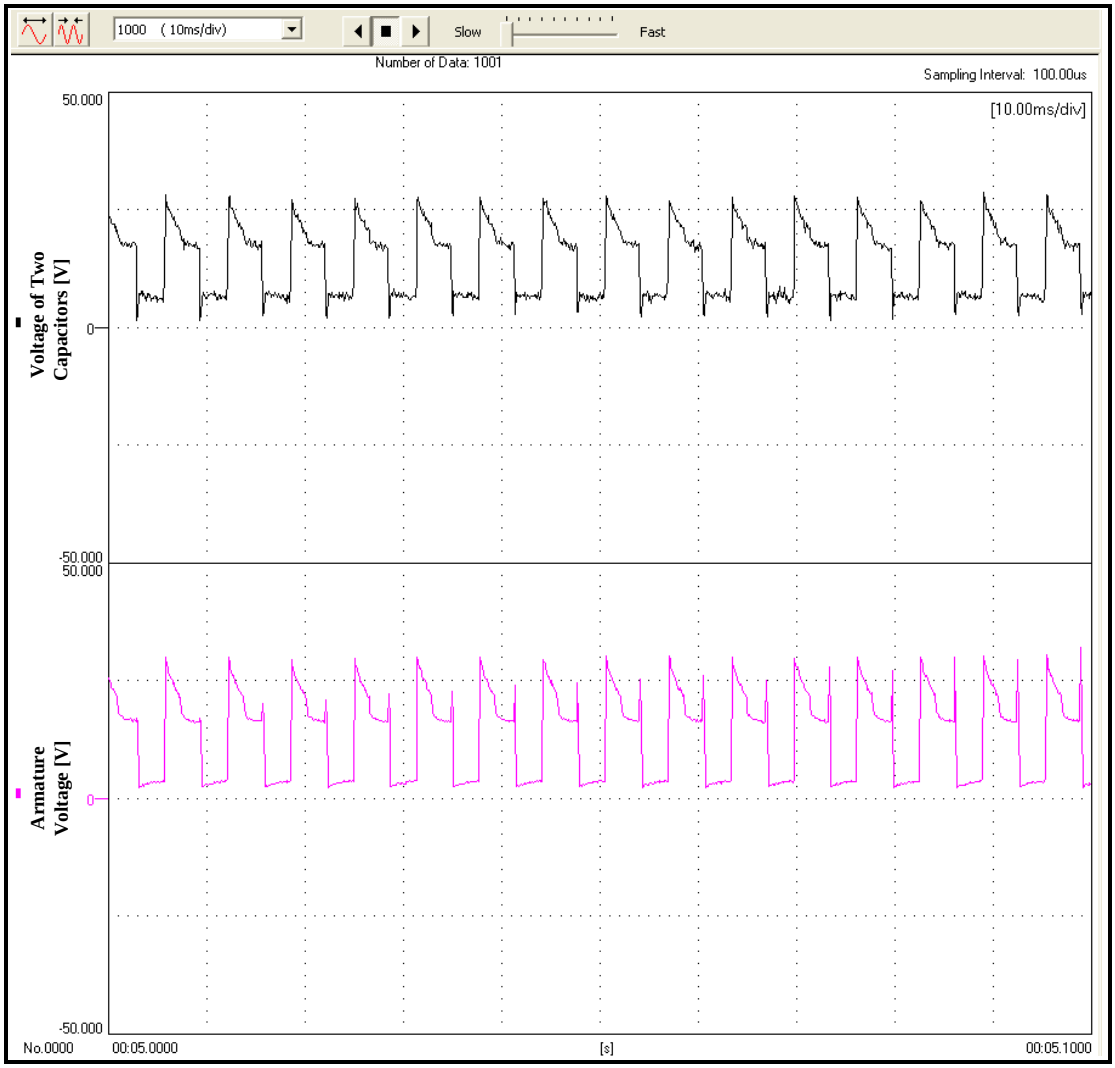

Fig. 4-19. Voltage across of the two capacitors and DC motor during operation in codes zero and 12.

Fig. 4-20 shows the voltage across of the UC modules, which gradually increases, because motor supplies its power to the modules. Fig. 4-21 represents gate-to-source voltages of S_{12} and S_9, motor current (from source of S_6 until C_2), and UC module current, respectively.

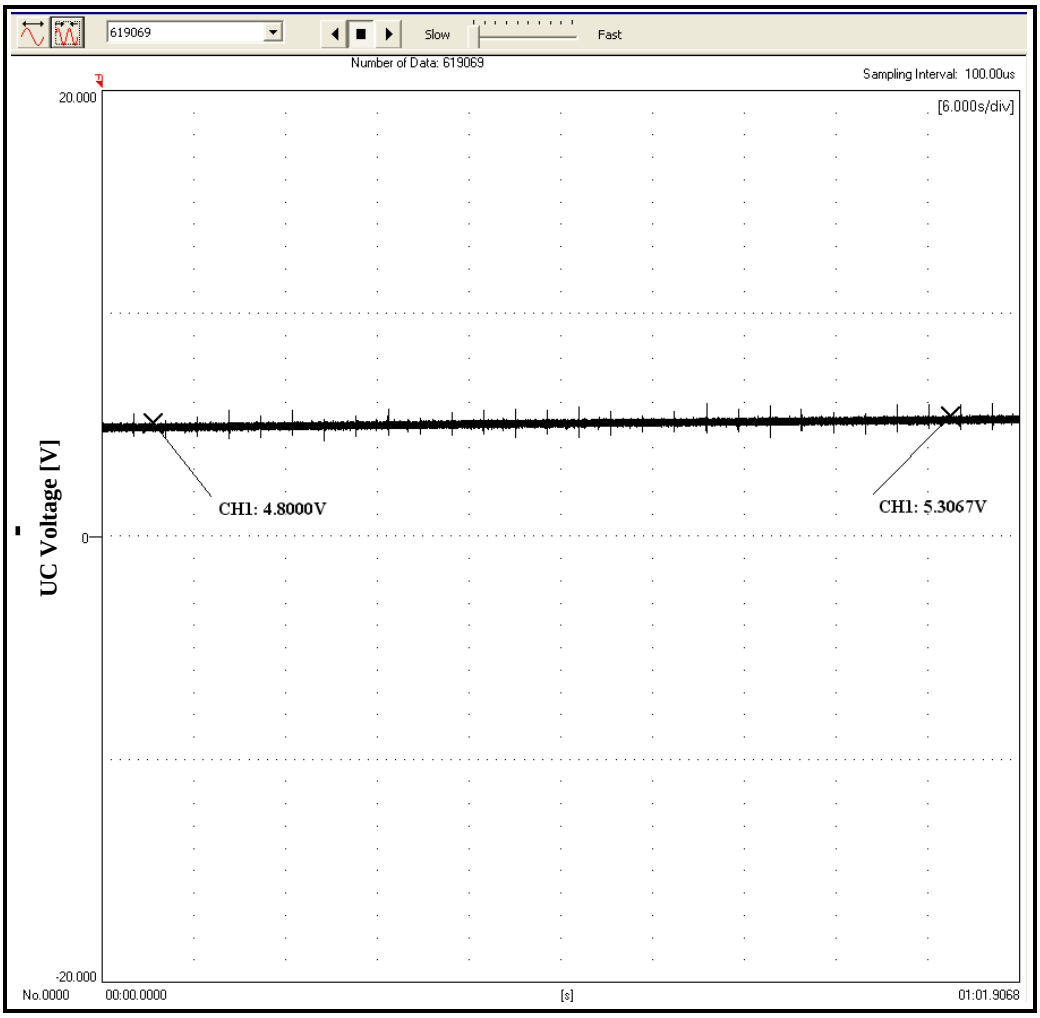

Fig. 4-20. Voltage across of the UC modules.

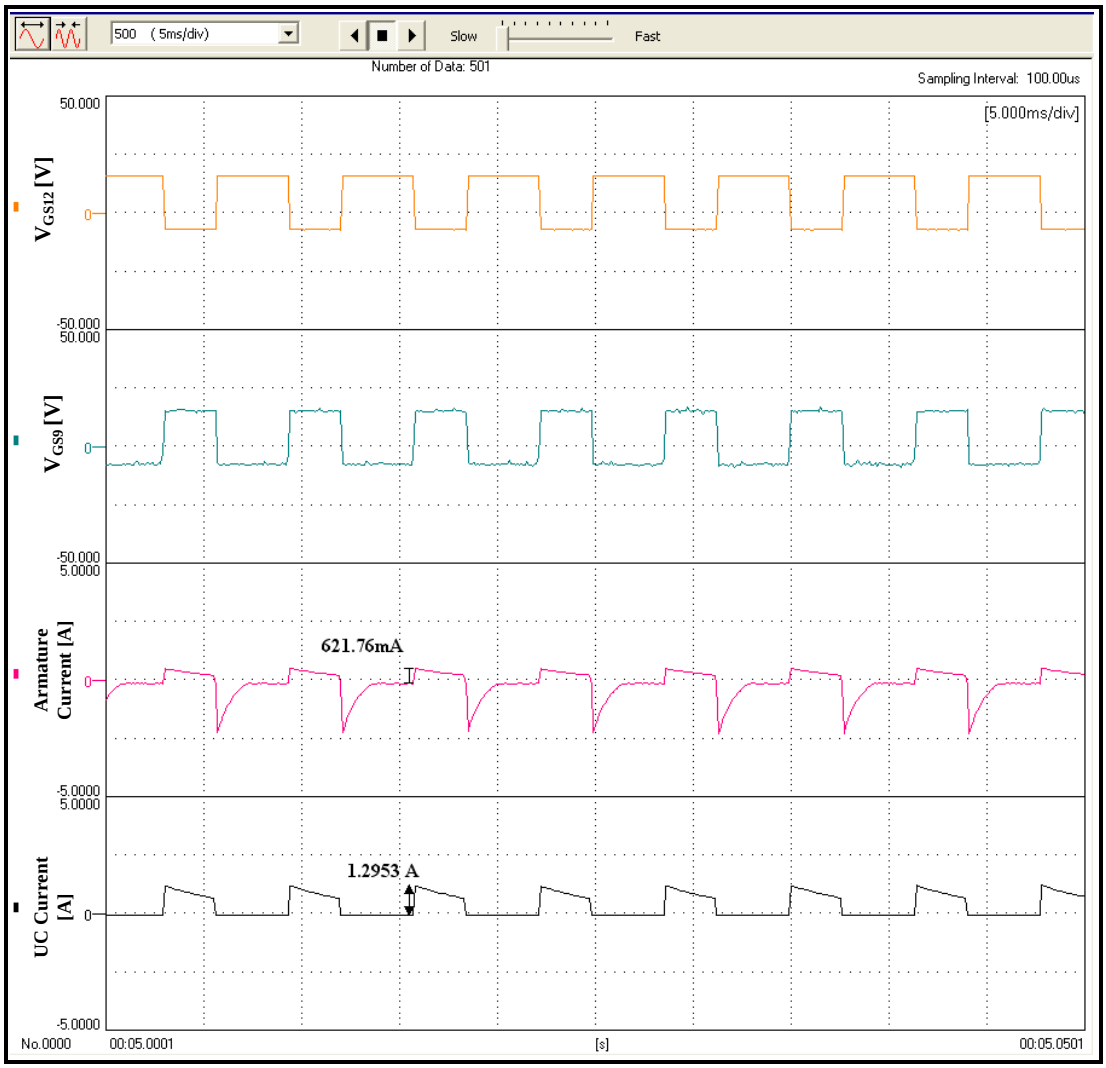

Fig. 4-21. Operation of switches S_{12} (V_{GS12}) and S_9 (V_{GS9}), motor current, and UC modules current.

Fig. 4-22 depicts operation of switches S_{12} and S_9, and motor current and voltage, respectively. As is clear, when S_{12} is on, armature current and voltage decrease, until voltage across of the two capacitors is equal to armature voltage. Also, when S_9 is on, armature current and voltage increase, because capacitors C_1 and C_2 are disconnected from motor side.

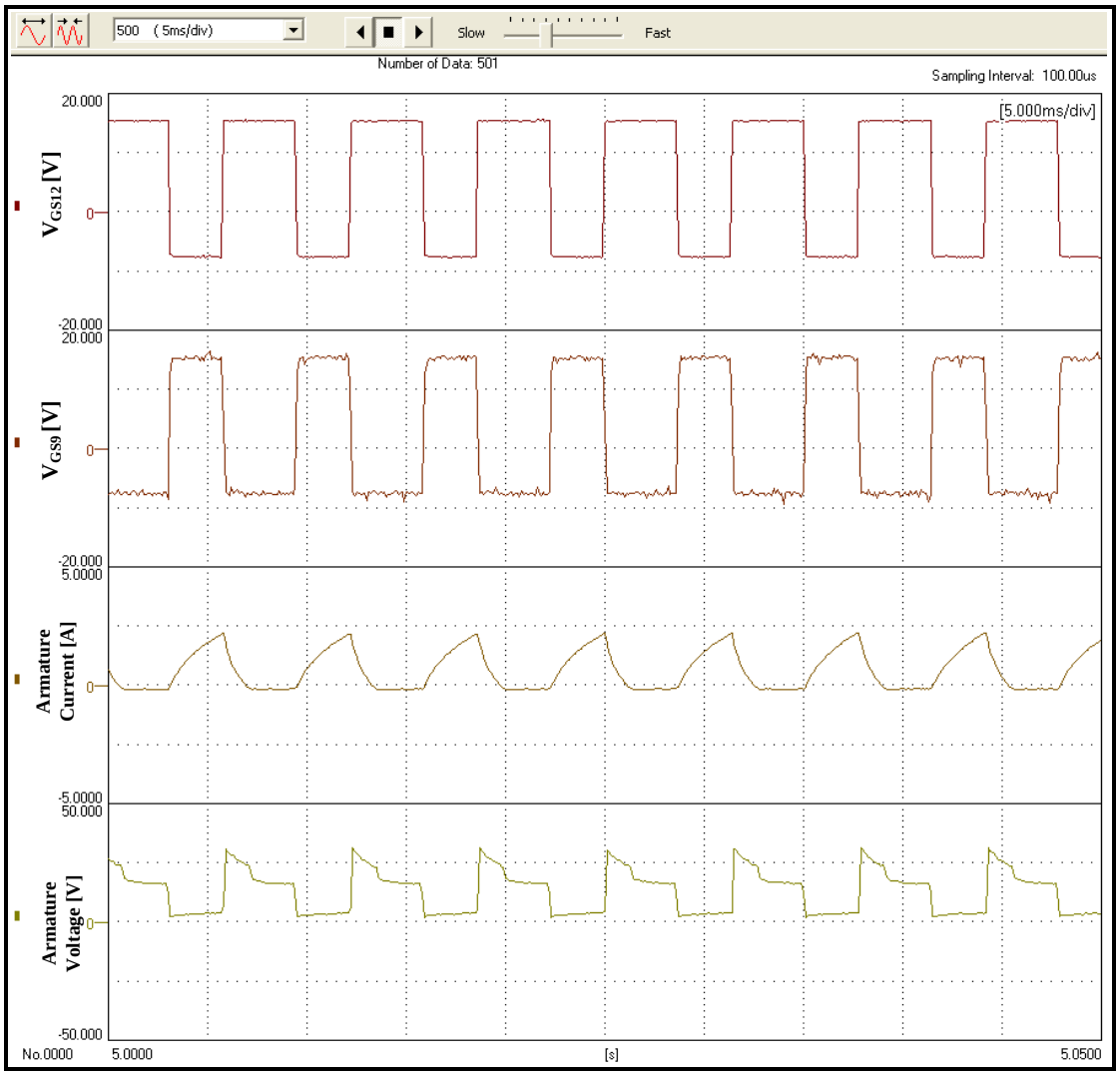

Fig. 4-22. Operation of switches S_{12} (V_{GS12}) and S_9 (V_{GS9}), and motor current and voltage.

Operation of switches S_3, S_{12}, S_7, S_1, S_9, and S_{15} are shown in Fig. 4-23. As is clear, when the converter is operated under code zero, S_3, S_{12}, and S_7 are on, and D_4, D_{11}, and D_6 start conducting (capacitors C_1 and C_2 are charged by the motor side). Under code 12 operation, S_6, S_9, S_{13}, and S_1 are on, and D_7, D_{10}, D_{14}, and D_2 start conducting. Capacitors C_1 and C_2 are discharged and transfer their stored energy to LV side.

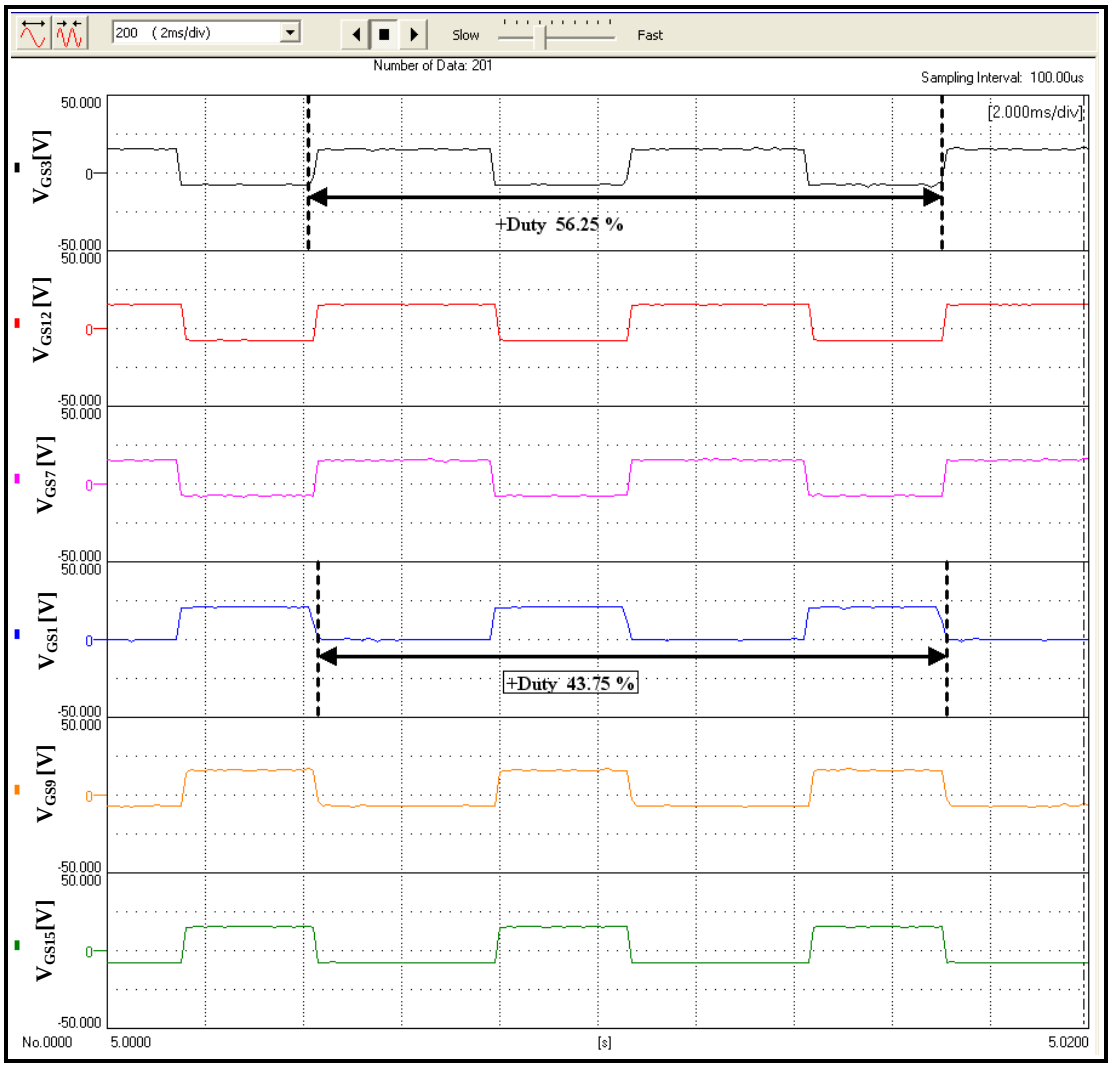

Fig. 4-23. Operation of switches S_3, S_{12}, S_7, S_1, S_9, and S_{15}.

Fig. 4-24 shows the overall computed energy transfer efficiency (η) versus varying conduction duty cycle, *k*, under codes zero and 12. Average transfer efficiency in this mode is calculated to be about 80%. Table 4-2 shows the efficiency comparison between the conventional 4-Q SC *Luo* converter and proposed 4-Q SC *Luo* converter [31]. Considering code 5, when battery modules are fully discharged or half charged, and they demand energy, motor supplies its energy to them.

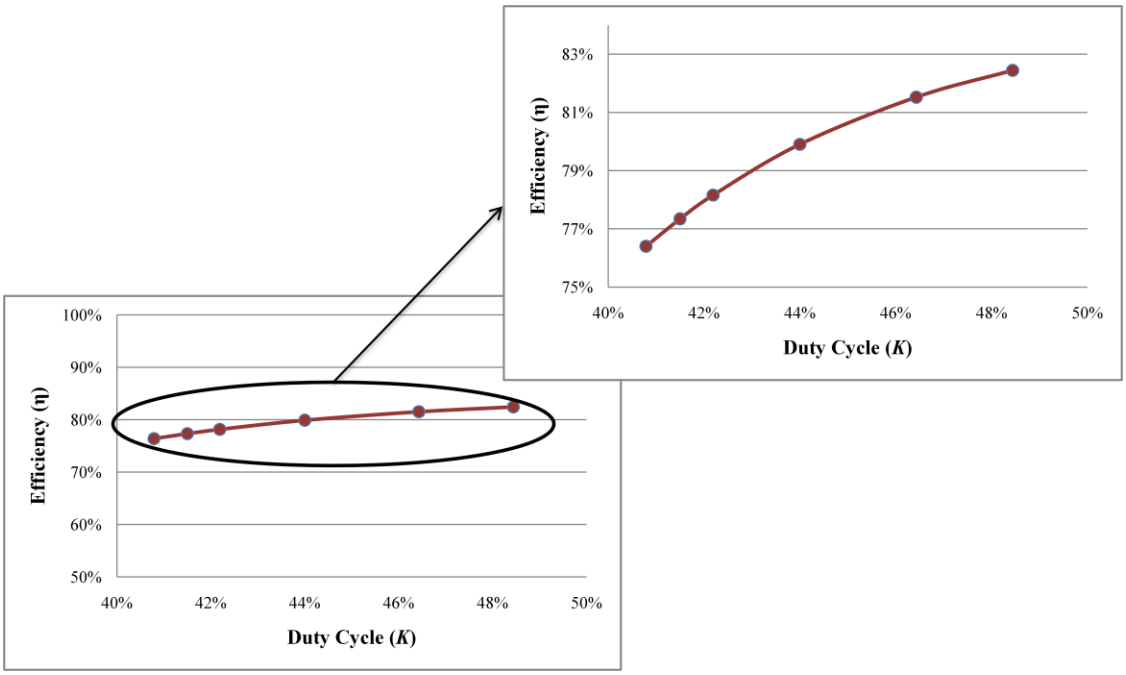

Fig. 4-24. Overall transfer efficiency versus varying duty cycle.

Table 4-2. Efficiency comparison between classic and proposed 4-Q SC *Luo* bi-directional DC/DC converters.

Converter Characteristics	Forward Motoring	Forward Regenerative
Conventional 4-Q SC *Luo* Converter	75%	67%
Proposed 4-Q SC *Luo* Converter	87%	80%

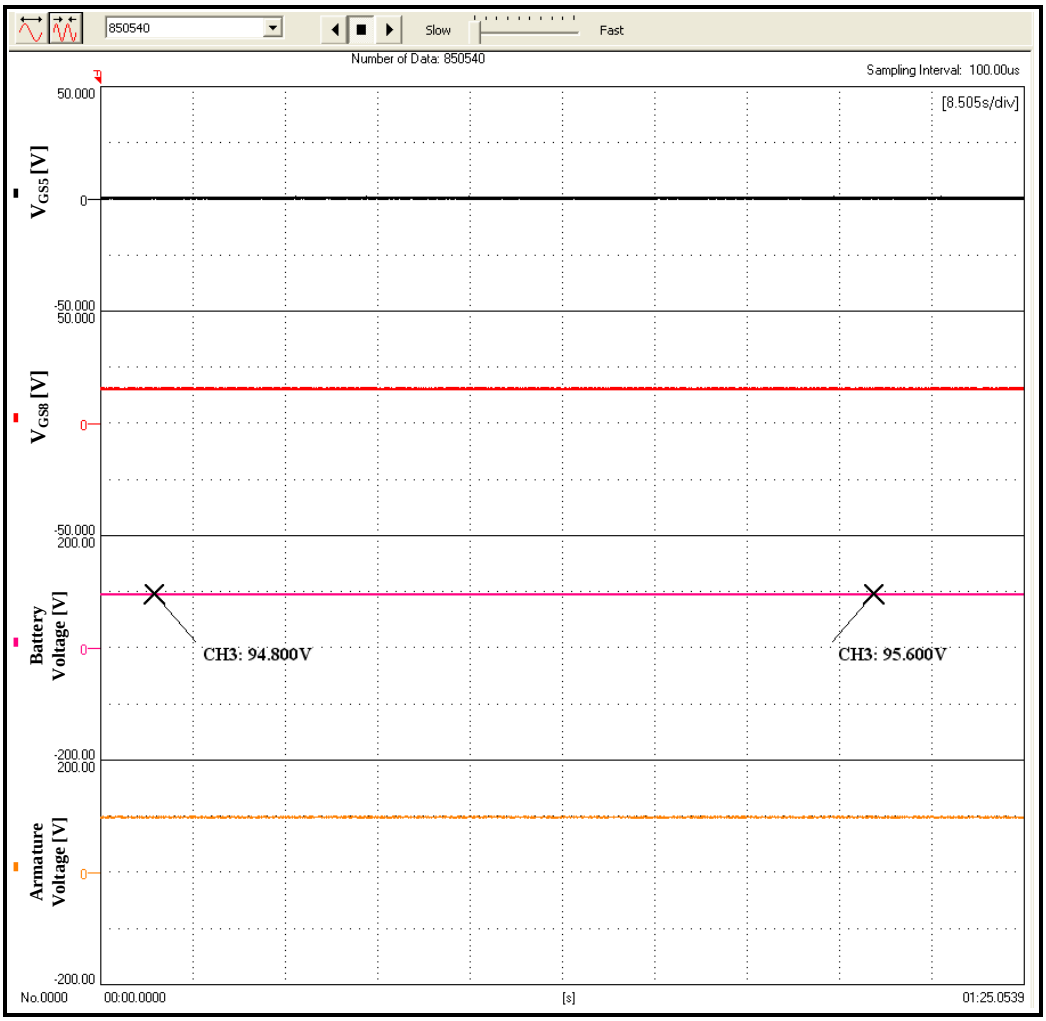

Fig. 4-25. Operation of switches S_5, and S_8, and battery and motor voltage.

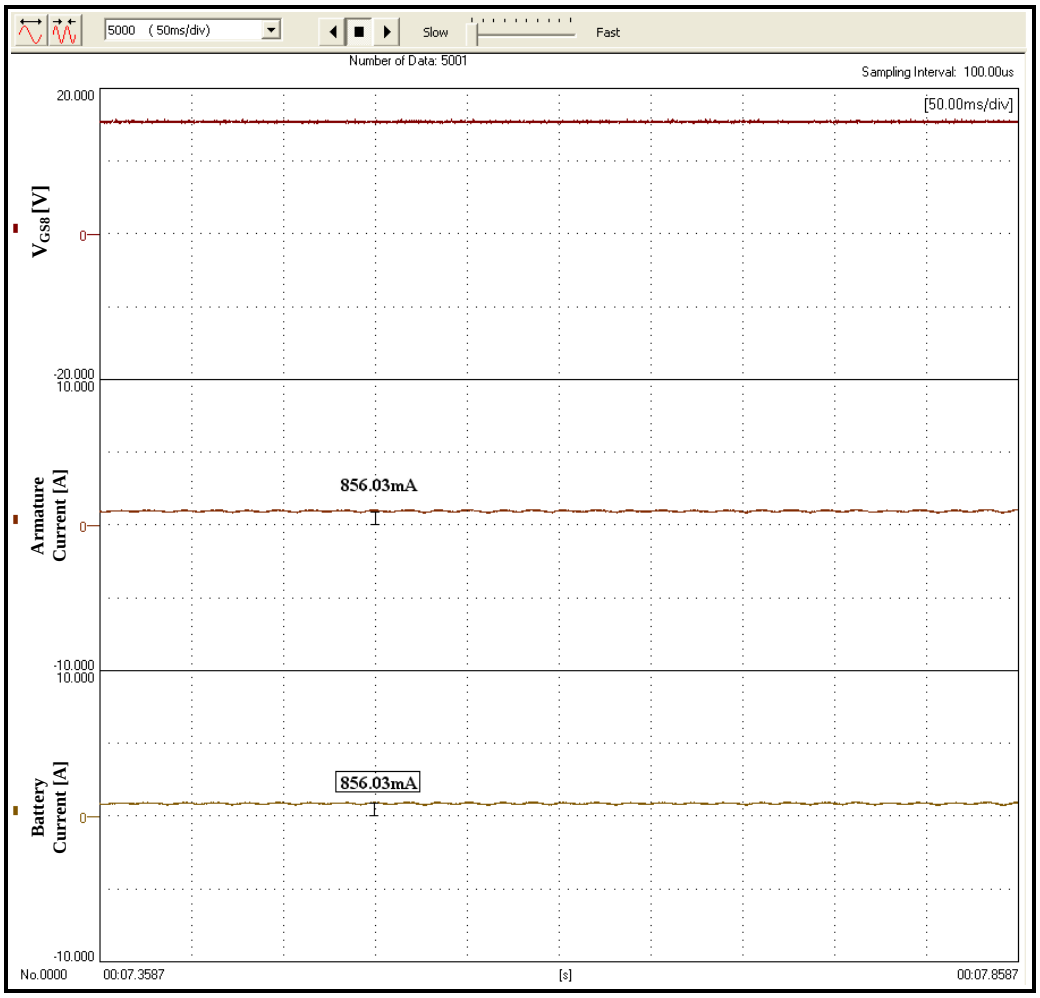

Fig. 4-26. Operation of switch S_8, and motor armature and battery current.

Fig. 4-25 represents operation of switches S_5, and S_8 as well as battery and motor voltage, respectively. Fig. 4-26 shows operation of switch S_8, and motor and battery current. As is clear from Fig. 4-26, the gate-to-source voltage of switch S_8 (V_{GS8}) conducts throughout the duration of this mode (code 5).

CHAPTER 5

CONCLUSIONS AND FUTURE WORK

5.1. CONCLUSIONS

The increasing popularity of EVs and PHEVs can be attributed to the savings in fuel costs, compared to conventional internal combustion engine (ICE) vehicles. EVs and PHEVs save energy due to the employment of reverse regenerating braking during the deceleration cycle. This recuperated energy can be proficiently stored in batteries and/or ultra-capacitors. A hybrid arrangement, with a parallel combination of batteries and ultra capacitor's (UCs), can significantly reduce the volume and weight of the overall EV energy storage system. Furthermore, overall battery life can be drastically improved, due to the decrease in the output current.

The main objective of this dissertation was to provide a detailed analysis and novel hybrid controller design for an advanced hybrid SC *Luo* bi-directional DC/DC converter, applicable for HEV/PHEV ESS applications. More specifically, a novel digital control technique is proposed for the popular 4Q switched-capacitor (SC) DC/DC converter as well as the *Luo* DC/DC converter. The main advantage of using SCCs for EV/PHEV energy management is the absence of transformers and inductors, which makes the complete integration of switching converters possible. In addition, switches are controlled by capacitors, which are charged and discharged through different paths, and transfer their stored energy to either the high voltage (HV) battery side, or the low voltage (LV) ultra-capacitor side.

In a 4-Q SC *Luo* converter, the buck mode uses the *current-amplification technique* and boost mode implements the *voltage-lift technique*, which elevates output current and voltage, respectively. Comparison between the hybrid SCC, interleaved SCC, and 4-Q SC *Luo* converter was presented, which offers features of voltage step-down, voltage step-up, and bidirectional power flow, associated with two or more HEV energy storage devices. A critical inference that can be drawn based on the comparative study between the three SCC topologies investigated in this dissertation, is that the 4-Q SC *Luo* converter has the highest overall transfer efficiency compared to a regular SCC and interleaved SCC. This is due to the fact that, during both operation modes (buck and boost) of the SC *Luo* converter, the converter equivalent resistance (especially the resistances of capacitors C1 and C2) are in parallel. As a result, reduced overall losses can be experienced, and the resulting transfer efficiency is enhanced.

5.2. RECOMMENDED FUTURE WORK

In regards to future work on hybrid electric vehicle energy storage design, the following directions are proposed:

- Using a zero-voltage-switching (ZVS) bidirectional DC/DC converter for hybrid electric vehicle energy storage application.

ZVS has the advantages of simple circuit topology, soft-switching implementation without additional devices, high efficiency, and simple control. These advantages make a new converter topology capable of handling medium and high power; especially as an auxiliary power supply in fuel cell vehicles or for on-board power generation, where high power density, low cost, light weight, and high reliability converters are required.

- Using a typical 3-way plug-in hybrid electric vehicle (PHEV) energy storage system, employing the proposed novel digital control technique.

A possible arrangement for a typical 3-way PHEV ESS could consist of a regenerative fuel cell (RFC), an ultra-capacitor (UC) bank, and a battery pack. The RFC generator acts as the main energy source. However, it has a poor efficiency at light loads, thus relying on the battery pack, for light-load energy requirements. As aforementioned, for transferring energy from each source to the DC link, a step-up operation mode could be used, while for charging both the UC bank and the battery storage system, as well as recovering braking energy, the step-down operating mode could be used.

- Zero-current-switching (ZCS) switched-capacitor bidirectional DC/DC converter using the proposed digital hybrid controller technique.

A ZCS converter possesses conventional features of resonant switched-capacitor converters: low weight, small volume, increased efficiency, low electromagnetic interference (EMI), reduced switching losses, and reduced switch current stress.

- Flywheel energy storage system

A flywheel stores energy in the form of kinetic energy, which can then be transformed into electricity. A flywheel consists of a large rotating disk, where the kinetic energy is stored, and a motor or generator, which is coupled to the flywheel, can convert kinetic energy to electrical energy. The electric traction motor is used to increase the energy stored in the flywheel, while the generator is used to supply energy to the load. Flywheels are predicted to find applications in a wide range of HEV propulsion systems. The kinetic energy in a flywheel can be expressed as:

$$E = \frac{1}{4} M r^2 \omega^2$$

Here, E is kinetic energy in the flywheel, ω is flywheel rotor rotational speed, M is flywheel rotor mass, and r is flywheel rotor radius. The proposed novel control strategy could be extended for effective energy management of the on-board electro-mechanical hybrid energy storage system. Steep demands of acceleration and braking can be attributed to the flywheel system, whereas steady braking and acceleration could be attributed to the battery pack.

REFERENCES

[1] Z. Amjadi and S. S. Williamson, "Power-electronics-based solutions for plug-in hybrid electric vehicle energy storage and management systems," *IEEE Trans. on Industrial Electronics*, vol. 57, no. 2, pp. 608-616, Feb. 2010.

[2] A. Emadi, K. Rajashekara, S. S. Williamson, and S. M. Lukic, "Topological overview of hybrid electric and fuel cell vehicular power system architectures and configurations," *IEEE Trans. on Vehicular Technology*, vol. 54, no. 3, pp. 763-770, May 2005.

[3] S. K. Biradar, R. A. Patil, and M. Ullegaddi, "Energy storage system in electric vehicle," in *Proc. IEEE Power Quality*, 1998, pp. 247-255.

[4] X. Yan and D. Patterson, "Improvement of drive range, acceleration and deceleration performances in an electric vehicle propulsion system, " in *Proc. IEEE Power Electronics Specialists Conf.*, June 1999, vol. 2, pp. 638-643.

[5] R. M. Schupbach, J. C. Balda, M. Zolot, B. Kramer, "Design methodology of a combined battery-ultracapacitor energy storage unit for vehicle power management," in *Proc. IEEE Power Electronics Specialists Conf.*, Acapulco, Mexico, June 2003, vol. 1, pp. 88-93.

[6] H. V. Venkatasetty and Y. U. Jeong, "Recent advances in lithium-ion and lithium-polymer batteries," in *Proc. 17th Annual Battery Conf. Applications and Advances*, Jan. 2002, pp. 173-178.

[7] J. McDowell, A. Brenier, M. Broussely, and P. Lavaur, "Industrial lithium-ion batteries: from the laboratory to real telecom application," in *Proc. IEEE Annual International Telecommunications Energy Conf.*, Sept. 2002, pp. 373-378.

[8] H. S. Park, C. E. Kim, C. H. Kim, G. W. Moon, and J. H. Lee, "A modularized charge equalizer for an HEV lithium-ion battery string," *IEEE Trans. on Industrial Electronics*, vol. 56, no. 5, pp. 1464-1476,May 2009.

[9] G. X. Dong, Y. S. Yan, Y. Wei, and H. Jun, "Analysis on equalization circuit topology and system architecture for series-connected ultra-capacitor," in *Proc. IEEE Vehicle Power and Propulsion Conf.*, Harbin, China, Sept. 2008, pp. 1-5.

[10] S. M. Lukic, S. G. Wirasingha, F. Rodriguez, J. Cao, and A. Emadi, "Power management of an ultra-capacitor/battery hybrid energy storage system in an HEV," in *Proc. IEEE Vehicle Power and Propulsion Conf.*, Windsor, UK, Sept. 2006, pp. 1-6.

[11] J. Moreno, M. E. Ortuzar, and J. W. Dixon, "Energy-management system for a hybrid electric vehicle, using ultracapacitors and neural networks," *IEEE Trans. on Industrial Electronics*, vol. 53, no. 2, pp. 614-623, April 2006.

[12] M. E. Ortuzar, J. Moreno, and J. W. Dixon, "Ultracapacitor-based auxiliary energy system for an electric vehicle: implementation and evaluation," *IEEE Trans. on Industrial Electronics*, vol. 54, no. 4, pp. 2147-2156, Aug. 2007.

[13] C. A. Ramos-Paja, C. Bordons, A. Romero, R. Giral, and L. Martinez-Salamero, "Minimum fuel consumption strategy for PEM fuel cells," *IEEE Trans. on Industrial Electronics*, vol. 56, no. 3, pp. 685-696, March 2009.

[14] A. Lidozzi and L. Solero, "Power balance control of multiple-input DC-DC power converter for hybrid vehicles," in *Proc. IEEE International Symposium on Industrial Electronics*, Ajaccio, France, May 2004, pp. 1467-1472.

[15] H. Matsuo, W. Lin, F. Kurokawa, T. Shigemizu, and N. Watanabe, "Characteristics of the multiple-input DC-DC converter," *IEEE Trans. on Industrial Electronics*, vol. 51, no. 3, pp. 625-631, June 2004.

[16] A. Di Napoli, F. Crescimbini, S. Rodo, and L. Solero, "Multiple input DC-DC power converter for fuel-cell powered hybrid vehicles," in *Proc. IEEE Power Electronics Specialists Conf.*, June 2002, vol. 4, pp. 1685-1690.

[17] M. H. Todorovic, L. Palma, and P. N. Enjeti, "Design of a wide input range DC–DC converter with a robust power control scheme suitable for fuel cell power conversion," *IEEE Trans. on Industrial Electronics*, vol. 55, no. 3, pp. 1247-1255, March 2008.

[18] A. Emadi, Y. J. Lee, and K. Rajashekara, "Power electronics and motor drives in electric, hybrid electric, and plug-in hybrid electric vehicles," *IEEE Trans. on Industrial Electronics*, vol. 55, no. 6, pp. 2237-2245, June 2008.

[19] Y. M. Chen, Y. C. Liu, and S. H. Lin, "Double-input PWM DC-DC converter for high/low voltage sources," in *Proc. IEEE International Telecommunications Energy Conf.*, Oct. 2003, pp. 27-32.

[20] K. P. Yalamanchili and M. Ferdowsi, "Review of multiple input DC-DC converters for electric and hybrid vehicles," in *Proc. IEEE Vehicle Power and Propulsion Conf.*, Sept. 2005, pp. 160-163.

[21] A. Emadi, S. S. Williamson, and A. Khaligh, "Power electronics intensive solutions for advanced electric, hybrid electric, and fuel cell vehicular power systems," *IEEE Trans. on Power Electronics*, vol. 21, no. 3, pp. 567-577, May 2006.

[22] S. M. Lukic, J. Cao, R. C. Bansal, F. Rodriguez, and A. Emadi, "Energy storage systems for automotive applications," *IEEE Trans. on Industrial Electronics*, vol. 55, no. 6, pp. 2258-2267, June 2008.

[23] M. Ehsani, Y. Gao, S. E. Gay, and A. Emadi, *Modern Electric, Hybrid Electric, and Fuel Cell Vehicles Fundamentals, Theory and Design*, CRC Press, Boca Raton Washington, D.C., 2005.

[24] M. B. Camara, H. Gualous, F. Gustin, and A. Berthon, "Design and new control of DC/DC converters to share energy between supercapacitors and batteries in hybrid vehicle," *IEEE Trans. on Vehicular Technology*, vol. 57, no. 5, pp. 2721-2735, Sept. 2008.

[25] Z. Amjadi and S. S. Williamson, "A novel control technique for a switched capacitor converter based hybrid electric vehicle energy storage system," *IEEE Trans. on Industrial Electronics*, vol. 57, no. 3, pp. 926-934, Feb. 2010.

[26] H. S. H. Chung, W. C. Chow, S. Y. R. Hui, and S. T. S. Lee, "Development of a switched-capacitor DC-DC converter with bidirectional power flow," *IEEE Trans. on Circuits and Systems*, vol. 47, no. 9, pp. 1383-1389, Sept. 2000.

[27] Y. Berkovich, B. Axelrod, S. Tapuchi, and A. Ioinovici, "A family of four-quadrant PWM DC-DC converters," in *Proc. IEEE Power Electronics Specialists Conf.*, Orlando, FL, June 2007, pp 1878-1883.

[28] H. S. Chung and A. Ioinovici, "Development of a general switched-capacitor DC/DC converter with bi-directional power flow," in *Proc. IEEE International Symp. on Circuits and Systems*, Geneva, Switzerland, May 2000, vol. 3, pp. 499-502.

[29] O. C. Mak, Y. C. Wong, and A. Ioinovici, "Step-up DC power supply based on a switched-capacitor circuit," *IEEE Trans. on Industrial Electronics*, vol. 42, no. 1, pp. 90-97, Feb. 1995.

[30] A. Ioinovici, H. S. H. Chung, M. S. Makowski, and C. K. Tse, "Comments on: unified analysis of switched-capacitor resonant converters," *IEEE Trans. on Industrial Electronics*, vol. 54, no. 1, pp. 684-685, Feb. 2007.

[31] F. L. Luo and H. Ye, *Advanced DC/DC Converters*, CRC Press, Boca Raton, FL, 2004.

[32] M. Veerachary and N. T. Reddy "Voltage-mode control of hybrid switched capacitor converters," in *Proc. Annual Conf. of the IEEE Industrial Electronics Society*, Paris, France, Nov. 2006, pp. 2450-2453.

[33] A. C. Baughman and M. Ferdowsi, "Double-tiered switched-capacitor battery charge equalization technique," *IEEE Trans. on Industrial Electronics*, vol. 55, no. 6, pp. 2277-2285, June 2008.

[34] Z. Amjadi and S. S. Williamson, "Advanced digital control for a switched capacitor and interleaved switched capacitor hybrid electric vehicle energy management system," *Journal of Electrical Engineering and Technology*, Feb. 2010.

[35] M. Veerachary, "Control of switched capacitor step-down buck converter," in *Proc. Annual Conf. of the IEEE Industrial Electronics Society*, Paris, France, Nov. 2006, pp. 2073-2076.

[36] M. Veerachary and S. B. Sudhakar, "Peak-current mode control of hybrid switched capacitor converter," in *Proc. IEEE International Conf. on Power Electronics, Drives and Energy Systems*, New Delhi, India, Dec. 2006, pp. 1-6.

[37] F. L. Luo, “Luo converters, voltage lift technique,” in *Proc. IEEE Power Electronics Specialists Conf.*, Fukuoka, Japan, May 1998, pp. 1783-1789.

[38] F. L. Luo, “Luo-converters, a series of new DC-DC step-up (boost) conversion circuits,” in *Proc. IEEE International Conf. on Power Electronics and Drive Systems*, Singapore, May 1997, vol. 2, pp. 882-888.

[39] F. L. Luo, “Negative output Luo converters: voltage lift technique,” *IEE Proc. on Electric Power Applications*, vol. 146, no. 2, pp. 208-223, March 1999.

[40] F. L. Luo, “Re-lift circuit: a new DC-DC step-up (boost) converter,” *IEEE Electronics Letters*, vol. 33, no. 1, pp. 5-7, Jan. 1997.

[41] Z. Amjadi and S. S. Williamson, “Modeling, Simulation, and Control of an Advanced Luo Converter for Plug-In Hybrid Electric Vehicle Energy Storage System,” *IEEE Transactions on Vehicular Technology*, vol. 60, no. 1, pp. 64-75, Oct. 2010.

[42] H. Chung, O. Brian, and A. Ioinovici, “Switched-capacitor-based DC-DC converter with improved input current waveform,” in *Proc. IEEE International Symp. on Circuits and Systems*, Atlanta, GA, May 1996, vol. 1, pp. 541-544.

[43] O. C. Mak and A. Ioinovici, “Switched-capacitor inverter with high power density and enhanced regulation capability,” *IEEE Trans. on Circuits Systems*, vol. 45, no. 4, pp. 336-347, April 1998.

[44] Z. Amjadi and S. S. Williamson, “Design and implementation of a bidirectional HEV energy management strategy using a switched capacitor *Luo* converter, ” in Proc. *IEEE Canadian Conf. on Electrical and Computer Engineering*, Calgary, Alberta, May 2010, pp. 1-5.

[45] Z. Amjadi and S. S. Williamson, “Review of alternate energy storage systems for hybrid electric vehicles,” *in Proc. IEEE Canada Electrical Power and Energy Conf.*, Montreal, QC, Oct. 2009, pp. 1–7.

[46] Z. Amjadi and S. S. Williamson, “Efficiency Modeling and Comparison of Switched Capacitor, Luo, and Interleaved Switched Capacitor Converters for Electric Vehicle Energy Storage Systems,” in Proc. *IEEE Industrial Electronics Society Annual Conf.*, Phoenix, AZ, Nov. 2010, pp. 1811–1817.

[47] Z. Amjadi and S. S. Williamson, “Novel controller design for a *luo* converter electric vehicle energy management system,” in Proc. *IEEE Canada Electrical Power and Energy Conf.*, Halifax, Nova Scotia, Aug. 2010, pp. 1–6.

[48] Z. Amjadi and S. S. Williamson, “Performance comparison and efficiency modeling of a *Luo* converter and 2-quadrant switched capacitor converter for HEV energy management,” in Proc. *IEEE Vehicle Power and Propulsion Conf.*, Lille, France, Sept. 2010.

[49] (Invited) Z. Amjadi and S. S. Williamson, “Comparative analysis between a 2-quadrant DC/DC converter and a *Luo* converter for a battery/ultracapacitor HEV energy storage system,” in Proc. *IEEE Vehicle Power and Propulsion Conf.*, Lille, France, Sept. 2010.

[50] Z. Amjadi and S. S. Williamson, “Efficiency modeling and analysis of a switched capacitor converter for a plug-in hybrid electric vehicle energy storage system,” in Proc. *35th Annual Conf. of the IEEE Industrial Electronics Society*, Porto, Portugal, Nov. 2009, pp. 3723-3728.

[51] Spectrum Digital, see: http://www.spectrumdigital.com.

APPENDIX

APPENDIX A: ELECTRONIC CIRCUITS FOR GATING SIGNALS OF THE SWITCHES

Fig. A-1 shows the electronic circuit that provides the gating signals for the switches. It provides the required current for the drive circuit of the switches.

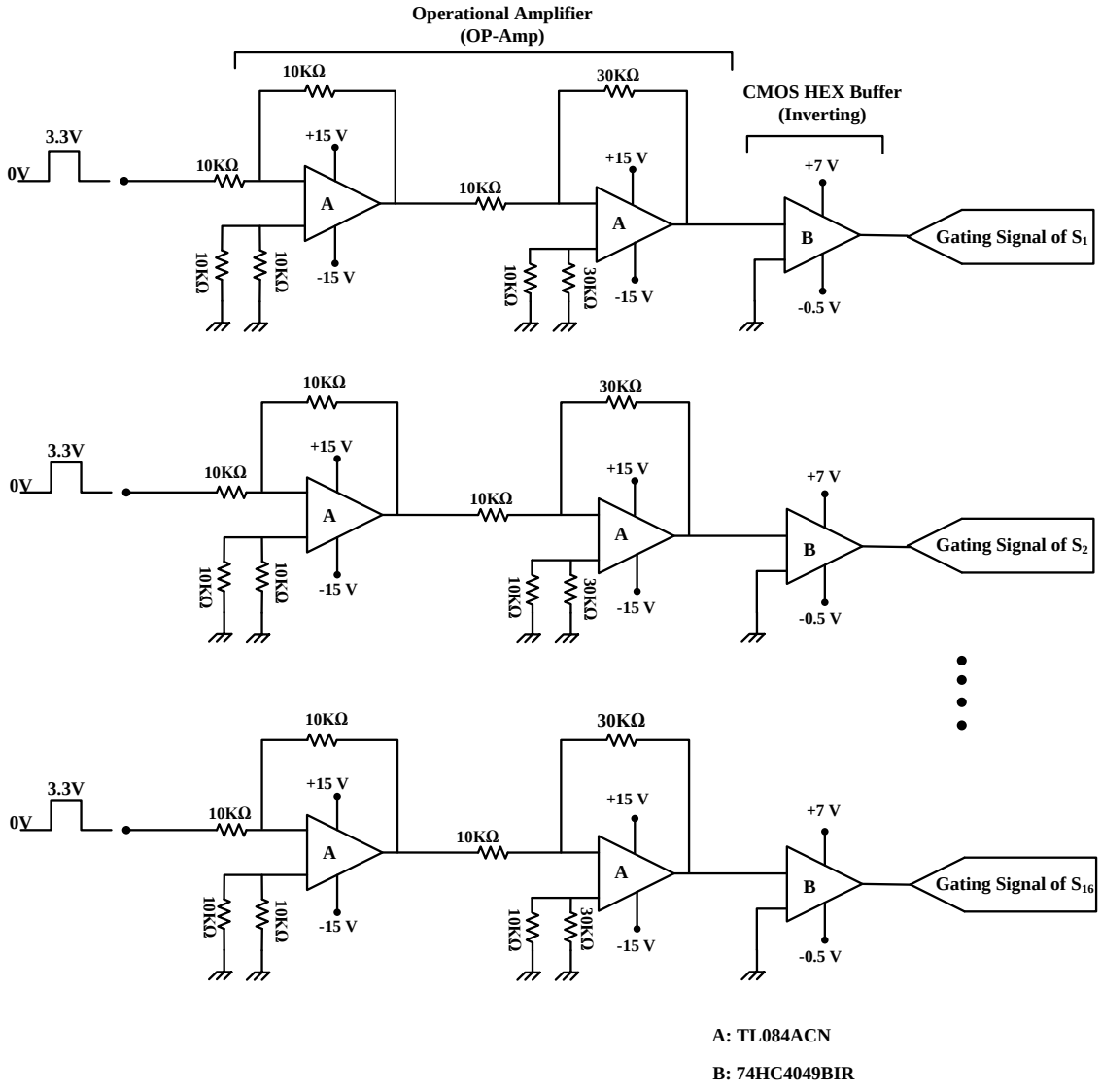

Fig. A-1. Electronic circuits for gating signals of the switches.

APPENDIX B: DSP SYSTEM

This project uses two types of connectors: 1) I/O interface connector (DAC) and 2) Analog interface connector (ADC). I/O interface connector consists of P4, P8, and P7, which interface the I/O signals from the DSP to the switch gating circuits. The layout of these connectors is shown in Fig. B-1. The pin definition of P4 and P8 connectors are shown in Fig. B- 2. The pin definition of P7 connector is represented in Fig. B-3.

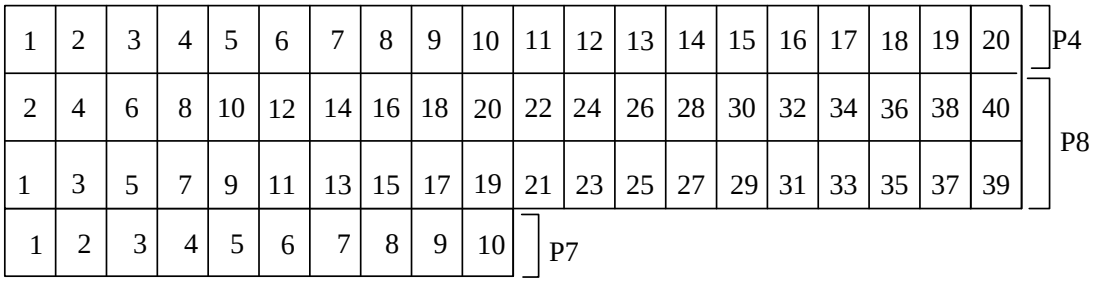

Fig. B-1. Layout of P4, P8, and P7.

P4 Pin #	P4 Signal	P8 Pin #	P8 Signal	P8 Pin #	P8 Signal
1	+3.3V/+5V/NC *	1	+3.3V/+5V/NC *	2	+3.3V/+5V/NC *
2	XINT2/ADCSOC	3	SCITXDA	4	SCIRXDA
3	MCLKXA	5	XINT1n/XBIOn	6	CAP1/QEP1
4	MCLKRA	7	CAP2/QEP2	8	CAP3/QEPI1
5	MFSXA	9	PWM1	10	PWM2
6	MFSRA	11	PWM3	12	PWM4
7	MDXA	13	PWM5	14	PWM6
8	MDRA	15	T1PWM/T1CMP	16	T2PWM/T2CMP
9	No connect	17	TDIRA	18	TCLKINA
10	GND	19	GND	20	GND
11	CAP5/QEP4	21	No connect	22	XINT1N/XBIOn
12	CAP6/QEPI2	23	SPISIMOA	24	SPISOMIA
13	T3PWM/T3CMP	25	SPICLKA	26	SPISTEA
14	T4PWM/T4CMP	27	CANTXA	28	CANRXA
15	TDIRB	29	XCLKOUT	30	PWM7
16	TCLKINB	31	PWM8	32	PWM9
17	XF/XPLLDISn	33	PWM10	34	PWM11
18	SCITXDB	35	PWM12	36	CAP4/QEP3
19	SCIRXDB	37	T1CTRIP/PDPINTAn	38	T3CTRIP/PDPINTBn
20	GND	39	GND	40	GND

Fig. B-2. I/O interface connector (P4 and P8).

P7 Pin #	P7 Signal
1	C1TRIPn
2	C2TRIPn
3	C3TRIPn
4	T2CTRIPn/EVASOCn
5	C4TRIPn
6	C5TRIPn
7	C6TRIPn
8	T4CTRIPn/EVBSOCn
9	No connect
10	GND

Fig. B-3. I/O interface connector (P7).

The analog interface connector includes 10 and 20 pins on the P5 and P9 connectors, respectively. These connectors are shown in Fig. B-4.

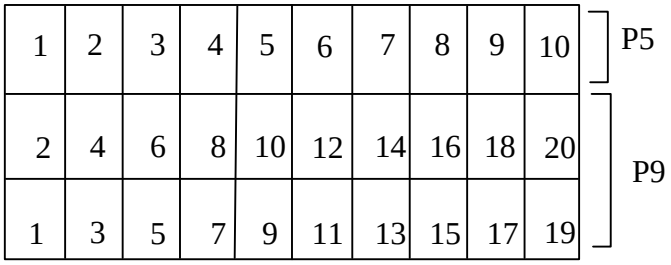

Fig. B-4. Layout of P5 and P9.

Pins P5 and P9 represent input signals to the DSP. The pin definitions of P5 and P9 signals are shown in Fig. B-5 [51].

P5 Pin #	Signal	P9 Pin #	Signal	P9 Pin #	Signal
1	ADCINB0	1	GND	2	ADCINA0
2	ADCINB1	3	GND	4	ADCINA1
3	ADCINB2	5	GND	6	ADCINA2
4	ADCINB3	7	GND	8	ADCINA3
5	ADCINB4	9	GND	10	ADCINA4
6	ADCINB5	11	GND	12	ADCINA5
7	ADCINB6	13	GND	14	ADCINA6
8	ADCINB7	15	GND	16	ADCINA7
9	ADCREFM	17	GND	18	VREFLO *
10	ADCREFP	19	GND	20	No connect

Fig. B-5. Analog interface connector (P5 and P9).